Kinematics-Based Modelling of Compact Footings

Auteur : Spada, Giorgia
Promoteur(s) : Mihaylov, Boyan
Faculté : Faculté des Sciences appliquées
Diplôme : Master en ingénieur civil des constructions, à finalité spécialisée en "civil engineering"
Année académique : 2018-2019
URI/URL : http://hdl.handle.net/2268.2/6778

University of Liège - Faculty of Applied Sciences

Département d'Architecture, Géologie, Environnement et Construction (ArGEnCo)

Graduation Studies conducted for obtaining the
Master's Degree in Civil Engineering in Constructions

Kinematics-Based Modelling of Compact Footings

Student:
Giorgia SPADA

Jury Members:
Boyan MIHAYLOV
Almila UZEL
Vincent DENOËL
Frédéric COLLIN
Stefano DE MIRANDA

Academic Year 2018-19
June 2019

Abstract

The main objective of this thesis work is the extension and validation of a Two-Parameter Kinematic Theory (2PKT) for shear behavior of deep beams to concrete compact footings. The foundations have the purpose to transfer the load of the superstructure and its weight to the soil layers. Generally, reinforced concrete footings are designed without shear reinforcement; therefore, these elements are susceptible to brittle failure according to the amount of diagonal cracking due to shear stresses. Large-scale tests provided by *Uzel* (2003) are the starting point for the analysis. It is known that there is a significant size effect in shear strength of lightly reinforced slender members without shear reinforcement, for that it is important to simulate during the test the real size of this kind of elements in order to correctly evaluate the influence of the size on the shear behavior of large concrete footings; therefore only large-scale tests of the *Uzel*'s series are considered. One-way shear is studied, thus the footings were modelled to represent a strip of the element subjected to point load (simulating the load coming from the column footing) and uniformly distributed load imposed by a set of hydraulic jacks equally spaced (which reproduce the simplified soil pressure, in practice it is not uniform, but it varies according to the soil type).

Then, Finite Element Models (by using program VecTor2) of tests are performed in order to obtain reliable and accurate predictions and enlarge the footings database, for which, in the literature, few suitable tests are available. Simultaneously, the 2PKT for shear behavior in deep beams was developed for footings, adapting the loading conditions and the shear resistance contributions. By means of the 2PKT it is possible to predict the shear failure load, the crack widths near failure, and the complete deformed shapes. The two parameters used in the models are the ultimate vertical displacement of Critical Loading Zone (CLZ) and the average tensile strain in the longitudinal reinforcement on the flexural tension side. In order to show the validity of the theory, a parametric study is developed by using FEM models. The parameters included in the study are the concrete strength, the longitudinal reinforcement ratio and the length of the footing. Based on the use of non-linear finite element calculations validated against experimental results, it is possible to validate the 2PKT extended to concrete compact footings. The 2PKT method reproduces well the observations and the measurements during the large-scale laboratory tests. The average experimental-to-predicted strength ratio obtained with the extended 2PKT calculations for the footings database and the FEM models is 1.04 and the Coefficient of Variation (CoV) is 14.2%. The shear resistance components, thus critical loading zone and aggregate interlock for footings without shear reinforcement, underline that the size effect for deep concrete footings is principally produced by the aggregate interlock mechanism. Specifically, increasing the dimension of the element, the critical loading zone deforms more, and the diagonal cracks are wider, therefore the shear stresses transmitted throughout the cracks reduce.

This thesis work is just the starting point for the validation of the 2PKT. The FEM models created for the parametric study could be actually validated by means of real laboratory large-scale tests, in order to experimentally demonstrate the shear predictions of the theory and enlarge its validity.

Acknowledgment

This master thesis is part of a larger project of research started years ago thanks to a collaboration between Professor *Boyan Mihaylov* and Professor *Almila Uzel*. The idea is to extend the Two-Parameter Kinematic Theory (2PKT) for shear behavior in deep beams, developed by *B. Mihaylov*, to deep footings studied and tested under one-way shear by *A. Uzel*. Therefore, I am grateful to Professors *B. Mihaylov* and *A. Uzel* for having introduced me in this interesting and advanced topic. With their experiences and knowledge, I was able to increase my understanding regarding this theme. I thank *Uzel* for her suggestions and for having provided me the experimental data. My supervisor, *B. Mihaylov*, guided me into the developing of this thesis work and during the weekly meeting with him I had the possibility to improve my knowledge and my communication skills, I am grateful to him and I am happy to have chosen him as guide for this concluding work.

Then, I thank all the other jury members *V. Denoël, F. Collin* and *S. De Miranda* for reading my thesis and being part of this project.

I would like to extend my thanks to *Jian Liu* for her support and advices, and to my office collogues *Renaud Franssen* and *Chathura Rajapakse* for the friendly environment created in the bureau during the semester.

It is important to mention that this opportunity was possible thanks to the double degree agreement between my home University of Bologna (Italy) and my hosting University of Liège. I owe to both universities for having allowed me to participate to this agreement and for the great possibility they gave me. The period I spent abroad was an unforgettable experience of life that allowed me to shape my future. I had the occasion to face with new methods of studying and researching, moreover I had the chance to undertake an internship in a company and merge the learning involvement with the work experience.

Many times, I missed my home, my university in Bologna and my country, but I am glad to have applied for the double degree because I had the possibility to grow as student and as a future engineer. Already during the International Master in Bologna, I understood how much important the intercontinental aspects were. Therefore, attending in my country classes with people and students from all over the world, studying in English and learning technical vocabularies made me raise. All of these aspects are necessary in order to enlarge the horizons and collect more views. Thus, especially, this year abroad allowed me to grow both personally and scholastically speaking.

For their unconditional support and help, I will be forever grateful to my family, my parents *Grazia* and *Andrea*, my brother *Giacomo* and all of my grandparents. I want to extend my thanks to old and new friends from all over the world for their friendship and care. Each of them was able to provide me support and attention. The distance was not a problem for true and

genuine friendship. Last but not least, I want to mention the strong and constant encouragement of *Alessio*, despite the vast distance, he was always ready to give me positive energy and the willingness to achieve my objectives. The current academic year was thought for both of us, far from our "comfort-zone", far from each other, far from our country (specially you) and families, but we overcame this challenge very well.

Table of contents

List of Figures

List of Tables

1. Introduction

1.1 Introduction to shear behaviour

Generally, it is important to predict the type of failure of concrete members and provide an adequate safety margin against flexural failure and shear failure. The latest, properly called diagonal tension failure, can be more dangerous than flexural one due to its suddenly occurrence, therefore with no advance warning. Typically, this failure mode is brittle.
By providing shear reinforcement (stirrups), the flexural failure commonly occurs before the shear failure, thus the element fails in a ductile manner.
Two types of inclined cracking occur in concrete beams: web-shear cracking and flexure-shear cracking. The failure modes are illustrated in Figure 1.1.
Web-shear cracking begins from an interior point in the concrete element when the principal tensile stresses exceed the tensile strength of the concrete. When flexural cracking occurs, the shear stresses in the concrete above the crack are increased. The flexure-shear cracks develop when the combined shear and tensile stresses exceeds the tensile strength of concrete.
When inclined cracking occurs in a non-prestressed concrete member, it is generally flexure-shear type. Web-shear cracking typically occurs near the supports of deep flexural members with thin web reinforcement, or near the inflection point or bar cutoff points of continuous beams, particularly if the beam is subjected to axial tension. [6]

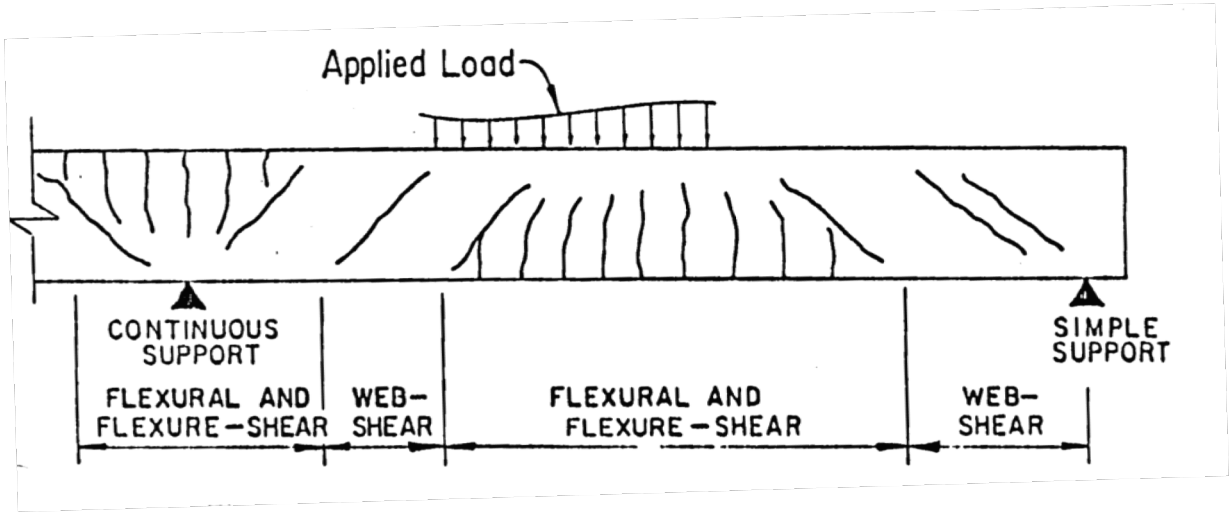

Figure 1.1: Types of cracking in concrete beams [6]

In order to determine the shear strength of concrete beams or shear resistance, two cases are possible for concrete elements: with or without shear reinforcement.
In the first case, so "if beams are equipped with shear reinforcement or stirrups, it is well known to predict the shear resistance of the web crushing with the truss analogy developed by *Ritter* and *Mörsch* that is based on the lower-bound theory of plasticity. The upper bound solution is used to minimize the strengthening effect of the stirrups". [18]

Secondly, "when there is no shear reinforcement, the shear transfer mechanism is the only thing responsible for forming the shear resistance. That is where Eurocode 2 lacks the support of an adequate theory and uses instead totally empirical procedures". [13]

The mechanisms assumed to be carrying shear force in cracked concrete to the supports when no shear reinforcement is provided for the member are:

- Concrete compression zone (V_C): Gradually inclined cracks widen in the concrete; the shear resistance decreases while the concrete and dowel action resistance increase. Finally, when the aggregate interlock reaches failure, large shear force transfers rapidly to the compression zone causing sudden and often explosive failure to the beam.
- Dowel action (V_d): This shear-load transfer mechanism occurs when cracks grow and cut across longitudinal reinforcements, providing an increase into the mechanical shear strength. Next, the crack lips transfer shear stresses to reinforcements. Consequently, a local bending and shear at reinforcements are observed. Shear resistance caused by dowel action can increase as the shear reinforcement decreases.
- Aggregate interlock (V_a): The aggregate interlock mechanism transfers a large part of the total shear force to the supports. Width of the cracks, aggregate size and concrete strength depend on aggregate interlock. When the longitudinal reinforcement ratio is increased with added bars to the beam, the width of the flexural cracks gets smaller due to increased shear resistance and consequently the contribution of V_a decreases.

Beam and Arch Mechanisms

If beams develop a flexure-shear interaction, the shear resistance consists of two different mechanisms, beam and arch mechanisms. The beam mechanism forms when the shear to effective span ratio *a/d* is above a transition point, shown in Figure 1.2, and the arch mechanism when it is below. Thus, the beam action relies on load transfer across the reinforcement-concrete interface. When the arch action begins to contribute more than beam action, the member can achieve considerably more load than at diagonal cracking. Therefore, arch action occurs in the uncracked concrete near the end of a beam, where load is carried from the compression zone to the support by a compressive strut. The vertical component of this strut transfers shear to the support, while the constant horizontal component is reacted by the tensile flexural reinforcement.
To predict failure mode of the member, *Russo* et al. [20] concluded that when arch action governs, shear-compression (SC) failure should be expected and if beam action governs, diagonal-tension (DT) should be expected.
The flexure-shear combined action is when bending moment and shear force act together in a cross section: $\frac{a}{d} = \frac{M}{Vd}$.

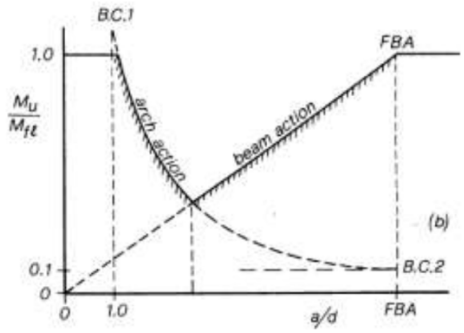

Figure 1.2: Model for flexure-shear interaction [20]

1.2 Failure modes

In this thesis work, footings without shear reinforcement will be studied, therefore in this paragraph the various failure modes without stirrups are described.

1.2.1 Shear Failure

Many types of structural concrete members have been reported to fail due to shear distress or diagonal failure. A combination of shearing force and moment is the fundamental cause of diagonal failure. [17]

Diagonal Tension Failure

The diagonal crack initiates from the last flexural crack formed. The failure occurs in beams when the shear to effective span ratio *a/d* is from 2.5 to 6.0. The crack propagates through the beam until it reaches the compression zone. When the beam reaches a critical point, it will fail as a result of splitting of the compression concrete, beam action is not likely to occur because it is not possible to transfer the load between the compression concrete zone and flexural reinforcement across the crack. Generally, the failure occurs without waring and the typical mode is brittle.

Figure 1.3: Diagonal tension failure of beams [27]

Shear Tension Failure

This type of failure is similar to diagonal tension failure but applies to short beams. The shear crack propagates through the beam, but without causing the failure of the beam on its own. Secondary cracks travel along the longitudinal reinforcement from the last flexural crack and can cause a loss of bond between the reinforcement and the concrete or anchorage failure.

Figure 1.4: Shear tension failure of beams [27]

Shear Compression Failure

If the diagonal shear crack propagates through the beam, causing failure when it reaches the compression zone without any sign of secondary cracks (contrarily to shear tension failure) it is referred to shear compression failure. This failure mode applies to short beams.

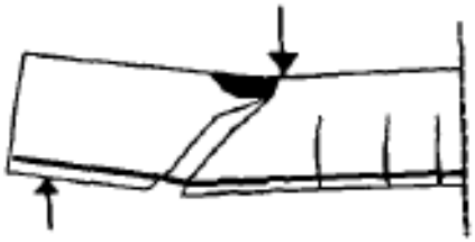

Figure 1.5: Shear compression failure for beams [27]

1.2.2 Flexural Failure

Flexural cracks are mostly moment dependent and typical of long beams. The cracks develop in proximity of the maximum moment. When the shear stress in the concrete reaches its tensile strength, cracks develop.
The cracks are almost vertical and cause failure to the beam due to either of these two cases [17]:

- Under-reinforced beams: the longitudinal reinforcement yields excessively resulting in failure in the concrete compression zone;
- Over-reinforced beams: concrete in the compression zone fails above the flexural crack before the longitudinal reinforcement yields.

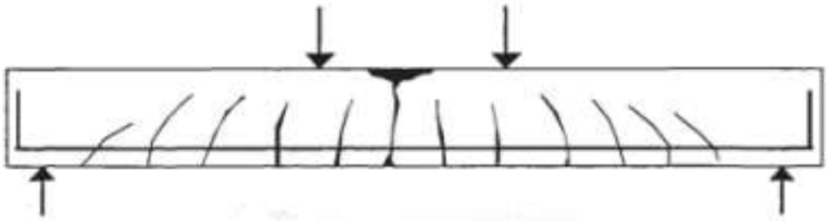

Figure 1.6: Flexural failure for beams [27]

1.3 Reinforced concrete deep footings

The previous section was a general overview of typical beam's failure modes (without shear reinforcement). For this thesis work, the main objective is the extension to concrete compact footings of the observations made for beams and deformation patterns predictions. Therefore, an introduction to this kind of elements is necessary. Reinforced concrete footings are designed in order to transfer the load of the superstructure and its weight to the soil. In order to achieve this purpose, the footings are commonly subjected to flexure and shear. Generally, this kind of foundation is designed without shear reinforcement (stirrups); therefore, the concrete footings are predisposed to brittle failure according to the amount of diagonal cracking due to excessive local shear stresses.

The shear failure can be localized around the column of the footing or around a plane across the footing width. The first failure mode is connected to two-ways shear failure (punching shear); while the second to one-way shear failure (beam action shear). For this thesis will be analyzed the one-way shear failure for compact reinforced concrete footings, considering a strip of the member.

Due to the absence of shear reinforcement, the resistance of the footing is often governed by the concrete contribution to shear strength (V_C). The specified critical section for beam action shear is located in a plane across the entire width of the footing.

Generally, for codes, such as for ACI shear previsions, the size effect is neglected, and it is considered that the failure shear stress for slender members without shear reinforcement decreases as the thickness of the structural member increases. *Richart* noted that "the factor of safety of thin footings appears greater than in thick footings." [2]

The ratio of shear length L_0 to the effective depth d is typically not very large, when it is low, an alternate force-resisting mechanism consisting of diagonal struts and tension ties can create, and this may provide adequate shear resistance even for very thick footings.

The applied shear is mostly transmitted to the sub-soil by diagonal compressive struts, in Figure 1.7 it is possible to observe the typical diagonal cracks on a reinforced concrete footing

subjected to shear force and supported by soil. Generally, the ratio of shear length L_0 to the effective depth d for compact footings is less than 2.

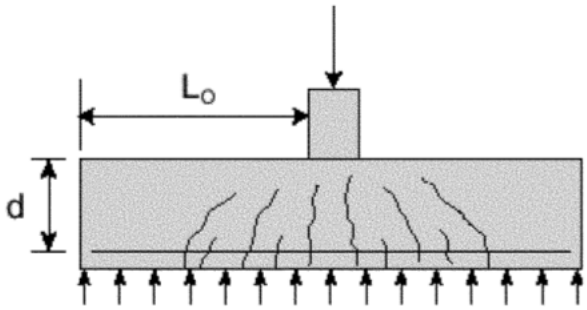

Figure 1.7: Diagonal cracks as a consequence of the diagonal compressive struts flow on a footing subjected to shear and supported by soil [11]

It is necessary to specify that for typical design purposes, the soil pressure is considered as uniformly distributed below the footing. In reality, the soil pressure is not uniform, therefore this is a simplifying assumption. Typically, the distribution of contact pressure depends principally on the stiffness of building foundation, the stiffness or compressibility of soil and the loading condition. If the foundation soil is a non-cohesive material (i.e. sand), the soil pressure is maximum at the mid span of the footing and minimum at the ends; while, if the soil foundation is composed of cohesive materials (i.e. clays), the pressure will be maximum at the extremities and minimum in correspondence of the geometrical mid span section. The concrete footing is compact; thus, it is considered as a rigid element and in Figure 1.8 it is possible to observe the real pressure if the soil material is sand (on the left) and it if is clay (on the right). This last situation is the most unfavorable one, due to the fact that it will produce a more critical stress distributions for shear design. The hypothesis done does not respect the reality, but, in practice, the contact pressure is assumed to be uniform in order to have also a general approach for all types of soils.

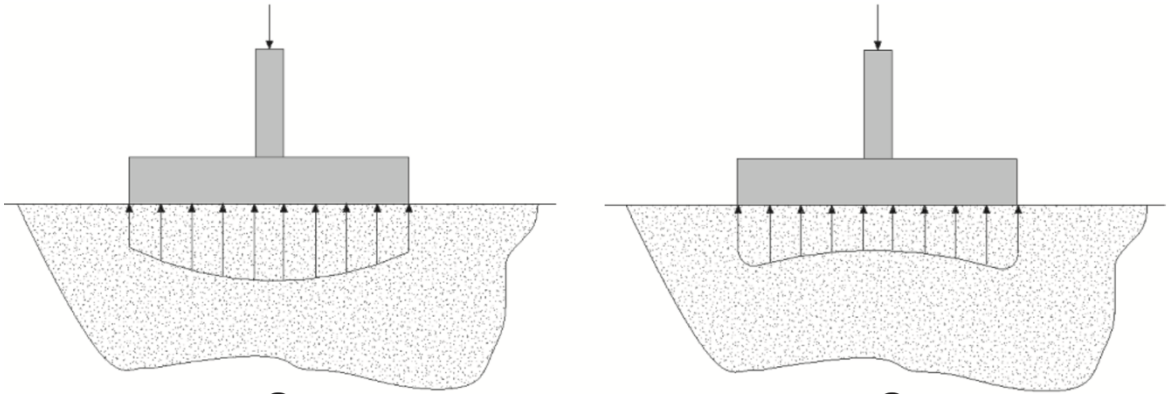

Figure 1.8: Distribution of the soil pressure under the footings (MacGregor and Wight [1])

Experimental and analytical data regarding shear behavior of reinforced concrete large footings are provided by *Uzel* (2003). The test specimens were designed to represent a strip of footing

member. Since the shear resisting mechanism of footings is a result of the beneficial loading and support conditions, special attention was given to the loading set-up. The test specimens were subjected to concentrated loads and uniformly distributed loads, which simulated column loads and soil pressure, respectively. [3]

1.4 Objectives of the research

The objectives of this master thesis work are:

- The extension of a Two-Parameter Kinematic Theory (2PKT) for shear behavior in deep beams, developed by *Mihaylov* (2013), to concrete compact deep footings. Specifically, the first step is the study of the theory for deep beams, consequently the development of the theory for large compact concrete footings with the necessary modifications and assumptions.
- The validation of the extended 2PKT for footings against experimental tests. Precisely, the starting point are large-scale samples provided by *Uzel*.
- The development of a larger footing database in order to validate the new model. Due to lack of tests in the literature review, Finite Element Models are validated against experimental tests. Thus, a parametric study is performed including validated models from the Finite Element Analysis by varying one parameter per time and conducting three analysis with two different *Uzel*'s tests as model.

1.5 Outline of the thesis

Below it is possible to read the plan and the skeleton of the following thesis work.

Chapter 1: Brief introduction of the studied topic and presentation of the developed work.

Chapter 2: Explanation of the failure modes for concrete footings and research for suitable tests in order to create a database of samples. Detailed description of *Uzel*'s (2003) tests, the procedure, the results and observations. They are the starting point to validate a Two-Parameter Kinematic Theory (2PKT).

Chapter 3: The presentation of the used modelling approaches and the theory behind the adopted software (VecTor2) to model the tests and create reliable samples to extend the 2PKT. The procedure of modelling is explained. Presentation of the 2PKT for beams and other approaches commonly used by codes.

Chapter 4: The 2PKT is extended to footings by means of some assumptions and modifications. The theory is developed, and the main hypothesis are presented in this part.

Chapter 5: Finite Element Models using VecTor2 are created for *Uzel*'s tests in order to obtain a reliable reproduction of real tests. The 2PKT strength predictions are compared with real test data in the literature. Before the validation of the theory applied to deep footings, a parametric study is developed using as starting point FEM validated against real laboratory test data. A MatLab code is developed in order to compute and to visually compare the theory's predicted displacements with the test results. Finally, the theory is validated after the discussion of the results and comparison between the experimental data and the predicted ones.

Chapter 6: The conclusions are presented and some suggestions for future steps are offered.

Appendix 1: The database of footings with their main parameters and data is presented.

Appendix 2: In this part some 2PKT calculations are shown, especially the last iterative step and the final results.

Appendix 3: Development of most significative FEM results from the parametric study.

Appendix 4: Comparison of actual load-displacement curves for *Uzel*'s tests with the 2PKT provisions.

2. Test of footings

2.1 Introduction

In order to properly transmit loads from the super structure (building or bridge, see also Figure 2.1) to the soil layers, concrete footings are designed. During the transferring of forces, the concrete element is subjected to flexure and shear. Generally, it is quite common to project the footing without shear reinforcement, so that it is inclined to brittle failure due to excessive local shear stresses.
The shear failure can be localized around the column of the footing, this mode is connected to two-ways shear failure (punching shear); or around a plane across the footing width while the second to one-way shear failure (beam action shear). For this thesis research the one-way shear failure for deep reinforced concrete footings will be analyzed and, in order to achieve this purpose, the footing is considered as a reinforced concrete beam, thus without representing the footing column, but just the loads coming from the superstructure.

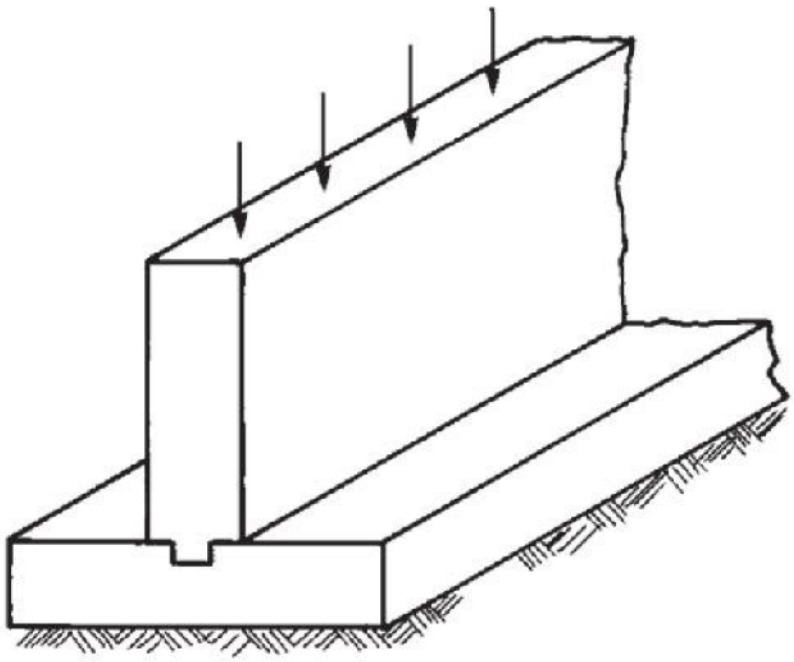

Figure 2.1: Example of compact footing for linear wall [Mihaylov]

2.2 Failure modes of footings

The foundation is the part of the structure that transfers the loads to the supporting soil in such a way that the resulting bearing pressures are kept under acceptable limits.
The first failure mode for concrete footing is when it may fail in shear as a wide beam along a critical section at a distance *d* from the column face in each direction. This is called “beam shear” or “one-way shear” as it resembles the shear crack in a concrete beam. This failure mode is shown in Figure 2.2. Generally, to avoid one-way shear failure of foundations, the shear

stress at the critical section of footing should be less than the shear strength of concrete with given percentage of reinforcement used.
The second failure mode considers that the column may penetrate, or punch, the footing. Therefore, it is called “punching shear” or “two-way shear” and occurs not along a straight plane, but along a 3D plane at a distance *d/2* all around the column (where *d* in both failure modes is the effective depth and it is represented in Figure 2.2 and Figure 2.3).
Normally, codes and standards include the two checks in the calculation of the concrete shear strength, the computation of the shear acting at the critical plane described above, and then the comparison of both. Usually the shear strength is provided by the concrete only, otherwise a special and expensive shear reinforcement would be necessary. The punching shear failure, also known as diagonal tension failure of foundation, produces the formation of inclined cracks around the perimeter of the column. In order to avoid punching shear failure, the ultimate upward shear force at this section in the foundation should be less than the shear resistance of concrete for the given percentage of concrete. The failure of foundation in this mode materializes as truncated cone or pyramid around the column (Figure 2.3).
The last possible failure mode for footings is the flexure failure: during the design, M_u/bd^2 is calculated to get the amount of reinforcement needed to resist to the bending moment the foundation is exposed to. Where M_u is the ultimate (already increased or factored moment) and *b* is the width of footing. The critical section for flexure is considered at distance *d* from the face of footing. The standard codes take care of flexure failure during design by providing percentage of reinforcement required to resist the bending moment. When bending moment increases, the footing fails as shown in Figure 2.4.

As previously mentioned, for this thesis research the one-way shear failure is considered.

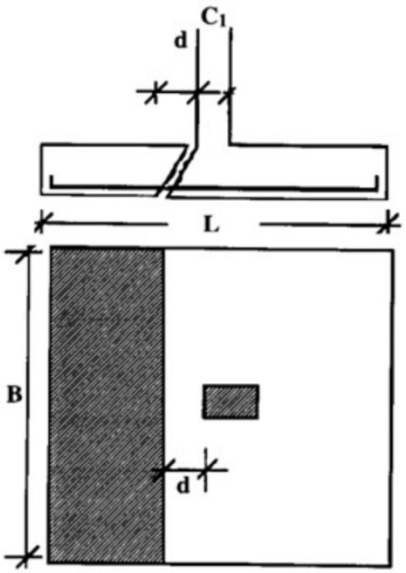

Figure 2.2: One-way shear failure [11]

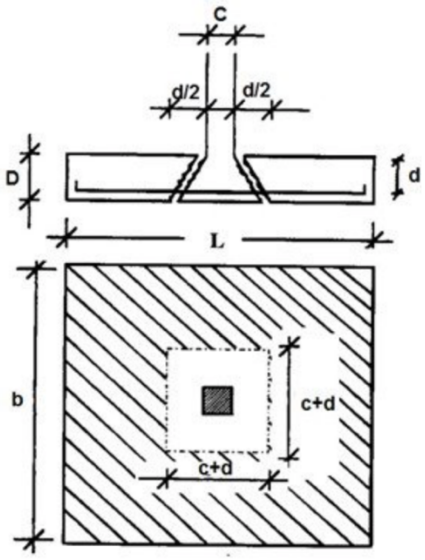

Figure 2.3: Two-ways shear failure [11]

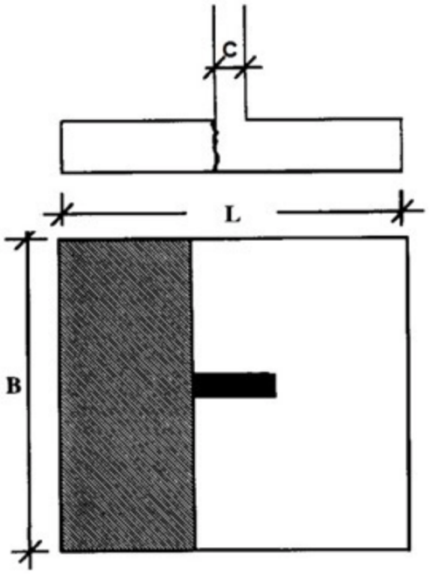

Figure 2.4: Flexural failure [11]

2.3 Tests in the literature

A number of experimental tests focusing on the shear behavior and strength of footings have been performed so far, the first works were carried out in the United States of America in 1948 by *Richart*, who presented two papers on experimental investigations, the tests follow the *ACI Building Code* of that period (1947). The point load on the top, which represents the loads coming from the column, was applied by a testing machine; on the bottom the specimens were sustained by a bed of spaced car springs in order to make the reaction of the soil uniform, even if, as specified in the introduction (in *Chapter 1*), it is actually not uniformly distributed, but it depends on the soil material. The resistance of the concrete footings, the failure modes, the

bond between steel and concrete, the diagonal tension and the tension in the steel were examined. For the following section, the database creation, it is important to say that the specimen of series 5 from 501 to 506 (a and b) perfectly match with the objective of the thesis. The considered last footings present three types of observed failure modes:

a) Punching failure;
b) Failure by inclined crack developed across the whole width of the member (as in beams);
c) Combination of the previous failure modes.

It is necessary to mention that all the tests performed by *Richart* had effective depth smaller than 400 mm. Generally, in practice works, the used value for real constructions is bigger than 400 mm, therefore, the size effect is not always considered. Commonly, it is possible to take into account the size effect when the effective depth is greater than 300 mm. The presented and considered tests are, consequently, handled with caution and always remembering that not always they are suitable with the input parameters used for the analysis of the shear behavior as objective of the research.

Recently, various interesting experimental findings have been produced with lightly reinforced large compact members without shear reinforcement (*Kani* (1967), *Collins* and *Kuchma* (1999)). The evidence from that tests is that for lightly reinforced slender members without stirrups, the failure shear stress decreases as the length increases. The shear capacity of footings is enhanced by the transverse clamping stresses that are introduced to these members by the loading support conditions.
The tests performed by *Uzel* (2003) for her PhD thesis fit into this context and the objective was the observation of the actual shear behavior. She performed experimental research regarding small-scale test, medium-scale tests and large-scale tests. The tests considered for this thesis work are an example of full-scale tests on compact reinforced concrete footing without shear reinforcement. As *Uzel* stated, the literature reveals that there is a lack of tests where the support introduces tension to a member subjected to uniformly distributed loads, thus the purpose of the experimental research is also the study of shear behavior of large footings where the support force introduces tension to the member. [3]
Concluding, the literature review shows few available experiments data for the one-way shear in large concrete footings and limited researches development regarding this topic.

2.4 Large-scale test specimens

For the objective of this research the large-scale test specimen (called AF) by Professor *Uzel* are used, in addition the test AF1 UN100 by *Bogdan Podgorniak-Stanik* was chosen as reference test for the creation of successive FEM analysis and parametric study.
All the full-scale tests were loaded by a set of hydraulic jacks which simulates the uniformly distributed loads from the soil. The tests were designed to represent a strip of a footing member subjected to point load and uniformly distributed loads. They contained only longitudinal

reinforcement and were casted from normal density concrete. Concrete strength for most of the specimens was around 30 MPa, which is widely used for footings in practice. [3]
Regarding the longitudinal reinforcement, the ratio of steel reinforcement varies and generally the diameter of the bar was 30 mm.
In Figure 2.5 it is possible to observe all the large-scale tests designed for the experimental program, the specimens were created to detect the behavior of the members under different load conditions, geometry and configurations. The elements underlined in red are the ones considered for the following extension of a Two-Parametric Kinematic Theory for footings because they satisfy the assumption of deep compact footing subjected to one-point load along the symmetry axis of the member and uniformly distributed loads on the bottom. The selection procedure will be explained in the subsequent sections. Note that AF6 apparently does not satisfy the previously mentioned assumption because of the two vertical loads, instead of one applied along the symmetry axis, but by making some considerations and studying just the ends of the footings the test can produce remarkable results for the following analysis.

Name	Loading	Length L (m)	Depth h (m)	Width b (mm)	Effective Depth d (mm)	Longitudinal Reinforcement		L_o (mm)	L_o /d
						Top	Bottom		
AF1 (UN100)	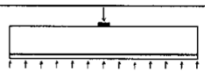	6	1	300	925	-	3-No.30 ρ=0.76 %	2925	3.16
AF2	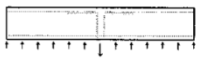	6	1	300	925	3-No.20	3-No.30 ρ=0.76 %	2925	3.16
AF3	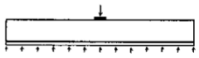	6	0.670	300	617	-	2-No.30 ρ=0.76 %	2925	4.74
AF4	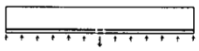	6	0.670	300	617	2-No.20	2-No.30 ρ=0.76 %	2925	4.74
AF5	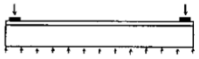	6	0.670	300	617	2-No.30 ρ=0.76 %	-	2800	4.54
AF6	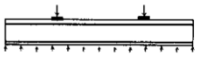	6	0.670	300	617	2-No.30 ρ=0.76 %	2-No.30 ρ=0.76 %	1815	2.94
AF7		6	1	300	925	-	3-No.30 ρ=0.76 %	2925	3.16
AF8		6	1	300	925	-	3-No.30 ρ=0.76 %	1925	2.08
AF9	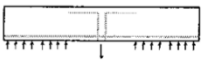	6	1	300	925	-	3-No.30 ρ=0.76 %	2925	3.16
AF10	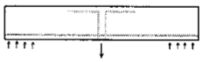	6	1	300	925	-	3-No.30 ρ=0.76 %	2925	3.16
AF11	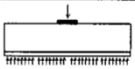	4	1	300	925	-	3-No.30 ρ=0.76 %	1850	2
AF12	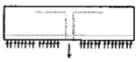	4	1	300	925	-	3-No.30 ρ=0.76 %	1925	2.08
AF13	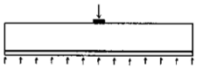	6	1	300	865	-	8-No.30 ρ=2.16 %	2925	3.38

Figure 2.5: Large-scale test specimens (Adapted from Uzel, 2003 [3])

All the considered specimens have a longitudinal reinforcement ratio equal to 0.76%, except AF13, which has 2.16%. They have all a length L of 6 m, except AF11, which has L = 4 m. From Figure 2.6 to Figure 2.10 all the considered specimens are shown in details.

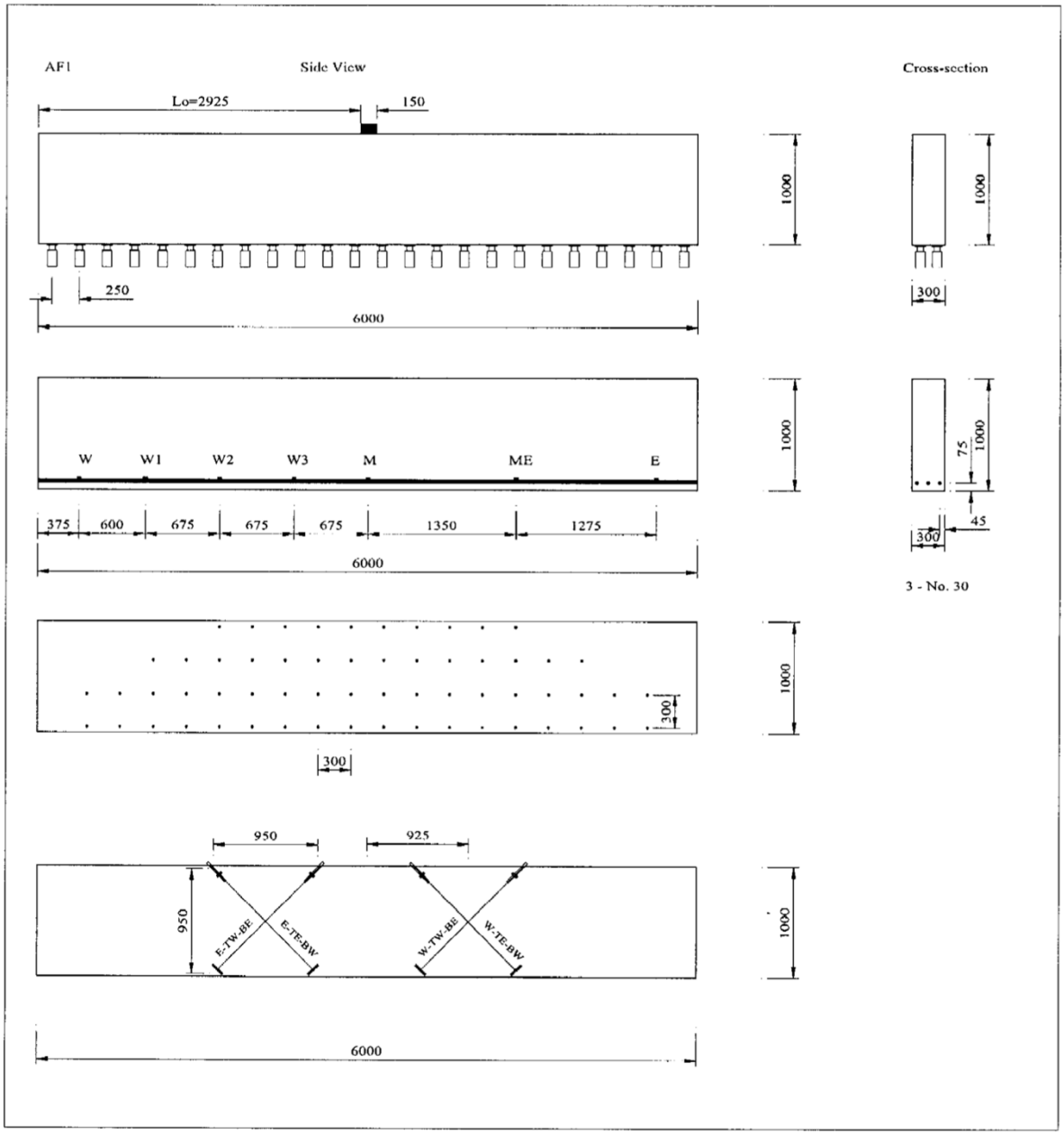

Figure 2.6: Specimen AF1 UN100 (Uzel, 2003 [3])

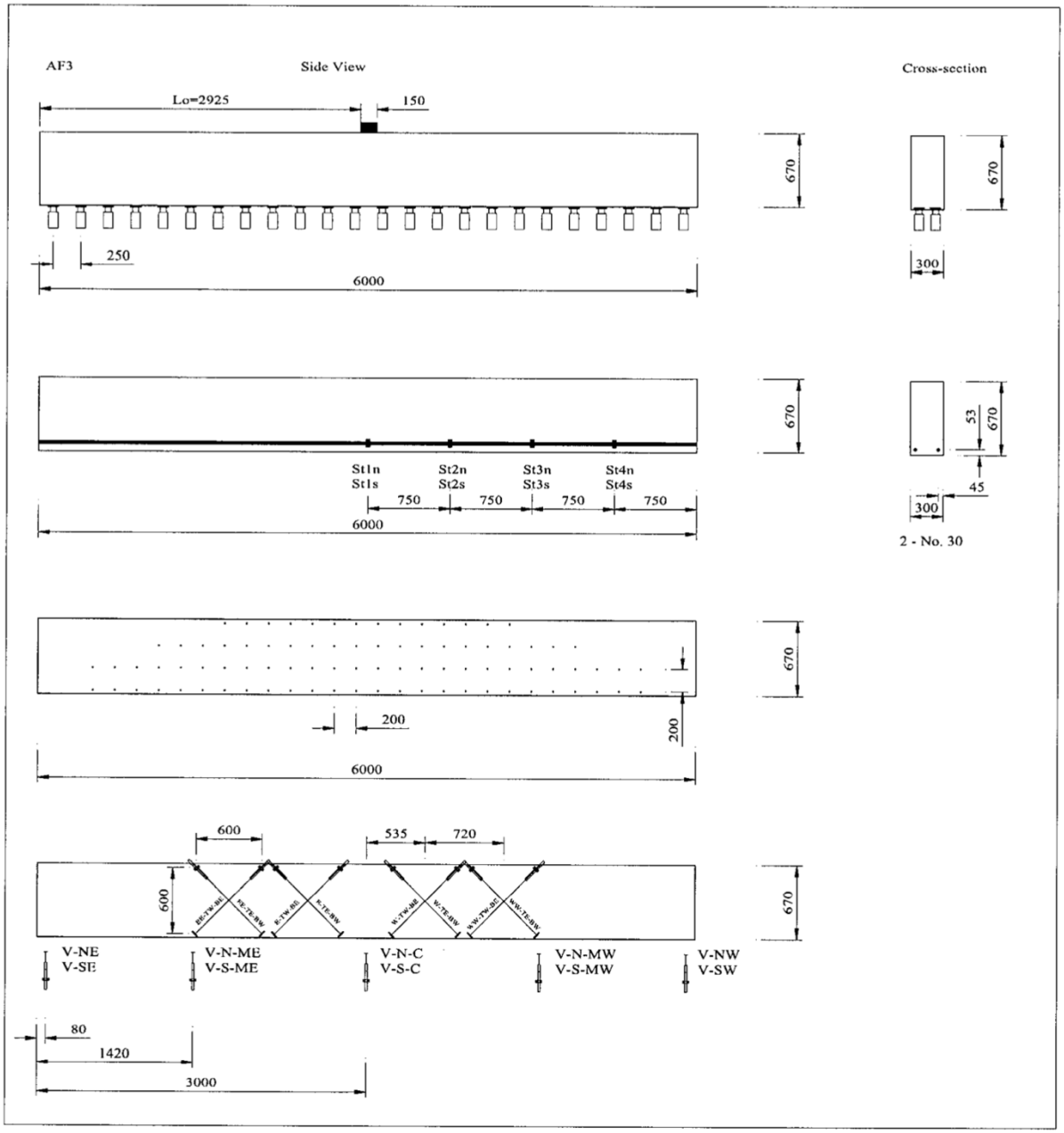

Figure 2.7: Specimen AF3 (Uzel, 2003 [3])

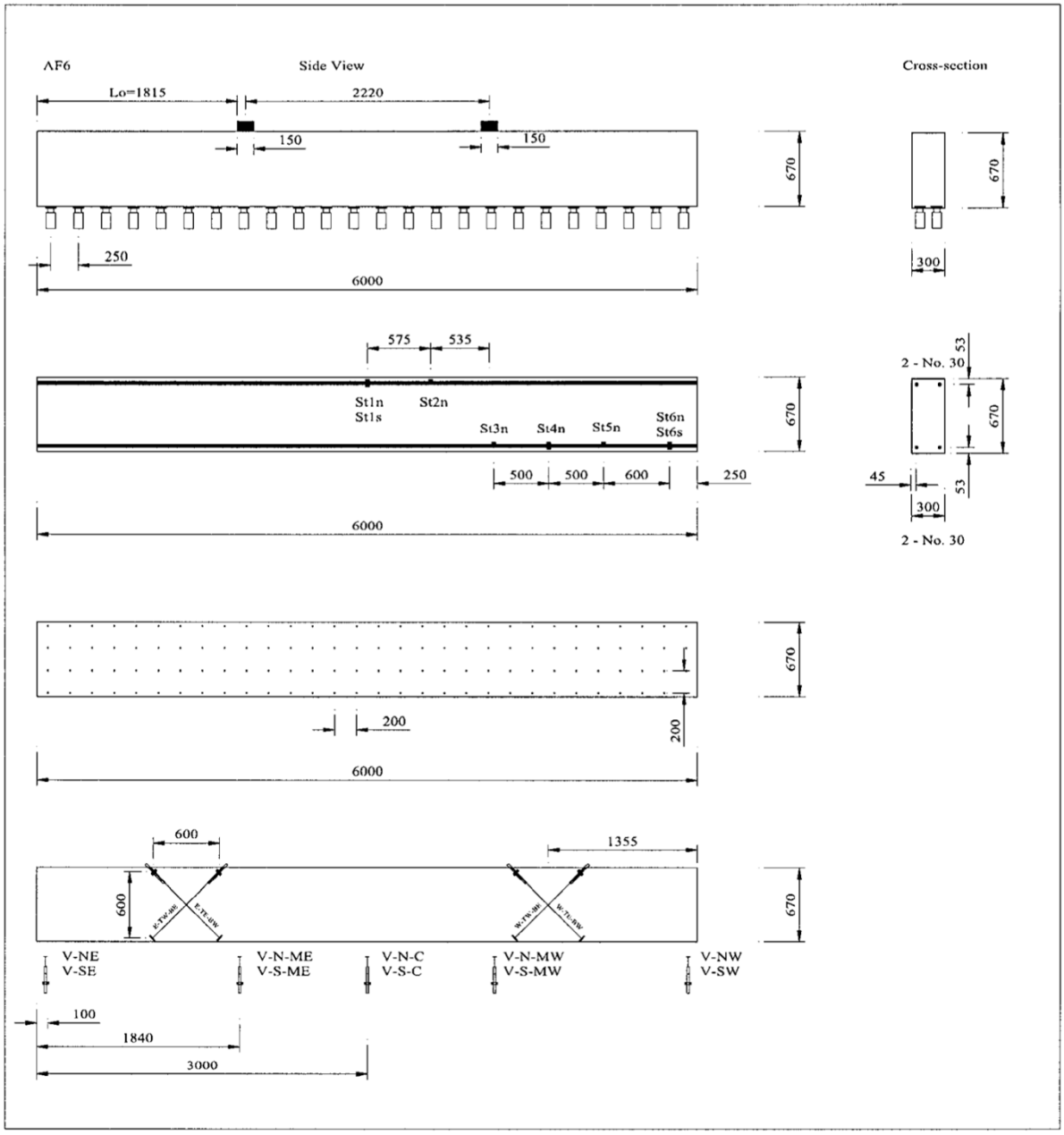

Figure 2.8: Specimen AF6 (Uzel, 2003 [3])

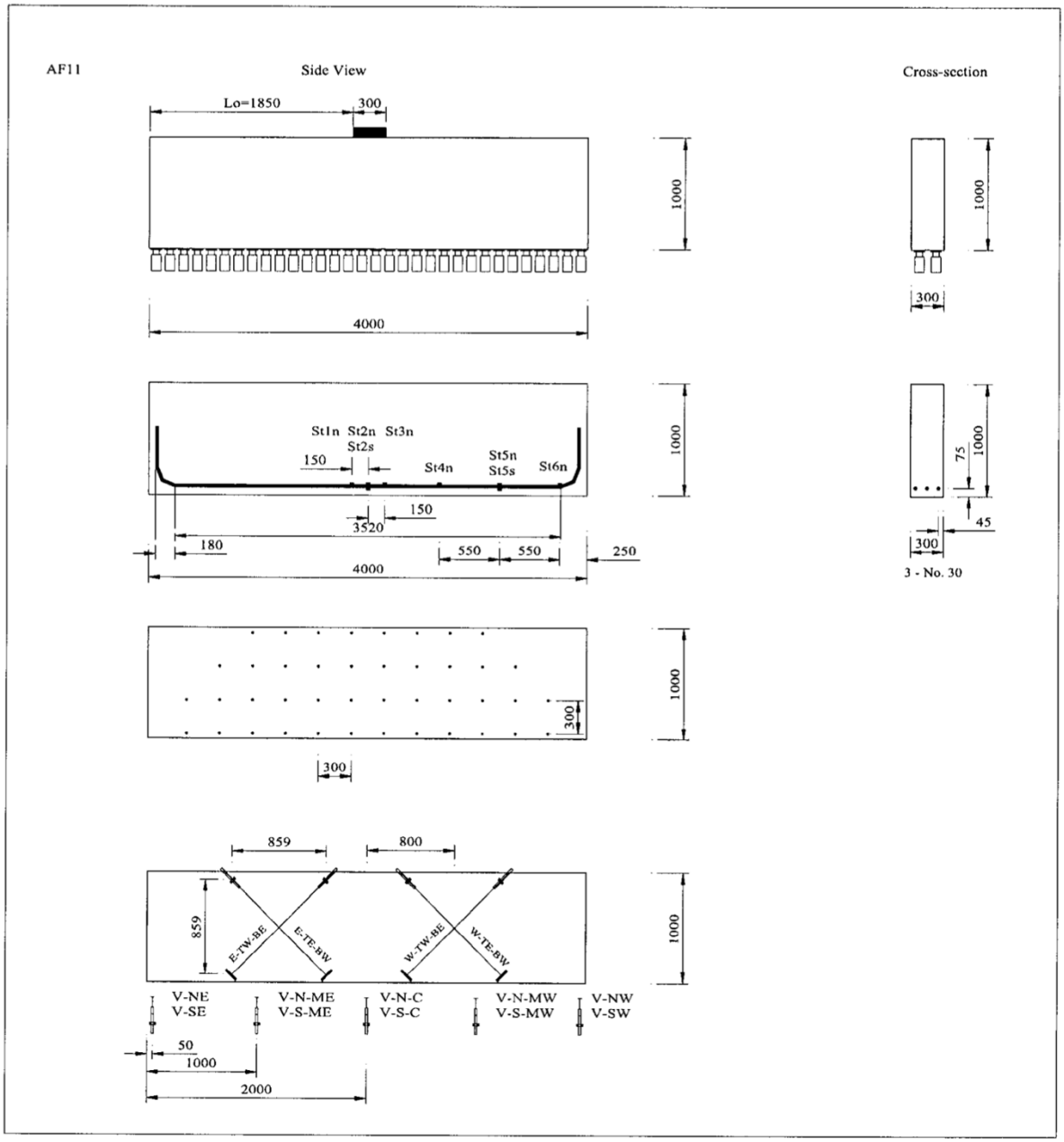

Figure 2.9: Specimen AF11 (Uzel, 2003 [3])

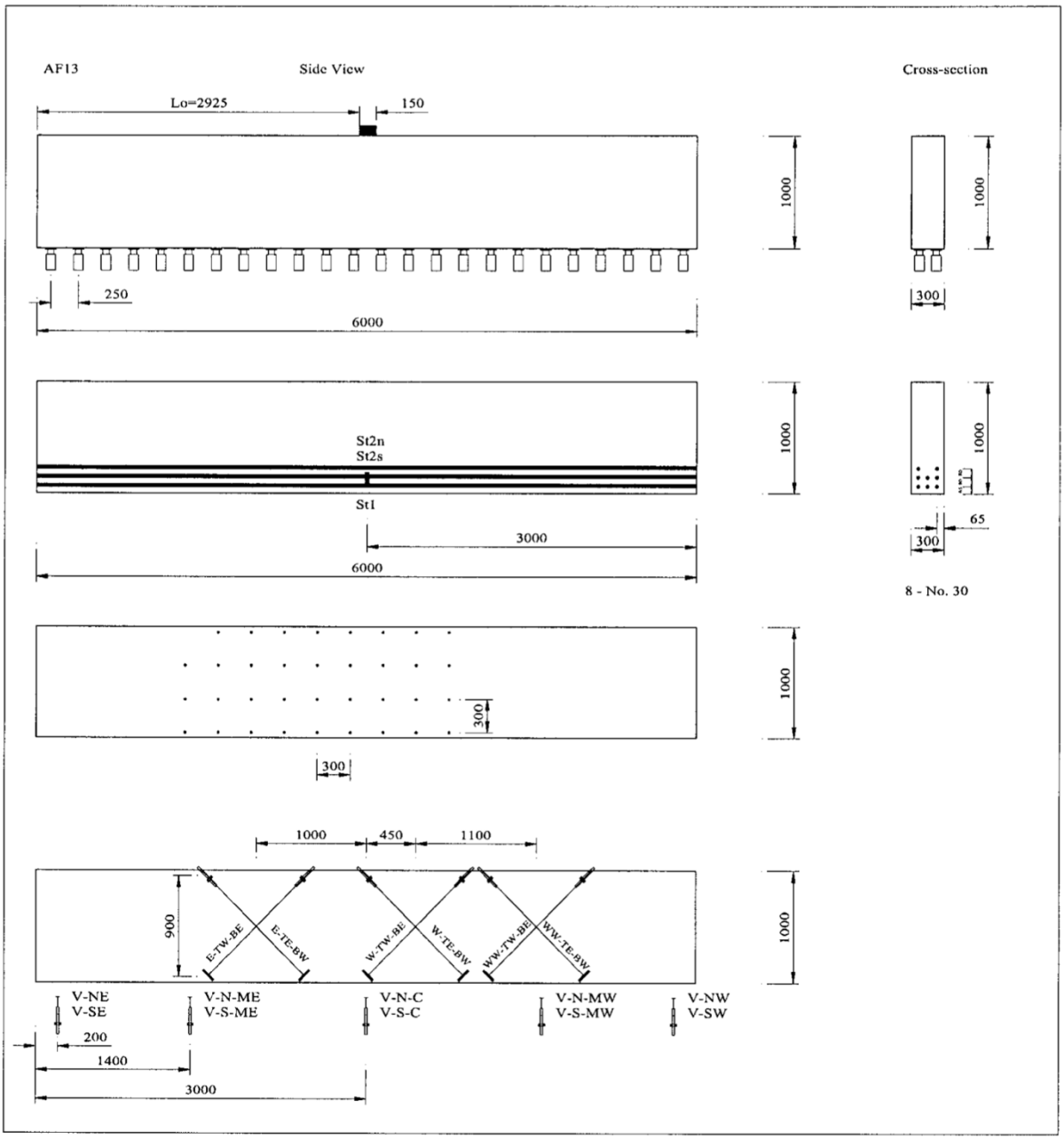

Figure 2.10: Specimen AF13 (Uzel, 2003 [3])

The specimen AF1, AF3 and AF6 were subjected to C-type loading (defined deeply in 2.4.1 Test set-up and loading procedure) in which the sample is pushed up towards the supports by hydraulic jacks spaced at 250 mm. The specimen AF11 was tested in the same way except for the fact that the hydraulic jacks are spaced of 125 mm.

The elongation of the longitudinal reinforcement was measured by strain gauges placed along the steel bars itself in many locations determined according to the loading conditions and support places. In order to measure the shear deformations, sets of two LVDT (Linear Variable Differential Transformer Transducers) transducers, placed diagonally on the face of the specimen, were used and mounted at the anticipated crack locations.

Furthermore, Zurich targets were glued on the face of the specimen in order to create a grid of measurements points for the surface strains.

2.4.1 Test set-up and loading procedure

Generally, footings are subjected to column loadings and the selected specimens from the experimental results of *Uzel*, described before, are all tested as Compression-type loaded (C-type loading). The specimens were subjected to uniform loading by hydraulic jacks equally spaced along the bottom part of the member and, thanks to the Baldwin testing machine, the footings were restrained in order to avoid vertical displacements and reproduce the column load. The total applied load was directly read from the load cell of the Baldwin testing machine. The jacks were positioned on steel plates and steel bearing plates were positioned between the jack ram and the specimen (detail B in Figure 2.11). A layer of Teflon was placed in order to remove the friction force.
By following the scheme of C-type loading, the specimens were pushed by hydraulic jacks until they were no longer sit from the support frames. Once the specimens started to float on the jacks, the supports were lowered, and the Baldwin testing machine was locked against vertical movement. [3]
For each specimen observations, data and results were collected from the transducers continuously during the loading phases; then the load-deflection diagrams (total applied load versus the characteristic displacement) were provided and the failure loads were measured. All the notes assembled during the different load stages are important and necessary (i.e. the formation of new diagonal cracks and widening of previous cracks) in order to make hypothesis regarding the failure mode, then to confirm by analytical methods. The load stages were determined by observing the diagonal cracks formation, generally the first load stage corresponded to the first sign of flexural cracking. The load increment between the load stages was lowered around the predicted failure load. At each new load stage, the new formed cracks were marked on the specimen and their width compared with measurement gauges. Finally, also the distance between the cracks and the Zurich targets were measured in order to have information about the surface deformations. The vertical, the lateral and the diagonal strains were computed by the changing of distance between the vertically, horizontally and diagonally placed target, respectively.
It is necessary to mention the constitutive laws used for materials (shown in Figure 3.8 and Figure 3.9) and to underline that the concrete strength value is the strength of the test day.

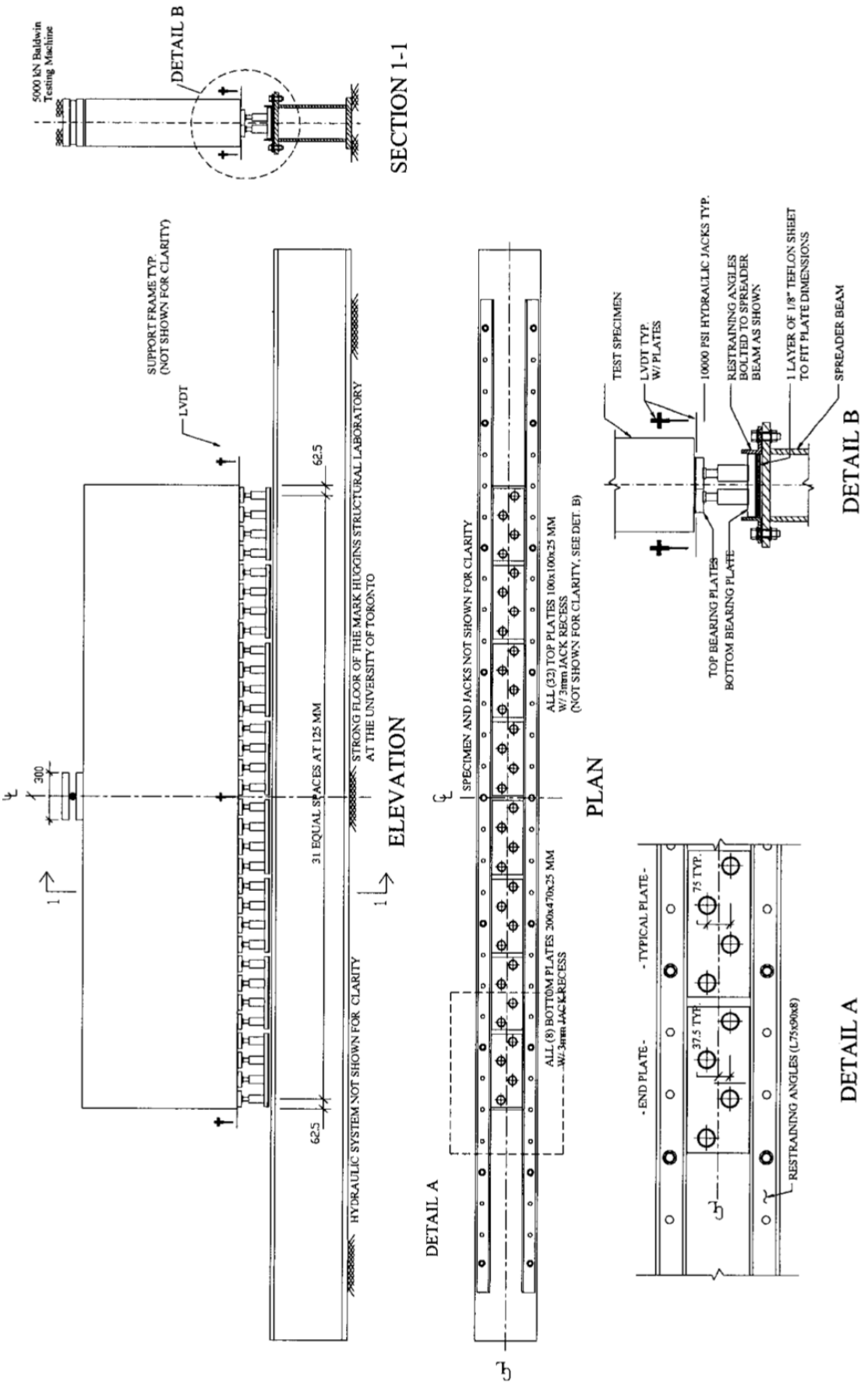

Figure 2.11: C-type loading set-up for specimen AF11 (Uzel, 2003 [3])

2.4.2 Deflection

The vertical deflection of the specimen, measured by using 10 LVDT (Linear Variable Differential Transformer Transducers) transducers mounted in five different positions, is calculated based on the readings taken from three different locations in which two transducers were located. The vertical displacement at each location is the mean value between the values given by the north and the south transducers. Finally, the deflection of the considered specimen is computed according to the support and load configuration.

2.4.3 Shear deformations

The shear deformation, measured by using LVDT transducers placed diagonally on the face of the specimen, is calculated as the difference between the measured elongation (D1) and shortening (D2) along the diagonal of the panel divided by the initial diagonal length:

$$\gamma = \frac{D1 - D2}{\sqrt{L_x^2 + L_y^2}}$$

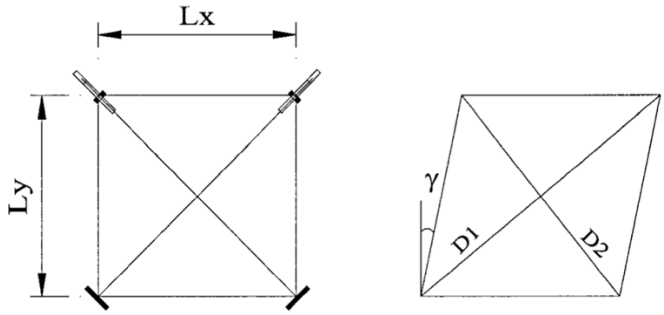

Figure 2.12: Shear deformation (Uzel, 2003 [3])

2.4.4 Zurich Targets

As it is possible to observe in the third part of Figure 2.6, Figure 2.7, Figure 2.8, Figure 2.9 and Figure 2.10 and as previously mentioned, additional Zurich Targets were glued on one face of the samples forming a grid of points in which the surface strain was measured. The initial readings, during load stage zero, were taken from the measurement equipment and Zurich Targets. A special gauge was used to record the spacing between the Zurich Targets. Then, the first load was generally taken where the first signs of flexural cracking were observed. The following load stages were taken at loads when new cracks formed or when previously formed crack widened or their length increased. The load increment between the load stages was lowered toward the estimated failure load of each sample. During the loading phases, the data were collected using the previously mentioned LVDT transducers and strain gauges. After the

reaching of each load stage, the peak load at that particular stage was decreased of 10% in order to stabilize the sample. At the end of each load stage the data were collected, and the new cracks formed were marked on the face of the specimen, photographs and recordings were also taken. The vertical, horizontal and diagonal distances between the Zurich Targets were measured by the specific gauges.
Surface deformations were measured by means of gauges on the created grid of Zurich Targets. The vertical and the lateral strains were then calculated based on the change in distance between vertically and horizontally placed targets. The diagonal strains were computed in the change of diagonal distance between the targets.
The strain measurements of the last load stage for the considered specimens are shown below. The specimen AF1 UN100 is not represented because it was not performed by *Uzel* (2003).

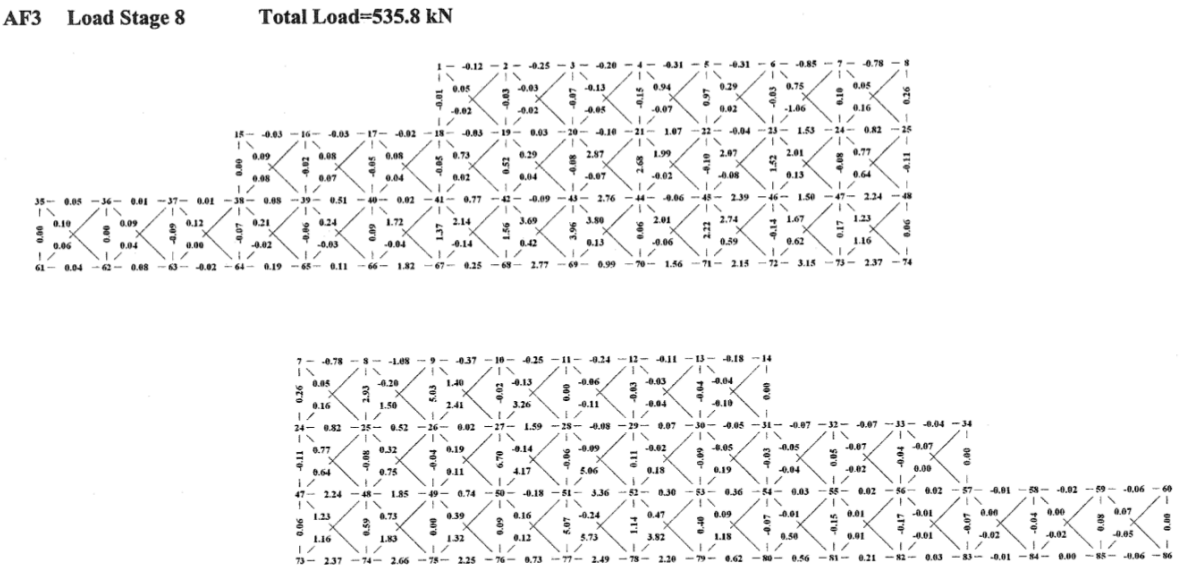

Figure 2.13: Shear strain measured at the Zurich Targets for the last load stage for sample AF3 [3]

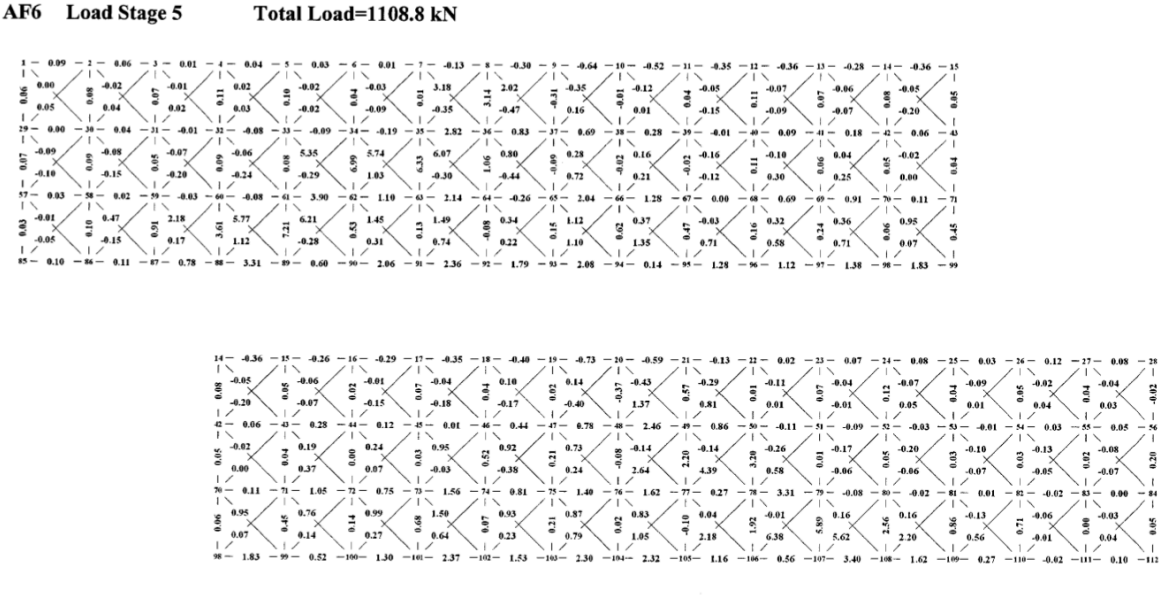

Figure 2.14: Shear strain measured at the Zurich Targets for the last load stage for sample AF6 [3]

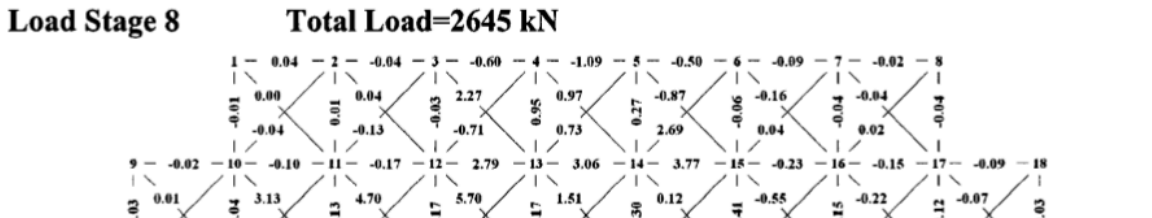

Figure 2.15: Shear strain measured at the Zurich Targets for the last load stage for sample AF11 [3]

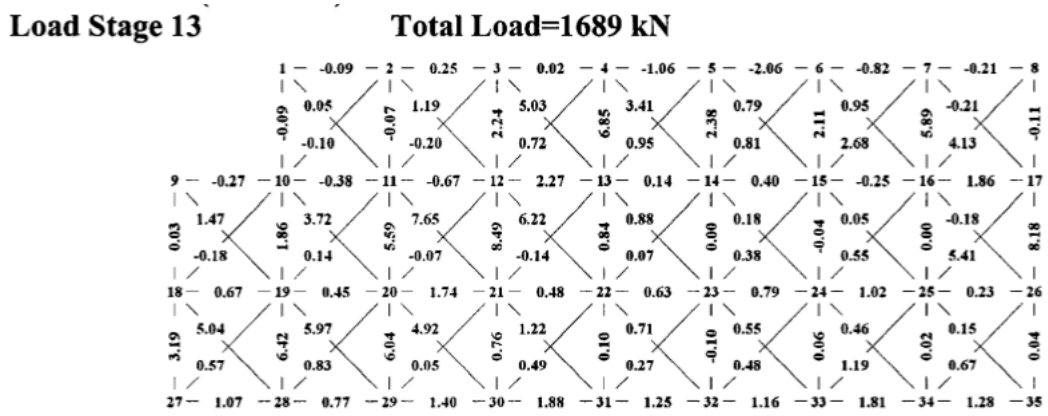

Figure 2.16: Shear strain measured at the Zurich Targets for the last load stage for sample AF13 [3]

2.4.5 Crack diagrams at failure

At each load stage, cracks were marked directly on both sides of the samples. Their widths were measured by means of a comparator gauge at a consistent location for all the load stages and also marked on the specimens [3].
The crack pattern for the last load stage of the considered samples are shown below by means of photos and plots.

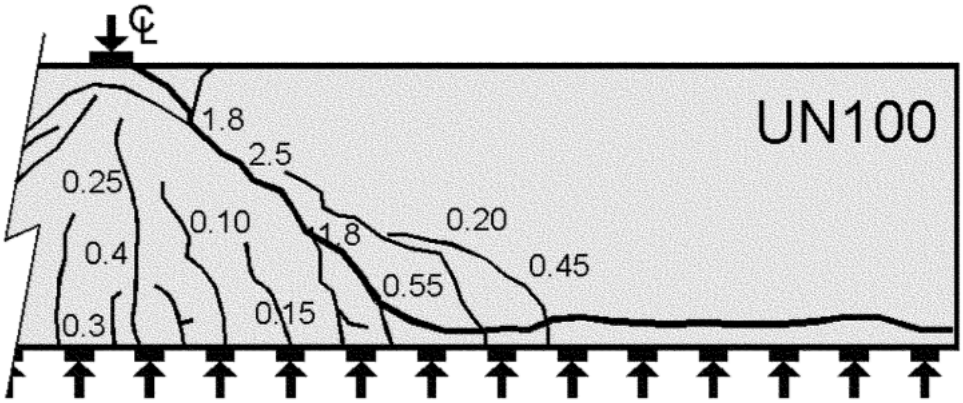

Figure 2.17: Crack diagram at failure for sample AF1 [10]

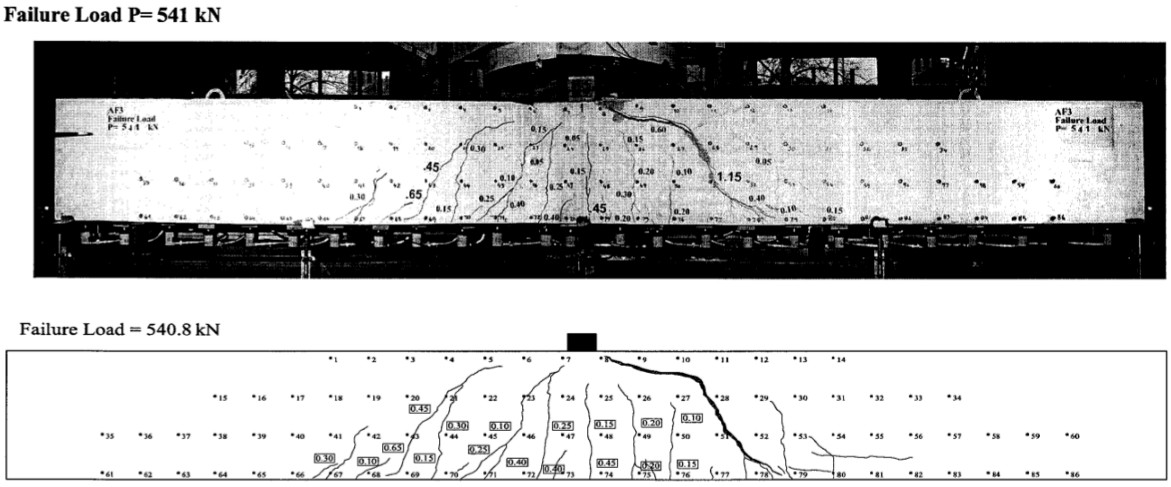

Figure 2.18: Crack diagram at failure for sample AF3 [3]

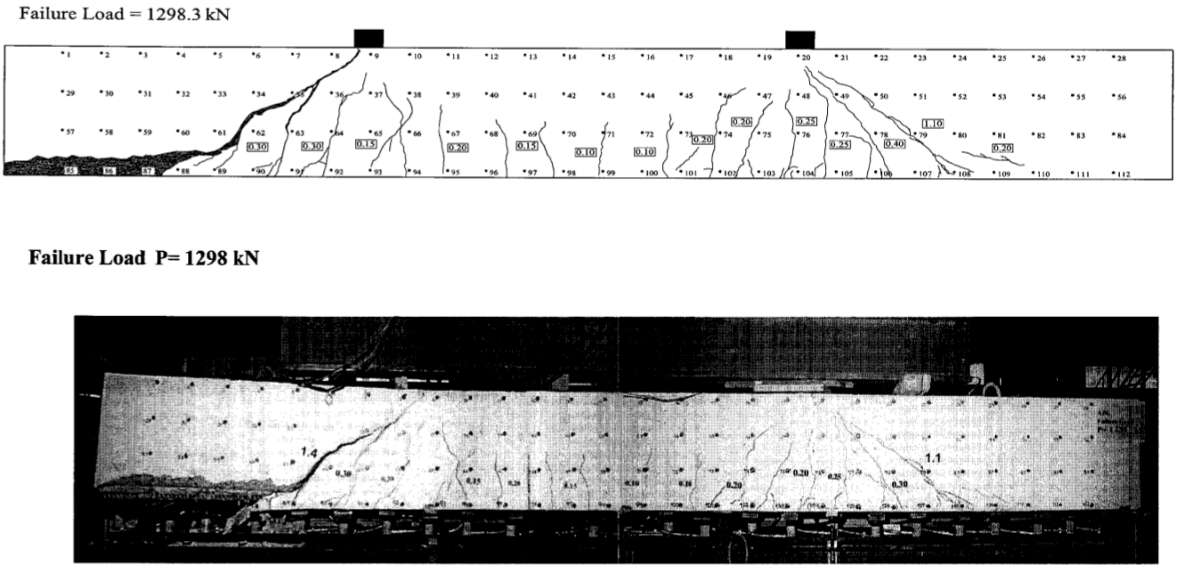

Figure 2.19: Crack diagram at failure for sample AF6 [3]

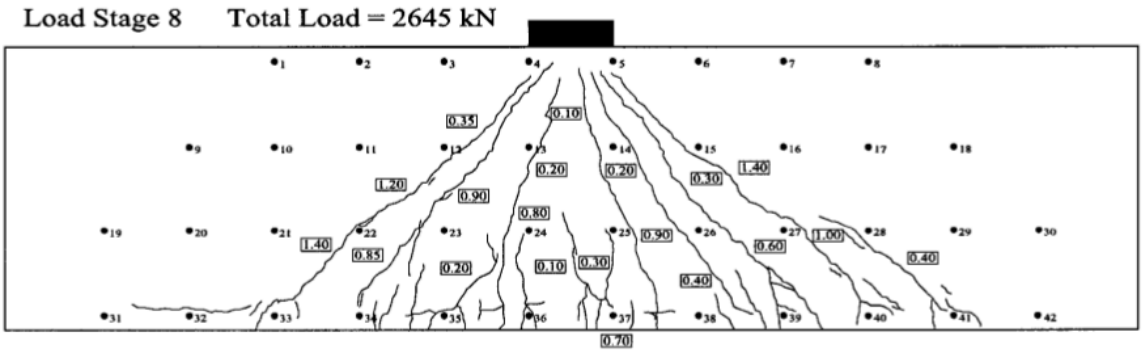

Figure 2.20: Crack diagram at failure for sample AF11 [3]

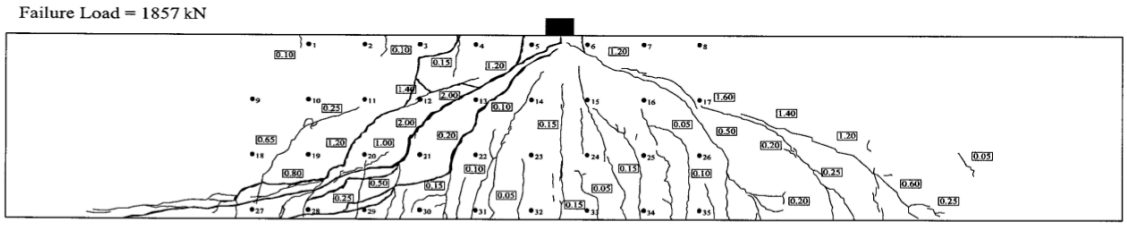

Figure 2.21: Crack diagram at failure for sample AF13 [3]

2.5 Summary and results of the considered tests

Footings can be considered as large beams supported by the soil in the bottom part of the member, therefore, the loading and the support condition introduce transverse clamping into the footings. Generally, the Codes prescriptions and the sectional models do not take into account the positive effects of clamping stresses on the shear capacity of the footings and most of the times these approaches are too conservative. In particular, from the experiments research of *Uzel* it is possible to observe that the clamping stresses decrease rapidly as the L_0/d ratio increases and hence, the shear stress at failure decreases accordingly. This is the reason why the specimens with higher L_0/d ratios (analyzing the whole research work conducted for the *Uzel*'s PhD Thesis and not only the sample considered for this specific work) failed at a lower shear stress than their companions. [3]

All the specimens failed in shear due to the rapid formation of a large number of diagonal cracks, except AF11 which had a flexural failure. The performed shear tests do not involve bond failures of the longitudinal bars, the slip of the longitudinal bars was in fact monitored during the tests. The obtained results for the considered tests conducted by *Uzel* are displayed in Table 2.1.

Specimen	**Concrete**	**Geometry**			**Deflection**	**Longitudinal Strain**	**Failure Load**
	f_c' [MPa]	L_0 [mm]	d [mm]	L_0/d	Δ [mm]	ε_{long} [mm/m]	P [kN]
AF1 UN100	43	2925	925	3.16	11.6	1.99	1186
AF3	27.3	2925	617	4.74	15.4	2.56	541
AF6	32.2	1815*	617	2.94	15.0	2.11	1298
AF11	36.2	1850	925	2.00	11.0	9.69	2645
AF13	35.7	2925	865	3.38	12.4	1.36	1857

Table 2.1: Summary of the considered experimental results

*For AF6 considering just the external side.

L_0 and d shown in Table 2.1. are illustrated in Figure 2.22. Precisely $L_0 = (L-l_b)/2$, l_b is the length of the loading plate and d is the effective depth.

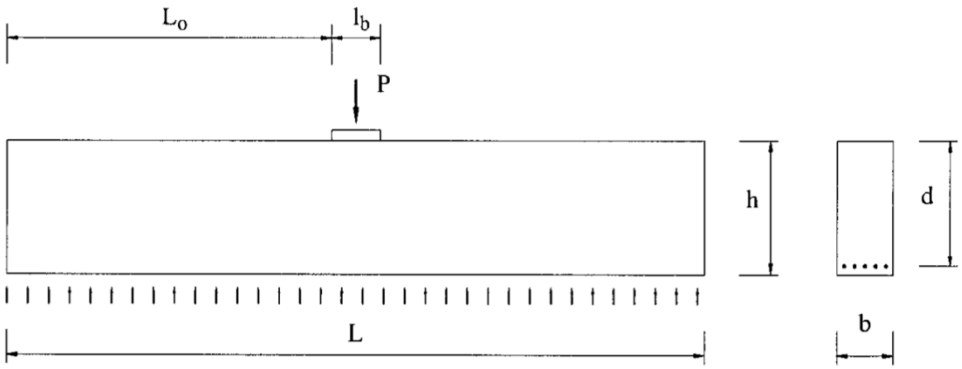

Figure 2.22: General typology of the considered footings and nomenclature [3]

Additional tests with different Boundary Conditions

As already mentioned, the database for the validation of the 2PKT was created for the simplest case of compact footing loading conditions: one vertical load along the symmetry axis of the member and uniformly distributed loads along the whole length of the footings in the bottom side of the considered footing's strip.
For the following parametric analysis (*Chapter 5*), thus the sensibility study, the tests resumed in Table 2.1 are considered because they suit with the initial hypothesis of one vertical load coming from the column and uniformly distributed loading over the whole overhang. Samples AF7 and AF11r will be involved subsequently in order to validate the Finite Element Modelling of the tests under different hypothesis (such as the uniformly distributed load in the bottom part of the footing just in the ends displayed in Figure 2.23). Hence, the characteristics of those two additional specimens are presented in Table 2.2.

Specimen	**Concrete**	**Geometry**			**Deflection**	**Longitudinal Strain**	**Failure Load**
	f_c' [MPa]	L_0 [mm]	d [mm]	L_0/d	Δ [mm]	ε_{long} [mm/m]	P [kN]
AF7	33.8	2925	925	3.16	11.8	1.82	713
AF11-r1	36.2	1850	925	2.00	9.4	2.03*	1408

Table 2.2: Additional sample test data

*Actual strain value is equal to the sum of this value and the residual plastic strain (4.55×10^{-3})

Specimen AF11 had a flexural failure before any indication of shear failure, therefore it was re-tested as AF11-r1 with the same geometrical characteristics, but under different loading conditions (as shown in Figure 2.23). With this loading set-up, before reaching failure, the maximum loading capacity of the hydraulic system was reached.

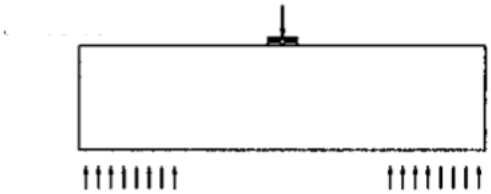

Figure 2.23: Loading set-up for additional specimen AF7 and AF11-r1 [3]

2.6 Conclusions

In the literature, tests that follow the required assumptions (no shear reinforcement, uniformly distributed pressure from the soil, one vertical point load coming from the column of the footing) are not available. Therefore, large-scale experimental tests are needed in order to create a larger database and validate the extended 2PKT (Two-Parameter Kinematic Theory) for shear behavior in deep footings. This will constitute the next step in the developing research connected to the treated topic. In order to prove the theory as well and its efficiency, FEM simulations are validated against *Uzel*'s tests and consequently a parametric study is developed by including the created Finite Elements Models. Therefore, the parametric study is a simulation of real laboratory tests and a first approach to possible future laboratory applications; all these created models will add to the database for footing tests. Finally, it is necessary to mention that also the *Richart*'s tests are included in the final database of footings (as shown in in Table A.1), without forgetting their peculiarity and their differences with respect to properly large-scale tests.
The complete footings database is shown in Appendix 1, also the FEM models are displayed as modifications of the original *Uzel*'s tests, but the modelling phase will investigated in next chapetrs.

3. Modelling approaches

3.1 Introduction

Shear failure in structural concrete members is generally a complex problem that has been investigated during the last century. The fact that makes even more difficult to predict the failure modes is that often the concrete elements fail in brittle ways, which can cause big consequences. Recently, many approaches were developed including the Modified Compression Field Theory (*Vecchio* and *Collins*, 1986) and Strut and Tie Models. These methods provide consistent and reliable prediction of the ultimate resistance. It is demonstrated that the traditional American Code ACI can be too permissive, in particular for members with deep cross-sections, high concrete strengths, or high stress levels in the longitudinal reinforcement.
Before analyzing and developing the modelling approach for footings with Finite Element Analysis (FEA), it is necessary to understand the researches developed to progress rational models for the shear behavior of reinforced concrete beams. The Modified Compression Field Theory (MCFT) (*Vecchio* and *Collins*, 1986) is a rational method and the sectional models based on the MCFT are capable of predicting accurately the shear behavior of reinforced concrete footings, this was verified thanks to experimental data of simply supported slender beams under point loads. It is necessary to specify that the behavior of one-way shear for uniformly loaded sustained footings is different, thus more investigations are required.
The MCFT, together with the Distributed Stress Field Model (DSFT) (*Vecchio*, 2000), is an analytical model for predicting the response of reinforced concrete elements subject to in-plane normal and shear stresses.
The used software to model the footings and to perform FEA (Finite Element Analysis) is VecTor2, developed following the Modified Compression Field Theory (MCFT) (*Vecchio* and *Collins*, 1986).
In this chapter, also the Two-Parameter Kinematic Theory (2PKT) (*Mihaylov*, 2013) for shear behavior in deep concrete beams is deepen. It represents a possible kinematic theory for shear behavior also in concrete compact footings.

3.2 Finite Element Models (FEM)

One of the models in the literature is the Modified Compression Field Theory (MCFT) (*Vecchio* and *Collins*, 1986), experimental researches regarding simply supported slender beams subjected to concentrated loads are verified using the MCFT, which predicts the shear behavior of reinforced elements in accurate way. The verified predictions for beams are quite different with respect to the footings model, for one-way shear behavior in compact footings the loads and support conditions change. Therefore, there is a need to adapt the theory and validate its prediction for the considered specific case.

The non-linear finite element analysis (NLFEA) considers non-linear deformations and redistribution of stresses in the compact footing. Therefore, the transverse clamping stress distribution is not equal to the one computed with linear assumptions.
As it is possible to observe in Figure 3.1, the non-linear finite element analysis was implemented on footings subjected to point loads (from the column) and uniformly distributed loads (which reproduce the pressure from the soil). The objective is to obtain and reproduce the experimental tests in a reliable and realistic way.
As explained in *Chapter 1*, in reality the reaction given by the soil is not uniformly distributed, but it depends on the type of the material of the soil foundation. The non-linear finite element analysis will be performed considering the uniform soil pressure, as it was assumed for the experimental tests.

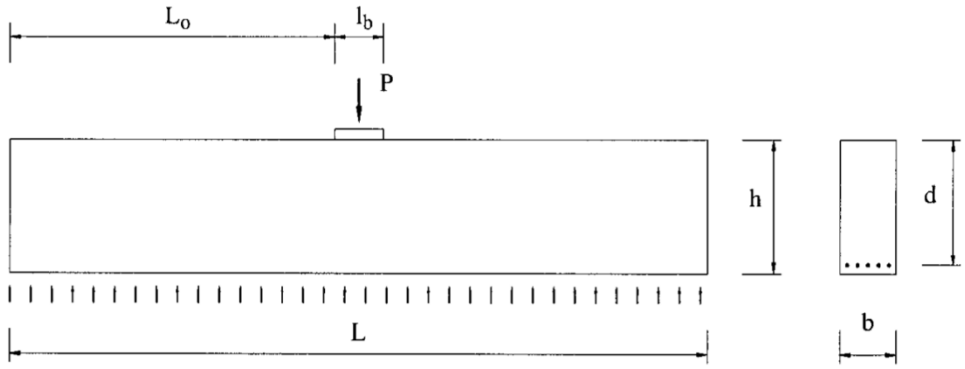

Figure 3.1: Typical beams subjected to point load and uniformly distributed loads (Adapted from Uzel, 2003 [3])

3.2.1 Modified Compression Field Theory (MCFT) (*Vecchio* and *Collins*, 1986)

The MCFT (*Vecchio* and *Collins*, 1986) is an analytical model for predicting the load-deformation response of reinforced concrete membrane elements subjected to shear and normal stresses (Figure 3.2). [7]
The theory was developed by observing the response of a large number of reinforced concrete elements loaded in pure shear or in shear combined with axial stress. While such tests were more difficult to perform, they gave experimental results that clearly illustrated the fundamental behavior of reinforced concrete in shear. [8]
The theory determines:

- the average and local strains and stresses of the concrete and reinforcement;
- the widths and orientation of cracks throughout the load-deformation response of the element;
- the failure mode of the element (based on the previous information).

The problem addressed by the MCFT is to predict the relationships between the axial and shear stresses applied to a membrane element (see Figure 3.3 and Figure 3.4 for membrane element

test) and the resulting axial and shear strains. The most accurate, but most complex, of these models involves representing the structure as an array of biaxial elements and then conducting a non-linear finite element analysis. This model gives accurate results both in flexural regions and in disturbed regions where high clamping stresses can significantly increase shear strength. If one assumes that plane sections remain plane and that the vertical clamping stresses are negligibly small, one can model a beam section as a vertical stack of biaxial elements. [8]

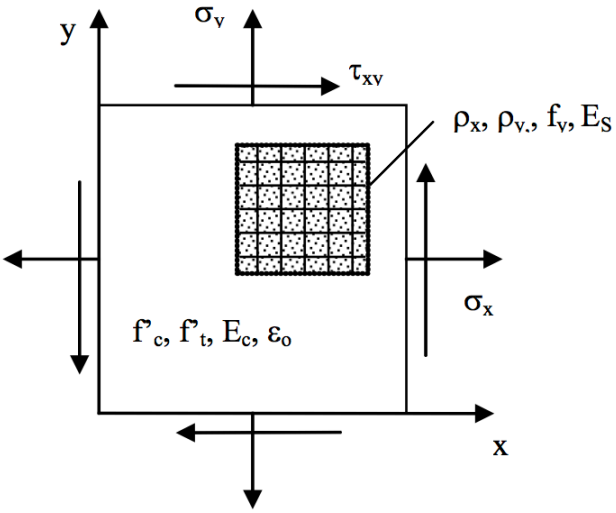

Figure 3.2: Reinforced concrete membrane element subject to in-plane stresses (Adapted from VecTor2 Manual, [7])

Figure 3.3: Membrane element test

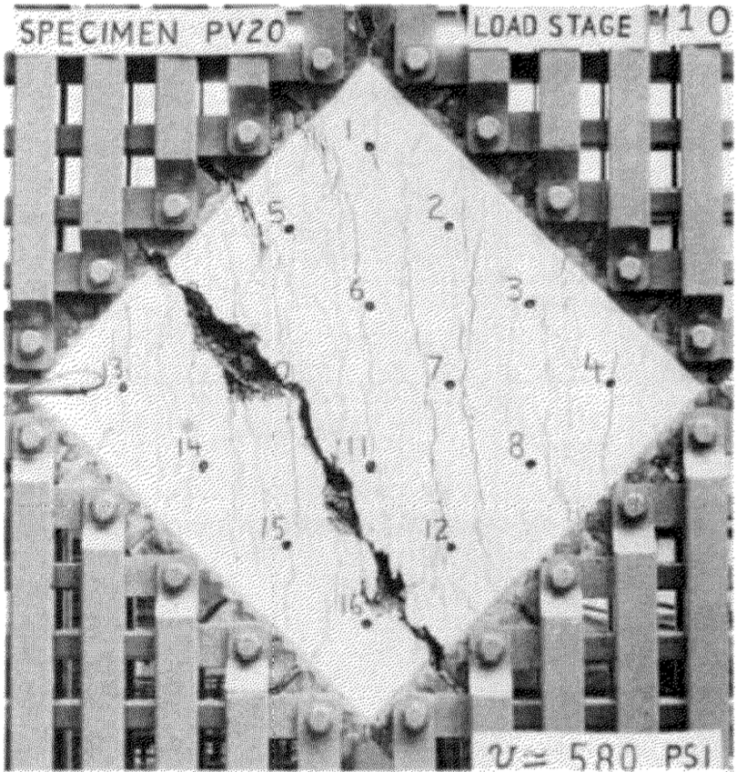

Figure 3.4: Specimen after failure [9]

The MCFT models cracked concrete as an orthotropic material, it is treated as a solid continuum with cracks distributed over the membrane element. The smeared cracks spontaneously reorient, remaining coaxial with the changing direction of the principal concrete compressive stress field. The smeared rotating crack approach is consistent with the distributed and twisting crack patterns observed in many reinforced concrete structures.
While cracks are smeared and the relationships are formulated in terms of average stresses and strains, a critical aspect of the MCFT is the consideration of local strain and stress conditions at cracks.

Assumptions of the MCFT [7]:

- uniformly distributed reinforcement;
- uniformly distributed and rotating cracks;
- uniformly applied shear and normal stresses;
- unique stress state for each strain state, without consideration of strain history;
- strains and stresses are averaged over a distance including several cracks;
- orientations of principal strain, θ_ε, and orientations of principal stress, θ_σ, are the same;
- perfect bond of materials, between reinforcement and concrete;
- independent constitutive relationships for concrete and reinforcement;
- negligible shear stresses in reinforcement.

Therefore, the hypothesis that change in the non-linear field and in particular in MCFT with respect to the linear assumption are the improved tension and compression response of concrete and the non-linear behavior of concrete and reinforcement.
The compatibility relationships pertain to the average strains in the concrete and reinforcement components (Figure 3.5). Due to the perfect bond hypothesis, it follows that average strains experienced by the concrete are equally experienced by the reinforcement. Therefore, the average strains in the concrete, ε_c, and reinforcement, ε_s, will be the same.

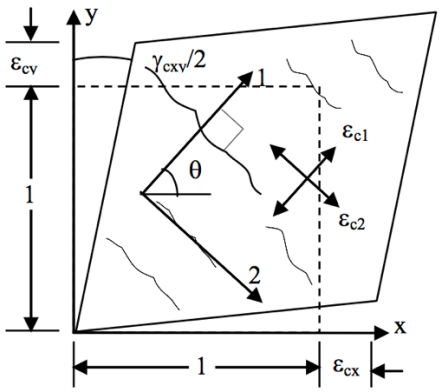

Figure 3.5: Average concrete strains due to average stress-strain response of concrete (Adapted from VecTor2 Manual, [7])

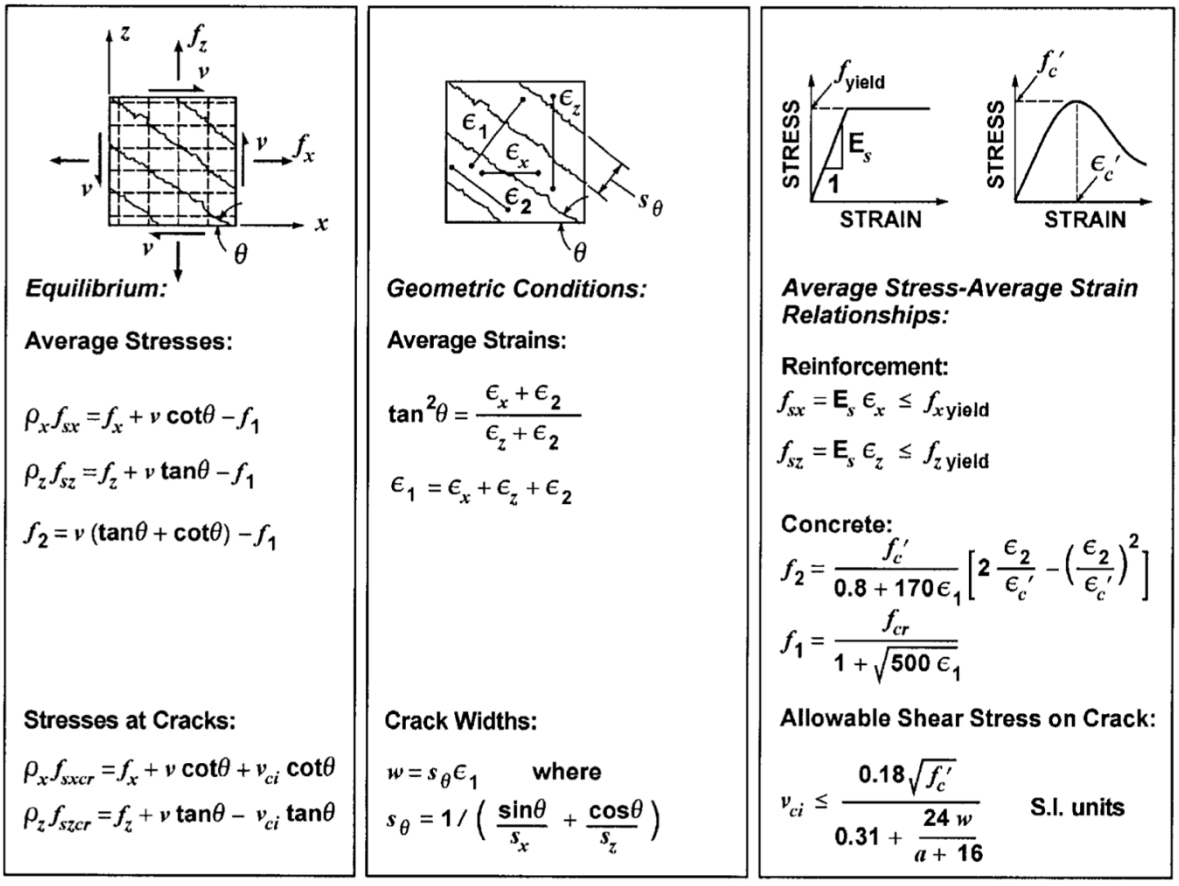

Figure 3.6: Modified Compression Field Model – Summary table [8]

Equilibrium equations, geometric conditions and stress-strain relationships used in the MCFT are summarized in Figure 3.6.
The central simplifying assumption of the theory is that the average direction of principal compressive stress in the cracked concrete corresponds to the average direction of principal compressive strain and the critical cracks are also inclined in this direction. In addition, in order to consider average stresses and average strains in the cracked concrete and the relationships between them, the theory considers how the stresses are transferred across the critical cracks. As an example, an element which does not contain shear reinforcement ($\rho = 0\%$), such as footing elements considered for this study, and is subjected to shear and uniaxial tension in the x direction must transmit a shear stress, v_{ci}, across the crack interface, which is equal to the applied shear stress, v. The ability of the crack to transmit this shear stress depends on the width of the crack (w), the maximum aggregate size (a_g), and the concrete strength (f_c').

3.2.2 Disturbed Stress Field Model (DSFM) (*Vecchio*, 2000)

The DSFM (*Vecchio*, 2000) integrates the MCFT in predicting the response of certain structures and loading scenarios. In lightly reinforced elements, where crack shear slip is significant, the rotation of the principal stress field tends to lag the greater rotation of the principal strain field. The MCFT generally underestimates the shear stiffness and strength, partly because the concrete compression response calibrated for the MCFT is overly softened for the effect of principal tensile strains. [7]
The DSFM expands the compatibility relationships of the MCFT to include crack shear slip deformations. The strains due to these deformations are distinguished from the strains of the concrete continuum due to stress. The DSFM decouples the orientation of the principal stress field from that of the principal strain field, resulting in a smeared delayed rotating-crack model. Moreover, by explicitly calculating crack slip deformations, the DSFM eliminates the crack shear check as required by the MCFT. Constitutive relationships for concrete and reinforcement are also refined.

While the MCFT assumes that principal strain and principal stress axes remain coaxial, the evidence demonstrates the principal strain field generally changes inclination at a larger rate than the principal stress field, resulting in a differential lag between the principal strain and principal stress axes.
This phenomenon is due to the manner in which the strain and stress fields are determined. The measured strains are total strains, which are attributable to straining of the concrete continuum in response to applied stresses as shown in Figure 3.5 and discontinuous shear slip is shown in Figure 3.7. Concrete stresses are attributable only to the continuum straining in response to applied stresses. [7]

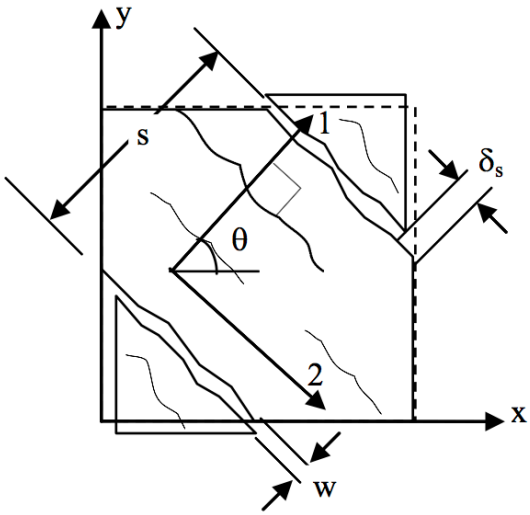

Figure 3.7: Deformation due to crack shear slip (Adapted from VecTor2 Manual, [7])

3.2.3 VecTor2

VecTor is a non-linear finite element program developed at the University of Toronto by researchers studying reinforced concrete behavior and applications of the finite element method. In particular, VecTor2 is a non-linear finite element software for the analysis of two-dimensional reinforced concrete membrane structures (*University of Toronto*, 1990). The original version is known as TRIX. This development has coincided with experimental tests to validate the ability of VecTor2 to predict the load-deformation response of a variety of reinforced concrete structures exhibiting well-distributed cracking when subject to short-term static monotonic, cyclic and reverse cyclic loading. [7]
The theoretical bases of VecTor2 are the Modified Compression Field Theory (*Vecchio* and *Collins*, 1986) and the Disturbed Stress Field Model (*Vecchio*, 2000), deepen in previous sections. VecTor2 models cracked concrete as an orthotropic material with smeared, rotating cracks. The program utilizes an incremental total load (introducing multiplying factors), iterative secant stiffness algorithm to produce a non-linear solution.
Some developments have incorporated alternative constitutive models for a variety of second-order effects including compression softening, tension stiffening, tension softening, and tension splitting. Also, the capabilities of modelling concrete expansion and confinement, cyclic loading and hysteretic response, construction and loading chronology for repair applications, bond slip, crack shear slip deformations, reinforcement dowel action, reinforcement buckling, and crack allocation processes. [7]
Finite element models constructed for VecTor2 use a fine mesh of low-powered elements, which suits to reinforced concrete structures, that require a relatively fine mesh to model reinforcement detailing and local crack patterns.
Then, the software Augustus provides graphical post-processing capabilities for the analysis results obtained with VecTor2.

3.2.4 General layout of Finite Element Mesh

Finite Elements Models of footings are possible with program VecTor2 and only half of the length of the footing can be represented due to the element's symmetry (Figure 3.10).
Thus, the appropriate restraints were used along the symmetry axis in order to prevent displacement along the horizontal axis (*x*-axis). In the bottom, the uniformly distributed loads are displayed. The specimen for the FEM model is loaded from the bottom and, therefore, it is restrained on the top where actually during the laboratory test a vertical incremental load is applied in correspondence of the column, modelled as a steel bearing plate. Obviously, the total load applied on the top during the real test is equal to the sum of the loads applied on the bottom for the FEM model. Then, the created model is a load-imposed test (and not imposed displacement). Generally, the modelled materials are three: the concrete, the steel for the loading plate and the reinforcement longitudinal steel (truss member). The constitutive laws for the materials are represented below in Figure 3.8 and Figure 3.9.

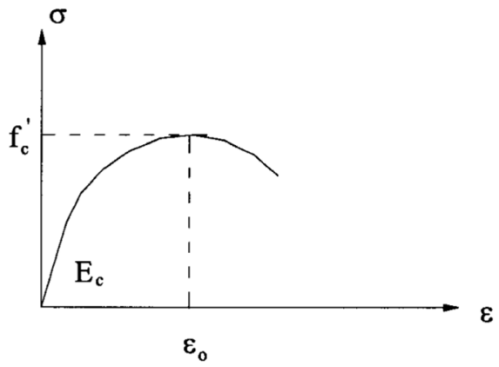

Figure 3.8: Concrete constitutive law

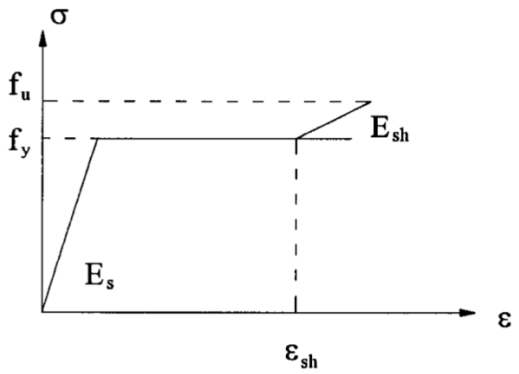

Figure 3.9: Steel constitutive law

Once defined the properties and the types of materials, the footings are modelled by creating the number of regions, finally the mesh is generated, and the number of elements varies for the different length *L* tested.
In Figure 3.10, it is possible to observe an example of footings modelled following what it is explained above using VecTor2 software.

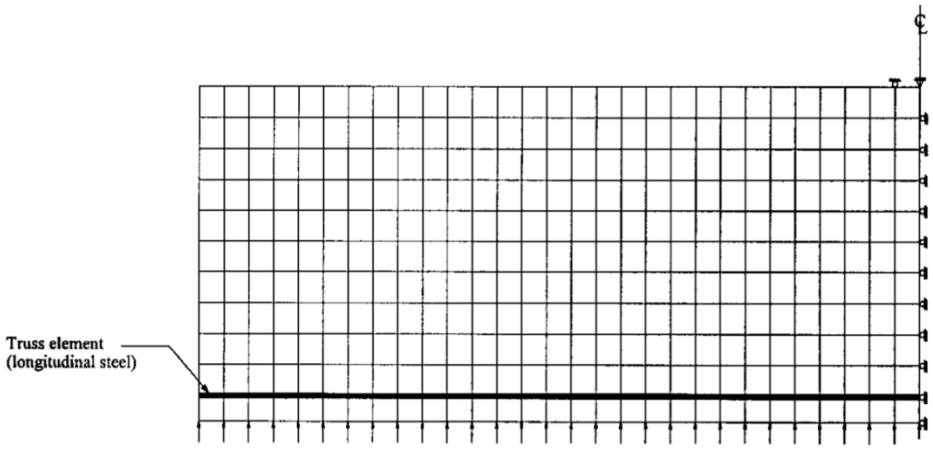

Figure 3.10: Example of footing modelled with VecTor2 (Adapted from Uzel, 2003 [3])

This modelling phase of members is part of previous works performed by *Uzel*. In her study, it was observed that the non-linear finite element analysis with dense mesh (880 elements) gives a failure loads that is about 47% less with respect to the one obtained with less dense mesh (220 elements). However, as the results from the analysis with less dense mesh are in good agreement with the experimental results, it is concluded that this mesh density is the more appropriate to use. [3]

The results obtained from her models and the experimental tests will be useful in the succeeding parts of the thesis. The procedure the get the best results, compatible and comparable with the results obtained by tests, required basically four different set of analysis. For each step the options regarding the modelling of materials and crack width behavior were improved until the fourth set of analysis which provided the best results, thus the more reliable and realistic ones. The first set of analyses was performed with coarse mesh, crack width check called "Advanced w-v_{ci} check" with different maximum crack width for distinctive specimens. Then, the second set of analyses was performed both coarse and dense mesh with different options for models: option 1 with crack stress control "Advanced (*Lee*, 2009)" and crack width check "Agg/2,5 max crack width"; while for option 2 crack stress control "Basic (MCFT/DSFM) and crack width check "No check". The advanced option regards "*Attard & Setung*" compression pre- and post- peak, "*Montoya/Ottosen*" confined strength and "*Gan-Vecchio*" confined concrete.

The third set of analyses is a dense mesh with bearing material defined under the plate, the chosen option is basic. The fourth set of analyses produces the best results, VecTor2 files are the same with respect to the third set, but with updated *.exe* file. It was observed that defining bearing material under the loading plate does not work as effectively as increasing the concrete strength of elements under the plate, consequently the performed final solution was the introduction of another material, high strength concrete, right below the steel loading plate.

As shown in Figure 3.10, the FEM model is created by imposing loads on the bottom, thus simulating the soil loads, and restraining the top, where the footing column transmits the load to the foundation itself. The total maximum load, for equilibrium, is the same on the top and on the bottom of the footing. In order to get the best results, the model is set with different concrete material (f_c = 70 MPa) under the steel bearing plate, even if during the laboratory tests, the samples were composed of the same concrete type everywhere, with this assumption the results

obtained with the non-linear finite element analysis are a good approximation of tests results. The main problem that brings to this final solution of different concrete strength was the fact that right under the plate there were a bad approximation of strain and cracks.

Summarizing, the suggestions for Finite Element Modelling for footings are:

- representation of half of the structure thank to the symmetry of the element;
- choice of the proper restraints along the symmetry axis and in proximity of the steel plate (in order to have incremental and uniformly distributed load in the bottom side of the element);
- basic options for the choice of the models;
- dense mesh option;
- definition of an additional type of material: bearing material defined under the plate with higher concrete strength in order to reproduce accurately in this portion the strain and the crack distribution.

The prescriptions and the suggestions explained above and given by *Uzel* will be useful and necessary also further on during the thesis work in order to validate Finite Element Analysis of the created models and enlarge the database of footings with Finite Element Models.

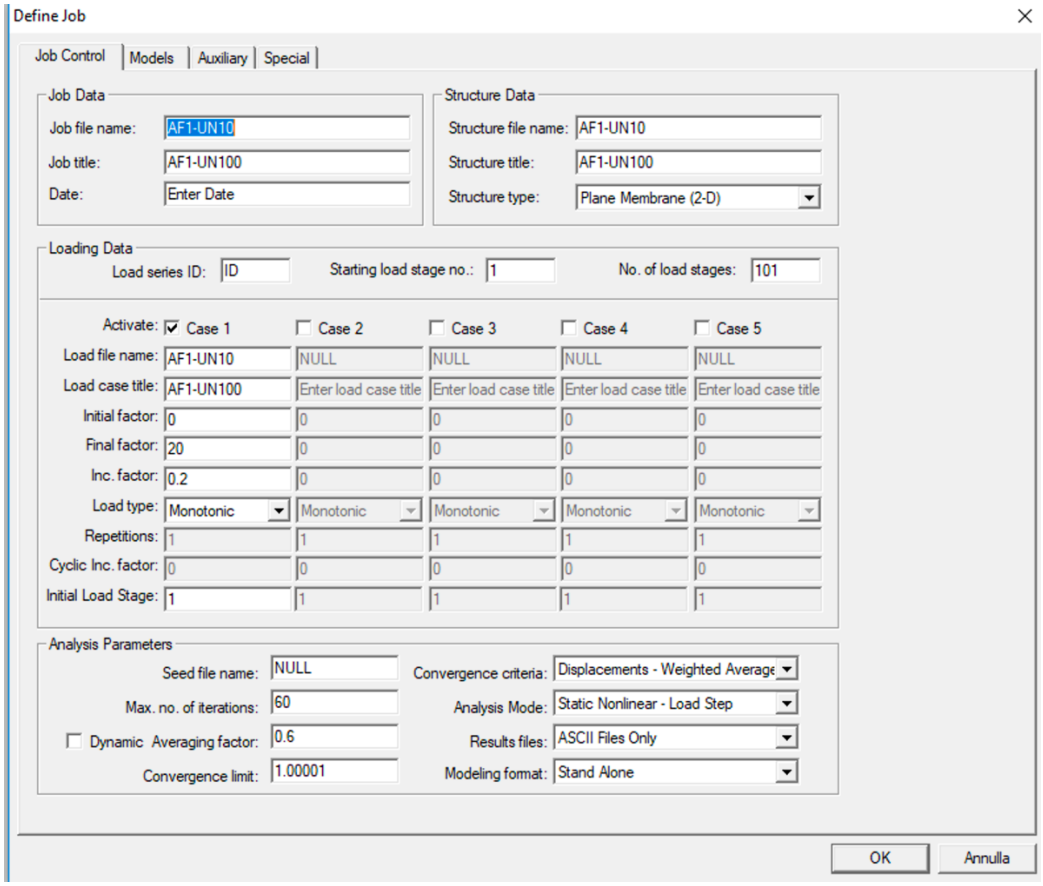

Figure 3.11: Job definition on VecTor2

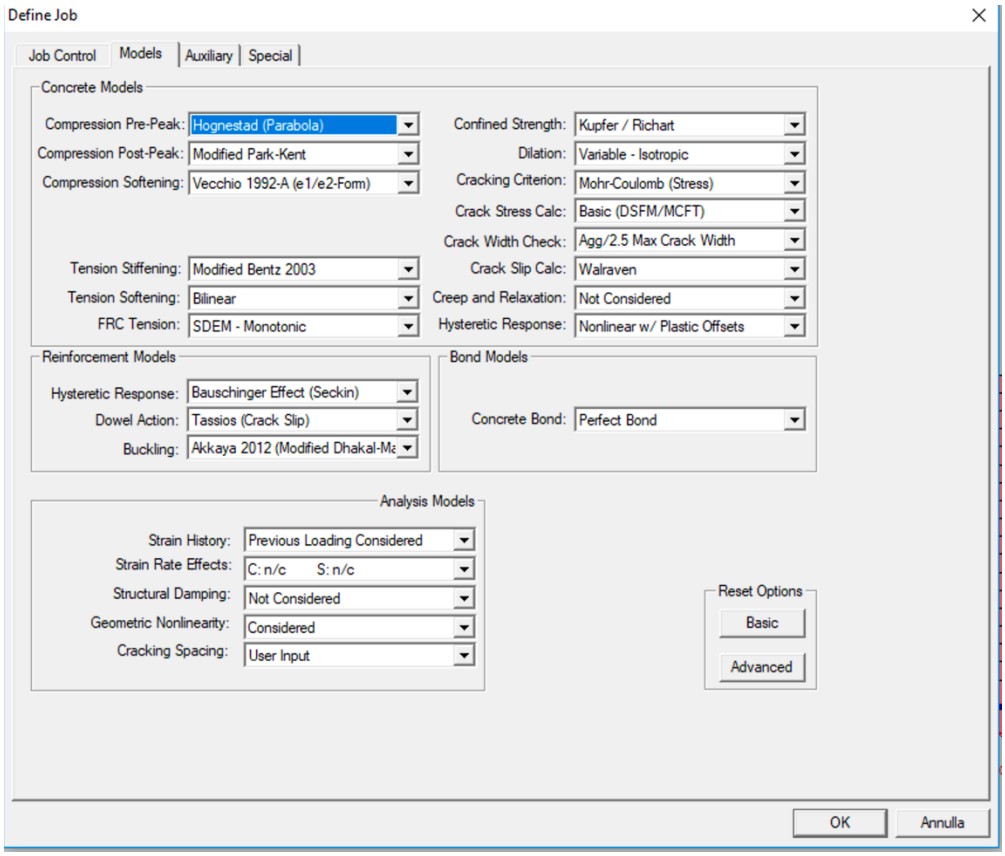

Figure 3.12: Options setting on VecTor2

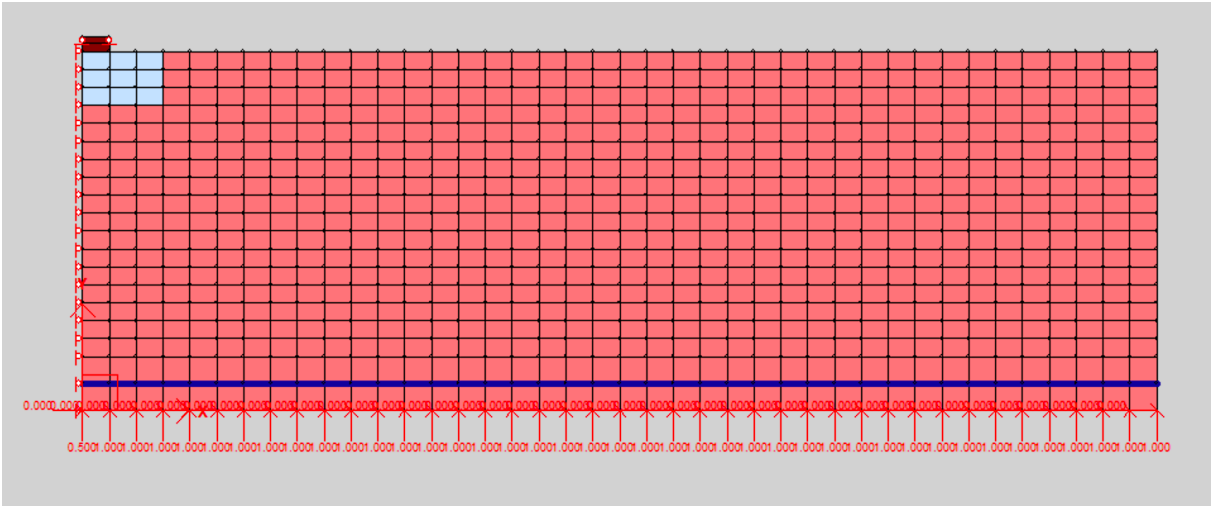

Figure 3.13: Mesh and materials areas on VecTor2

In Figure 3.11 and Figure 3.12 the job definition and the options setting on VecTor2 are respectively illustrated. In particular, in Figure 3.12, it is possible to understand the model used for concrete, pre- and post- peak behaviour, tension and compression softening, tension stiffening, confinement and crack control; dowel action and buckling for the steel.
Then, the Figure 3.13 represents the model of the beam AF1 UN100, it possible to observe the displayed loads, the restraints, the chosen mesh and the different types of materials. In fact, as previously mentioned, the pink part is the actual concrete with the real concrete strength, the

light-blue part is the high strength concrete, the blue truss is the longitudinal bottom reinforcement and the red rectangular on the top is the restrained steel loading plate.

3.3 Two-Parameter Kinematic Theory (2PKT) for Shear Behaviour of deep beams

3.3.1 General

The Two-Parameter Kinematic Theory (2PKT) (*Mihaylov*, 2013), validated with a large amount of experimental results, is a kinematic model for deep beams accomplished of defining the deformed shape of those members in terms of two parameters, two degrees of freedom: the average strain in the bottom reinforcement, $\varepsilon_{t,avg}$, and the vertical displacement of the critical loading zone, Δ_c. By combining the theory with the equilibrium equations and the stress-strain relationships, it is possible to predict the shear strength and the deformation patterns at shear failure. Remarkable is the prediction of how the shear strength components (and also the deformation patterns, crack width, maximum deflection, displacement field for deep beams) vary with different *a/d* ratios, where *a* is the shear span and *d* is the effective depth. Thus, it is evident a significant size effect for the shear strength of deep beams. The transition from deep beams to slender beams occurs at an *a/d* of approximately 2.3.
Before going into details of the theory, it is necessary to clarify the hypothesis and the main assumption of deep beams. First of all, the statement "plane sections remain plane" [*Hooke*, 1678] is no more valid for deep beams. The shear strain becomes dominant and the deformation pattern becomes more complex. Thus, for such members a different approach is required.

3.3.2 Kinematics of deep beams

The model assumes that the critical crack extends from the inner edge of the support to the far edge of the tributary area of the loading plate responsible for the shear force *V*. The concrete above the critical crack is modelled as a single rigid block, while the concrete below is represented by a series of rigid radial struts. The regions of the model on each side of the critical crack are connected by the critical loading zone (CLZ) at the top of the section, by the bottom flexural reinforcement and by the stirrups. The elongation of the bottom reinforcement causes the rigid radial struts to rotate about the loading point and the crack to widen. [4]
Both degrees of freedom cause tensile strain in the transverse reinforcement. By increasing the shear-to-span ratio (*a/d*), the angle of critical crack (α_1) should be taken smaller than the angle θ of the crack developed in the uniform stress field (calculated from the MCFT or taken equal to 35°). The formulae reported below represent the horizontal and vertical displacement of each point of the concrete beam expressed by assuming the previously mentioned Degrees of Freedom (DOFs).

Points below the main diagonal crack:

$$\delta_x(x,z) = \varepsilon_{t,avg} \cdot x \tag{1}$$

$$\delta_z(x,z) = \varepsilon_{t,avg} \cdot \frac{x^2}{h-z} \tag{2}$$

Points above the critical crack:

$$\delta_x(x,z) = \varepsilon_{t,avg} \cdot (h-z) \cdot \cot(\alpha) \tag{3}$$

$$\delta_z(x,z) = \varepsilon_{t,avg} \cdot x \cdot \cot(\alpha) + \Delta_c \tag{4}$$

The *x*-axis and *z*-axis are represented in Figure 3.14. Then, in Figure 3.15, the deformed shape of the entire surface of a tested deep beam (Specimen S1C) is represented in order to demonstrate and validate the prediction of the equations. The white circles indicate the displacement predictions by the 2PKT model with respect to the location of the targets and the measurements during the laboratory tests (the positioning of Zurich Targets was done also by *Uzel* for the same reason). For the sample in the picture it is possible to notice that 27 out of 28 targets are accurately predicted.

The explained kinematic model can also be utilized to estimate the width of the critical diagonal cracks:

$$w = \Delta_c \cdot \cos(\alpha_l) + \frac{\varepsilon_{t,min} l_k}{2\sin(\alpha_l)} \quad \text{(at mid-span)} \tag{5}$$

Where l_k is the length of the bottom reinforcement whose elongation contributes to the width of the critical crack. It is assumed that l_k is equal to the distance between the node that develop in the longitudinal bars near the support (see Figure 3.14).

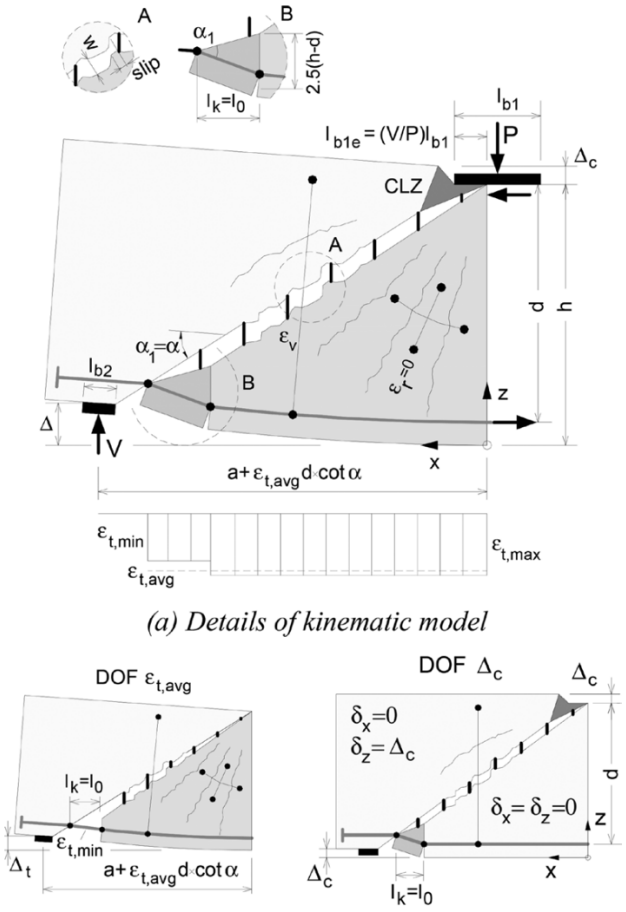

(a) Details of kinematic model

(b) Degrees of freedom of kinematic model

Figure 3.14: Kinematic model for deep beams [4]

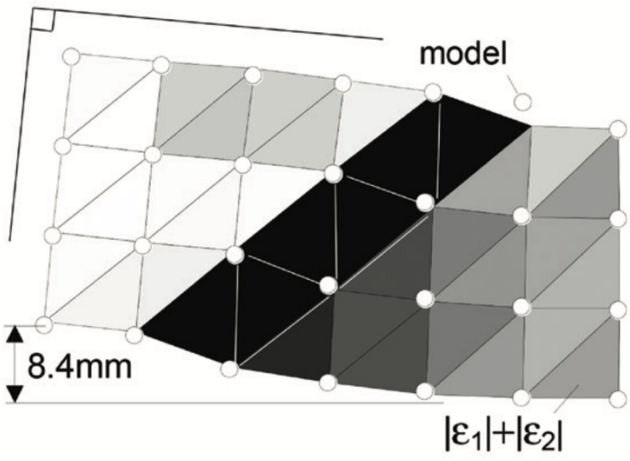

Figure 3.15: Deformation pattern at failure of Specimen S1C (Scale Factor = 30) [4]

3.3.3 Critical Loading Zone (CLZ)

At the base of the developing of the Two-Parameter Kinematic Theory, there is the Critical Loading Zone (CLZ). As it was possible to observe from numerous laboratory tests, this zone failed due to high diagonal compressive stresses as the spalled concrete and the cracks orientation showed. Therefore, an analytical method was advanced in order to calculate the dimension of CLZ. It is important to notice that the zone of concrete above the critical diagonal crack is exemplified as an elastic cantilever fixed in one end and loaded in the opposite side (Figure 3.16). the assumptions are that plane sections perpendicular to the bottom face of the cantilever remain plane and the tip section is subjected to uniform compressive stresses.
The analysis showed that the compressive stress along the bottom edge of the cantilever reaches its maximum value at a distance of $1.5l_{b1e}\cos(\alpha)$ from the tip section and returns to the applied stress at a distance of $3l_{b1e}\cos(\alpha)$ from the same section (where l_{b1e} is the effective width of the loading plate). This result is used to define a triangular critical loading zone with a bottom length of $3l_{b1e}cos(\alpha)$ and a top vertex located opposite to the location of the maximum compressive stress. [4]
In Figure 3.16, by relating images (a) and (b), it is also possible to observe that the chosen geometry reasonably agrees with the test result (in the picture the Specimen SC1 is represented).
In order to obtain accurate results for specimens loaded with very small loading plates, l_{b1e} should not be taken less than $3a_g$ (where a_g is the maximum size of coarse aggregate).
As *Mihaylov* states "knowing the geometry of the critical loading zone, the ultimate shear displacement Δ_c can be calculated by assuming values for the average strains along the bottom and top sides of this zone (refer to Figure 3.16 (c)). As the zone fails due to combined moment and compression, the bottom strain is assumed equal to –0.0035 and the top strain is assumed equal to zero."

$$\Delta_c = 0.0105 l_{b1e}\cot(\alpha) \tag{6}$$

Considering the triangle of forces shown in Figure 3.16 (c), the shear strength of the critical loading zone is as follow:

$$V_{CLZ} = k f_{avg} b l_{b1e} sin^2(\alpha) \tag{7}$$

Where k is the crack shape coefficient, it accounts that for slender beams the critical diagonal crack is not straight but has an S-shape and approaches the loading plate at a very flat angle. It is suggested that $k = 1$ for beams with $\cot(\alpha) \leq 2$ and $k = 0$ with $\cot(\alpha) \geq 2.5$, with a linear transition for intermediate values of $\cot(\alpha)$. [4]
By the use of tests, it is possible to demonstrate that a significant part of the shear in deep beams is carried by mechanisms other than diagonal compression in the CLZ.

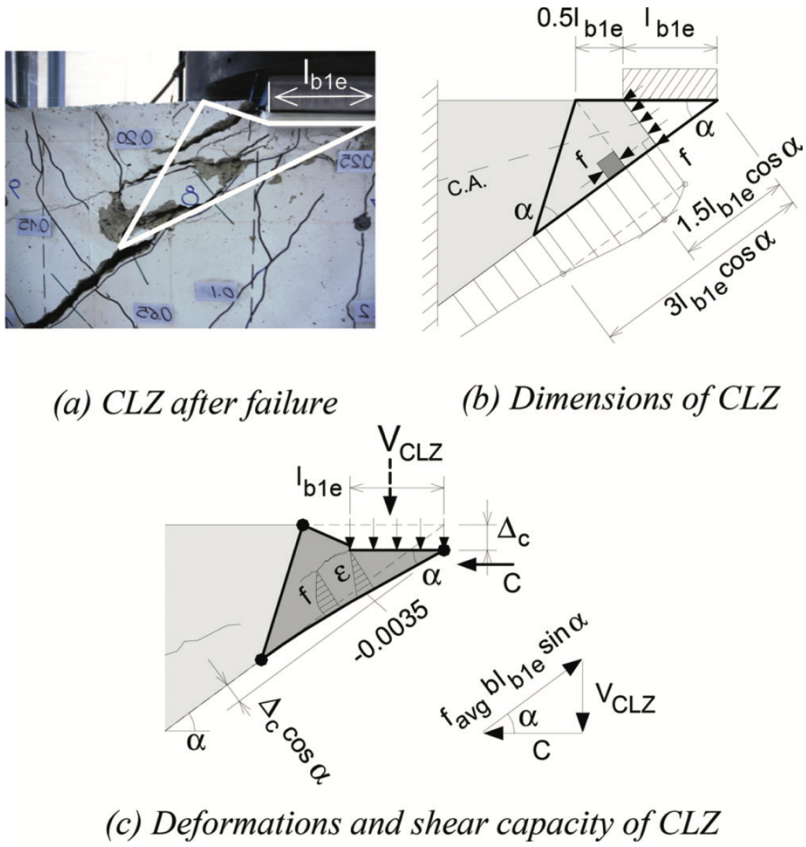

Figure 3.16: Modelling of CLZ [4]

3.3.4 Shear strength calculation in deep beams

Due to the displacement Δ_c, the critical diagonal crack moves down and opens (slip displacement). The slip, due to aggregate interlock forces, will produce substantial shear stresses that will contribute to the shear capacity resistance of the element.
As shown in Figure 3.14 (a) in detail B, the bottom longitudinal bars in deep beams are subjected to double curvature near the support and thus will resist shear by dowel action. [4]
Therefore, the shear resistance of deep beams is calculated as follow:

$$V = V_{CLZ} + V_{ci} + V_s + V_d \tag{8}$$

Where $V_{CLZ}, V_{ci}, V_s, V_d$ are respectively the shear forces resisted by the CLZ, by the aggregate interlock, by stirrups and by dowel action.
The shear resistance provided by aggregate interlock is:

$$V_{ci} = \frac{0.18\sqrt{f'_c}}{0.31+\frac{24w}{a_{ge}+16}} bd \tag{9}$$

Where a_{ge} is the effective aggregate size equal to a_g for $f'_c < 60\ MPa$ and zero for $f'_c > 70\ MPa$, with linear transition for intermediate values. The crack width w is computed using equation (5).

The shear capacity produced by the stirrups' contribution is equal to the following formula.

$$V_s = \rho_v b(dcot\alpha_1 - l_0 - 1.5l_{b1e})f_v \geq 0 \tag{10}$$

Where $(dcot\alpha_1 - l_0 - 1.5l_{b1e})$ indicates the length along the shear span within which the diagonal critical crack is wide enough to cause significant tension in the stirrups. The stress in the stirrups is calculated by assuming elastic-perfectly plastic behavior of the steel.

$$f_v = E_s\varepsilon_v \leq f_{yv} \tag{11}$$

Where ε_v, the transverse strain at the middle of the shear span, is derived from the kinematic model.

$$\varepsilon_v = \frac{1}{0.9d}(\Delta_c + 0.25\varepsilon_{t,avg}dcot^2\alpha_1) \approx \frac{1.5\Delta_c}{0.9d} \tag{12}$$

The shear resisted by the dowel action of the bottom reinforcement is computed as follow.

$$V_d = n_b f_{ye}\frac{d_b^3}{3l_k} \tag{13}$$

Where n_b is the number of longitudinal steel bars, d_b is the diameter of the bars. The formula (13) is derived under the assumption that the dowels of length $l_k = l_0 + d(cot\alpha + cot\alpha_1)$ in which $l_0 = 1.5(h-d)cot\alpha_1 \geq s_{max}$, work in double curvature with plastic hinges created at the ends. The moment capacity of the hinges is computed with an effective yield strength $f_{ye} \leq 500\ MPa$ in order to account for the tension effect of the bar. The limit of $500\ MPa$ accounts for the fact that the transverse displacement at the dowel might not be sufficiently large to cause plastic hinges in bars with high yield strength.

The previous equations are derived by assuming that the element fails along the critical diagonal crack, but beams with large amount of stirrups may fail by crushing of concrete along a steep section near the load (sliding shear failure).
The 2PKT method has been developed to apply to members with short shear spans where the shear strength predicted by this method will exceed the shear strength predicted by sectional design procedures intended for longer spans. [4]
It is observed from experimental tests and calculations that when *a/d* increases, the angle of the critical crack decreases, therefore, the stirrup contribution V_s will be larger. In addition, the shape of the critical loading zone becomes slenderer: strength and its stiffness will both decrease. As consequence of the stiffness reduction, the diagonal critical crack will be wider and, thus, when *a/d* increases, the aggregate interlock contribution V_{ci} decreases.

An important motivation for the development of the 2PKT model was the need for a better understanding of the size effect in deep beams. The question is whether very large beams will fail at lower shear stresses than geometrically similar, smaller beams. [4]
For beams without stirrups, so without the contribution of shear resistance V_s, it is predicted that the size effect in deep beams is caused mainly by aggregate interlock. With the increment of the dimension of the concrete element, the CLZ will be more deformed and therefore the diagonal cracks will be wider. This produces a substantial reduction of transmitted shear stresses across the cracks. The 2PKT and the database of tests collected by *Mihaylov* denotes that the supplement of stirrups might not exclude the size effect in deep beams.

3.3.5 Overview of solution procedure

Degree of freedom Δ_c is obtained by assuming that the CLZ is at failure under diagonal compressive stresses; while $\varepsilon_{t,avg}$ is obtained as illustrated in Figure 3.17. The thick black line in the plot shows the relationship between $\varepsilon_{t,avg}$ and the applied shear V, while the red line represents the shear resistance which decreases with increasing strains. As already mentioned, this resistance consists of four components: shear carried in the CLZ (V_{CLZ}), aggregate interlock component (V_{ci}), stirrups component (V_s) and dowel action of the bottom longitudinal reinforcement (V_d). It is possible to observe that the reduction of shear resistance is caused by the weakening of aggregate interlock and dowel action shear components, while component related to the Critical Loading Zone is not influenced by $\varepsilon_{t,avg}$.
The force resisted by the dowels decreases with increasing the strain. The longer the bars, the longer the lever arm of the dowels and the less the dowel effect is. At one point, the dowel action will have no effect when the bars have yielded. The yielding strain is given by:

$$\varepsilon_y = \frac{f_y}{E_s} = 3.26 \cdot 10^{-3} \tag{14}$$

Also, the aggregate interlock is affected by the strain in the bottom longitudinal reinforcement: by increasing the strain wider cracks will form and the aggregate interlock forces will decrease. In the example in Figure 3.17, the component V_s is almost constant because $\Delta_c = 0.41\ mm$ is sufficient to yield the stirrups even when $\varepsilon_{t,avg}$ is zero. Therefore, the solution of the equations of the 2PKT correspond to the intersection point of the black and red lines which relates to the equilibrium point for shear forces. This graphical representation of the 2PKT is similar to that used by *Muttoni* in a critical shear crack theory for punching of slabs [29]. As the equations of the model are not suitable for a closed-form solution, the shear strength is found by an iterative solution procedure. With the predicted DOFs, the 2PKT can also be used to evaluate the deformation patterns of the beam near shear failure, including crack widths, deflections, and the complete displacement field of the beam. It should be noted that in the 2PKT the flexural reinforcement is assumed to behave linearly, while yielding of the reinforcement can be taken into account by performing a flexural strength calculation based on code provisions. The final

predicted failure load will be the minimum load obtained from a 2PKT shear calculation and a standard flexural strength calculation.
In the case of Figure 3.17, the member considered is a deep beam subjected to rotational moment at one end. Therefore, from the equilibrium of moment, the shear force V can be calculated as follows:

$$V = \frac{T \cdot 0.9d}{a} \tag{15}$$

where T is the tension in the bottom longitudinal reinforcement, $0.9d$ is the assumed lever arm between the compression force C and T, and a is the shear span.

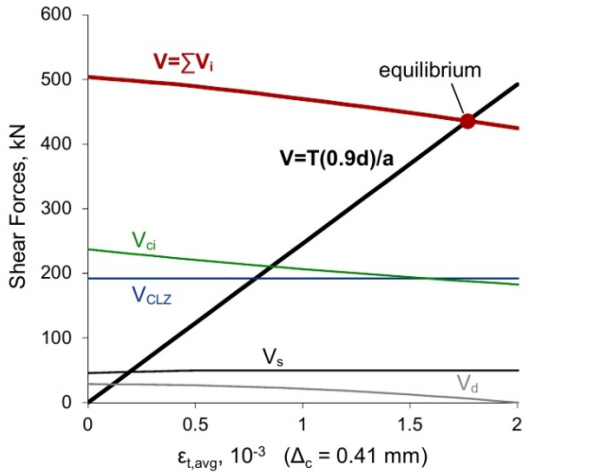

Figure 3.17: Components of shear resistance and equilibrium at peak load [4]

3.4 Sectional shear analysis

Sectional models are analytical procedures to predict the response of reinforced concrete beams in which it is assumed that plane sections remain plane after bending. Engineering beam theory studies the response of the member section-by-section and does not account for the local effects caused by the support and loading configuration. Therefore, *Schlaich, Schäfer* and *Jennewein* (1987) called "beam region" the part of the element in which the assumptions of engineering beam theory are accurate; while "disturbed region" is the part in which the stress distributions are influenced by the support and loading setting. Analysis based on sectional models are suitable to predict the behavior of beam regions, but not accurate for disturbed regions. Specifically, for the latest regions, analysis methods based on strut-and-tie methods or non-linear finite element models are able to predict the flow of forces of these regions. The strut-and-tie model is developed in the next section; while the FEM is deepened in 3.2 Finite Element Models (FEM).

Generally, in using the sectional analysis approach, the problem of determining the response of a reinforced concrete structure subjected to given loads is divided into two tasks.
First, the sectional forces at various locations in the structure caused by the applied loads are determined. This step is usually performed assuming that the structure remains linearly-elastic. Then the response of a local section to the sectional forces is determined. In this second step, which is the sectional analysis, the non-linear characteristics of cracked reinforced concrete are taken into account. [26]
The assumptions for the shear sectional analysis are that plane sections remain plane, thus, a straight line drawn on the element before deformation will still be a straight line after deformation, and no significant net stress in the transverse direction. Therefore, the concrete force and the steel force balance each other at every point across the depth of the element. These assumptions are respected when the analysis is being performed a distance away from the support and the load point. In fact, nearby to the load and to the reactions, there is a transverse clamping stress from the application of the load itself, which produces a local increment of the strength. Therefore, this is one cause of short beams are markedly stronger in shear than long beams with the same cross section.

The β-method is a simple hand-calculation developed by Collins and Mitchell in 1991, it is based on the Modified Compression Field Theory (MCFT) (Vecchio and Collins, 1986) and forms the basis of shear design methods for reinforced concrete elements in current design codes. In fact, the general procedure of the ACI318-11 and AASHTO LRFD specifications for shear is shown in Figure 3.18. Specifically, AASHTO LRFD provides a hand-based shear-design procedure derived from the simplified MCFT. The nominal shear capacity is taken as the sum of a concrete component and a shear-reinforcement component (for non-prestressed concrete elements).

	ACI 318-11	AASHTO LRFD (2010)*
Nominal strength, V_n =	$V_c + V_s$	$V_c + V_s \le 0.25 f_c' b_v d_v$
Concrete, V_c =	Simple: $2\sqrt{f_c'} b_w d$	$0.0316\beta\sqrt{f_c'} b_v d_v$
	Detailed: $\left(1.9\sqrt{f_c'} + 2500\rho_w \frac{V_u d}{M_u}\right) b_w d$	
Steel, V_s =	$A_v f_y d/s$	$A_v f_y d_v \cot\theta / s$

*Simplified MCFT (that is, AASHTO LRFD Method 2).

Figure 3.18: Sectional shear design provision for non-prestressed elements [25]

Concluding, the loading and support conditions induce transverse clamping stresses into deep beams and footing type beams. These stresses are not accounted by sectional models; therefore, it is not suggested to use them to predict the response of disturbed regions. In fact, the shear strength predictions for beams with *a/d* less than about 2 are extremely conservative. In deep beams, significant transverse clamping stresses are induced by the loading and support

conditions. It is believed that there is a need for more general sectional analysis method. *Uzel* presented a new approach to sectional analysis in order to predict the shear behaviour. [3]

Simple expressions for clamping stress distributions

Simple expressions for clamping stress distributions for beams subjected to uniformly distributed loads on the bottom and point load on the top are developed by *Uzel* also thanks to non-linear finite element analysis.
It is observed that the clamping stresses due to the point load disperse over a length *c* and the value of clamping stresses decreases when moving away from the load. [3] Moreover, the value of clamping stresses due to the applied uniformly distributed load is equal to the applied stress and decreases linearly over the height of the beam.
In Figure 3.19 (a) it is possible to observe the assumed clamping stress distribution along the overhang of a footing due to the point load.
The dispersion length *c* can be approximated as half of the distance from the point zero shear to the face of the column but not greater than *1.5h*.

$$c = L_0/2 \leq 1.5h \tag{16}$$

The highest clamping stress σ_z at section that is L_s away from the face of the column can be calculated as:

$$\sigma_z = \frac{V}{ab}\left(\frac{2.5}{0.6+4\frac{L_s}{c}} - 0.5\right) \qquad 0 < L_s < c \tag{17}$$

$$\sigma_z = 0 \qquad L_s \geq c \tag{18}$$

Where V is the shear force calculated at the face column, b is the width of the beam and a is calculated as:

$$a = \frac{l_b+2L_0}{4} \tag{19}$$

The value of h_z for a section at distance L_s away from the end of the bearing plate is:

$$h_z = h(1 - \frac{L_s}{c}) \tag{20}$$

Figure 3.19 (b) shows the clamping stress distribution due to the uniformly distributed load, the clamping stress is equal to:

$$\sigma_z = \frac{P}{bL} \tag{21}$$

Where P is the total column load, b is the width of the beam and L is the total length of the beam.

The total clamping stress distribution is given by superimposing the two cases of point load and uniformly distributed load. It is possible to obtain the distribution of clamping stresses over the height of the section assuming a linear distribution and that at the boundaries the clamping stresses should be equal to zero where no external force is applied.

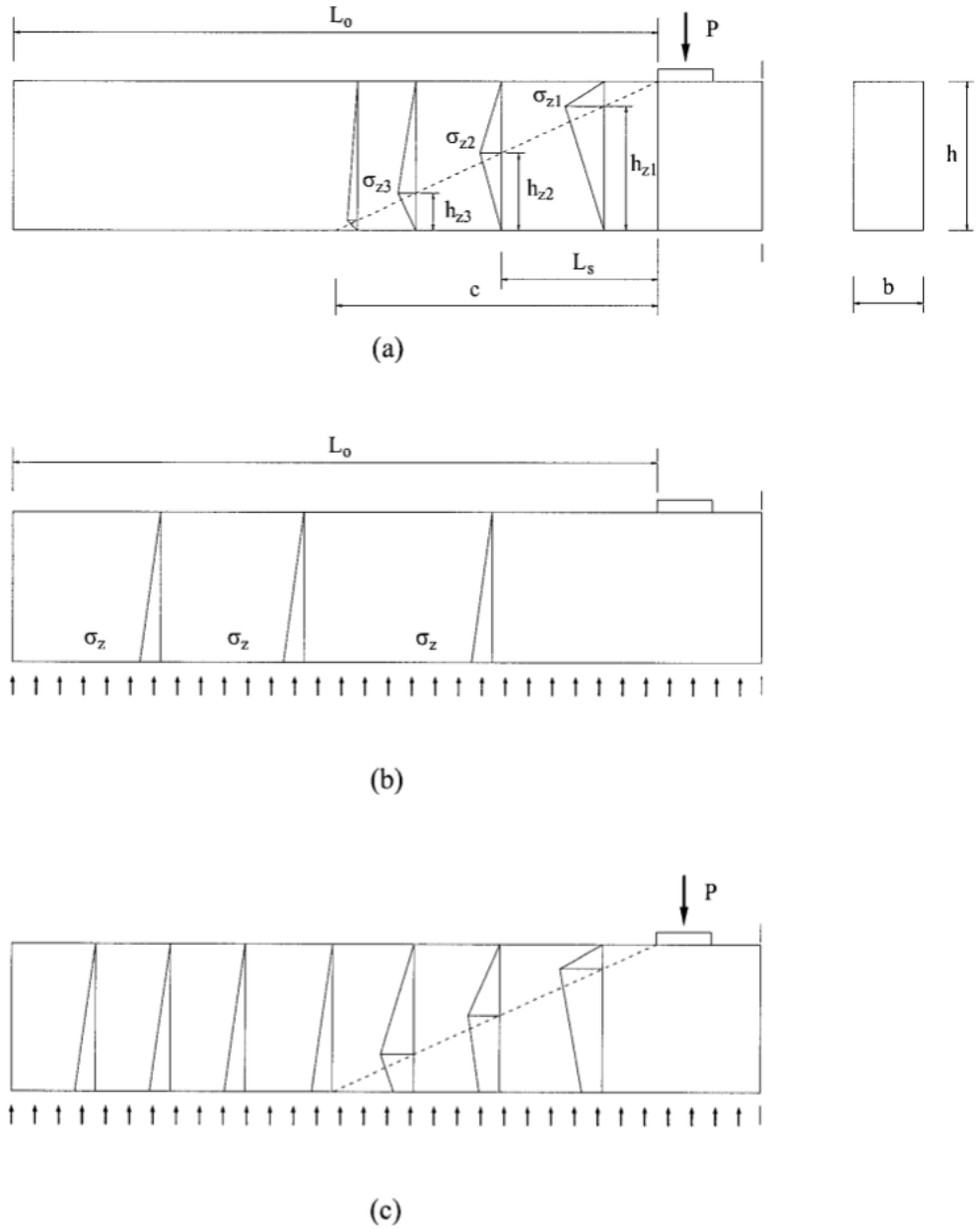

Figure 3.19: Clamping stress distributions along the overhang of a footing. (a) due to the point load; (b) due to the uniformly distributed load; (c) due to the combined action of the previous [3]

3.5 Strut-and-tie models (STM)

Many researches have been made to predict the behavior of disturbed regions, in particular, strut-and-tie methods were developed.
Ritter (1899) developed a truss model to explain the resistance in shear of cracked reinforced concrete beams. This model consists of horizontal compression and tension chords, vertical tension ties and compression diagonals inclined at 45° to the longitudinal direction. *Ritter*'s model was in 1909 refined by *Mörsch* and *Goodrich* by replacing the discrete diagonal compressive struts with a continuous field of diagonal compression. It is necessary to specify that these early models neglected the tensile stresses in the cracked concrete and assumed that after cracking the diagonal compression stresses would remain at 45°.
Leonhardt (1965) found that the inclination of the diagonal struts varies depending on cross-section and the properties of the shear reinforcement. He suggested consequent tensile forces in the principal tension direction along with tensile forces of stirrup. He also found that a constant amount of shear is resisted by the concrete.
Rogowsky and *MacGregor* (1986) empirically demonstrated that the tension force in the bottom chord decreases towards the support due to a series of diagonal strut members. Truss models were then developed by *Schlaich* and *Weischede* (1982) and *Schlaich* et al. (1987), they defined B- and D-regions and proposed to develop strut-and-tie models (STM) for use in D-region as shown in Figure 3.20. Then, they generalized the truss analogy in order to apply the strut-and-tie model to each part of any structure.

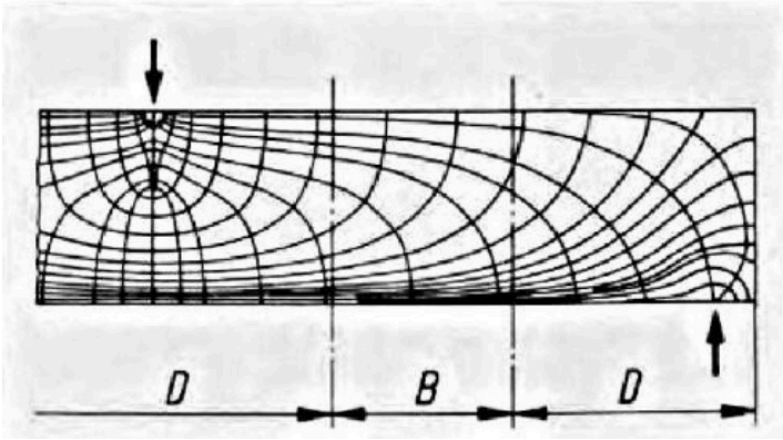

Figure 3.20: Stress trajectories, B- and D-regions (Schlaich et al. 1987)

For solutions of these two regions, it was suggested that the B-region could be modelled by beam theory and the D-region by a strut-and-tie model (STM). These two regions need to be compatible. The sectional forces on the boundaries of B-regions form the input forces to the STM to calculate internal forces in the D-regions. [12]
Concrete struts could be subjected to bidirectional strains, compressive strains in the strut direction and tensile strains in the perpendicular direction. *Collins* and *Mitchell* (1986) described the approach (see also paragraph 3.2.1 Modified Compression Field Theory (MCFT) (*Vecchio* and *Collins*, 1986)) using equilibrium conditions, strain compatibility, and material

stress-strain relationships. They demonstrated the crushing strength of a compressive strut with respect to the orientation of a tension tie passing through the strut based on the softening effect of concrete due to transverse tensile straining. [12] They modelled the internal flow of forced in distributed regions using compressive struts to represent the concrete uniaxial compression, tension ties to model the principal reinforcement and nodal zones which represent the part of concrete subjected to multidirectional stresses where the strut and tie meets. [3] The model considering the strain conditions of the concrete and the reinforcement in the vicinity of the strut is in use by the Canadian Code CSA Standard A23.3 (CSA, 1984) and the AASHTO LRFD (AASHTO, 1994).

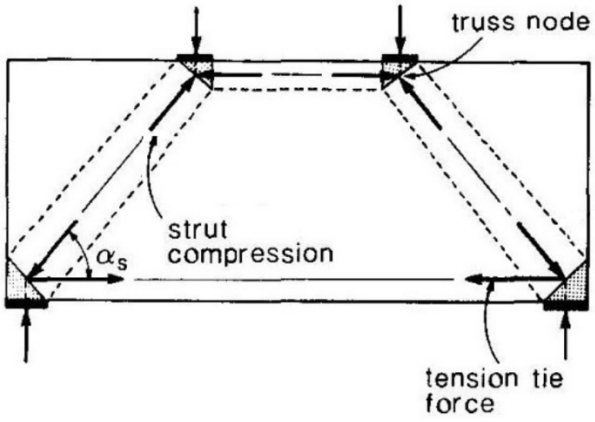

Figure 3.21: Truss model, Strut and tie model for a deep beam (Collins and Mitchell 1986)

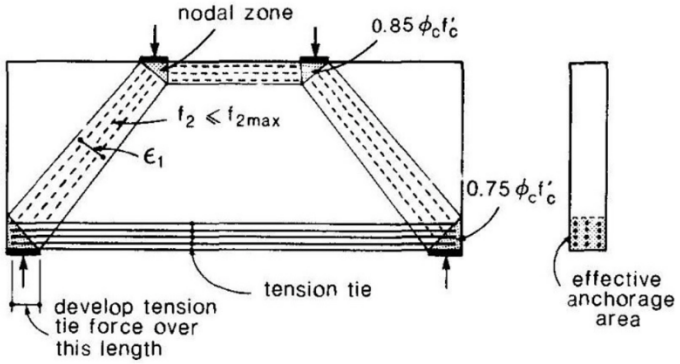

Figure 3.22: Flow of forces, Strut and tie model for a deep beam (Collins and Mitchell 1986)

It is demonstrated by the 2PKT that AASHTO29 strut-and-tie model, which does not account for the size effect, provides an approximate lower bound to the predictions of the 2PKT method. For these beams, the ACI strut-and-tie model, which also neglects the size effect, produces similar predictions. [4]

STM for footings

In a strut-and-tie model the struts represent concrete stress fields with prevailing compression in the direction of the strut. Accordingly, the ties normally represent one or several layers of tensile reinforcement. However, model ties can occasionally also stand for concrete tensile stress fields.
This method implies that the structure is designed according to the lower bound theorem of the theory of plasticity. However, since structural materials, in particular concrete, permit only limited plastic deformations, the internal structural system (the strut-and-tie model) has to be chosen in a way that the deformation capacity is not exceeded at any point, before the assumed state of stress is reached in the rest of the structure. [33]

It is interesting to mention that *Adebar* and *Zhou* developed a simple rational design method, strut-and-tie model, for deep pile caps in which the maximum bearing stress is considered a better indicator of shear strength than the "shear stress" on any prescribed critical section. In deep pile caps the shear stress is concentrated in zones (compression struts) between the column and piles, and is not uniform over the height, which makes it difficult to calculate a meaningful shear stress. The procedure suggested is based on the proposition proposed by *Schlaich* et al. that an entire D-region of a concrete structure can be considered safe if the maximum bearing stress is maintained below a certain limit. [34]

4. Extended 2PKT for footings

4.1 Introduction

As it is seen and explained in previous chapters, generally, footings are large beams supported by the soil. The loading and the support conditions induce significant clamping stresses into these elements. Shear design procedures based on sectional models and code prescriptions do not take into account the beneficial effects of the clamping stresses on the shear capacity of the member. Therefore, new models and theories are needed in order to capture the shear behavior of concrete compact footings. In *Chapter 3* some theories regarding the strength provision of such elements were explained and, in particular, the two-Parameter Kinematic Theory (2PKT) for shear behavior in deep beams developed by *Mihaylov* (2013) was explicated. By means of the 2PKT it is possible to predict the shear failure load, the crack widths near failure, and the complete deformed shapes of diagonally cracked point-loaded deep beams subjected to single curvature. The two parameters involved in the models are the ultimate vertical displacement of CLZ (Critical Loading Zone) and the average tensile strain in the longitudinal reinforcement on the flexural tension side. The theory allows to consider the size effect for deep beams; therefore, the obtained shear provisions are more accurate with respect to code's ones based on sectional models. In fact, the beam's mechanism of shear resistance strictly depends on the size of the element itself. A slender beam is a structural member with a shear span-depth ratio, *a/d*, greater than 2.3 and its behavior is consistent with "*plane sections remain plane*" and shear resistance is attributed to the ability of the cross section to transfer shear across a diagonal crack. While for deep beams the statement is no more valid, the shear strain becomes dominant and the deformation pattern becomes more complex. Shear resistance is attributable to stirrups contribute, aggregate interlock of concrete of the primary diagonal crack, dowel action of longitudinal reinforcement and shear capacity of the CLZ.
The extension of the 2PKT for shear behavior in concrete compact footings represents the main objective for this research and the principal topic of the current chapter.
Thus, the loading conditions and the shear resistance contributions are adapted to the practice of footings. It is necessary to remind the main assumptions for the considered elements: the one-way shear behavior is studied taking into account a strip of footing subjected to one vertical point load coming from the column of the superstructure and uniformly distributed load (UDL) which represents the soil pressure. In practice the pressure transmitted by the soil is not uniformly distributed along the length of the member, but it depends on the material type of the soil foundation. A simplified assumption allows to consider it as uniform.
In the following sections the main factors that contribute to shear resistance are explicated and the uniformly distributed load in the bottom part of the footing is now included in the theory. After the extension of the theory for footings, the following step in next chapter will be the validation of the theory by means of real tests and FEM analysis validated against real laboratory tests results.

4.2 2PKT adapted for shear behaviour of footings

The extended two-Parameter Kinematic Theory (2PKT) for footings is an expansion of the 2PKT developed by *Mihaylov* (2013), able to predict the whole force-displacement response of a deep beam under shear behavior. The two-Parameter Kinematic Theory (2PKT) adapted to compact concrete footings is capable of predicting the shear failure load, the crack widths near failure, and the complete deformed shapes of diagonally cracked point-loaded elements sustained by uniform soil pressure. At the basis of the theory there is the modeling of the Critical Loading Zone (CLZ). As for the 2PKT for beams, the CLZ is the most stressed area of concrete near the point of load application. The two parameters of the theory (two Degrees of Freedom, 2DOFs) are: the ultimate vertical displacement of the CLZ and the average tensile strain in the longitudinal reinforcement on the flexural tension side.
The extended 2PKT for footings, as the theory developed for beams, in addition to the kinematic conditions, includes equations for equilibrium and stress-strain relationships for the materials. The 2PKT estimates the components of shear resistance, evaluated at failure.

The 2PKT, computes four different shear resistant forces capable of giving contribution to the total shear resistance:

- V_{CLZ} is the shear contribution given by the Critical Loading Zone (CLZ);
- V_{ci} is the shear carried by the aggregate interlock;
- V_d is the shear contribution given by the dowel effect;
- V_s is the shear carried by transverse reinforcement (stirrups).

All shear contributions are calculated as a function of Δ_c and when summed, they provide the total shear resisted by the member.

While, the extended 2PKT for footings, estimates two different shear resistant forces capable of giving contribution to the total shear resistance:

- V_{CLZ} is the shear contribution given by the Critical Loading Zone (CLZ);
- V_{ci} is the shear carried by the aggregate interlock.

In this case the contribution of the stirrups is not considered because generally the footings are built without shear reinforcement and the dowel action effect is neglected in order to obtain conservative results, in fact, in practice, these elements are predisposed of light longitudinal reinforcement.

In Figure 4.1 it is possible to observe the general footing without stirrups and only with the longitudinal bottom reinforcement, it is subjected to a vertical point-load in correspondence of the symmetry axis and it is also sustained by uniform soil pressure. In order to extend the theory, some assumptions are performed. First of all, the uniform soil pressure below the main diagonal does not change the 2PKT calculations (of length $l_{b3} = L - l_{b2} = hcot\alpha_1$), in fact, this part was not considered also in the original theory for beams, but it affects P, thus:

$$P = \frac{V_{2PKT}}{l_{b2}} L \tag{22}$$

The remaining distributed load is supposed as concentrated in order to attribute it at the 2PKT for beams, in fact V_{2PKT} is predicted by the 2PKT at failure.
Therefore, the shear strength of the critical loading zone is, similarly to the one for beams, as follow:

$$V_{CLZ} = kf_{avg}bl_{b1e}sin^2(\alpha_1) = k \cdot 1.43f_c^{0.8}bl_{b1e}sin^2(\alpha_1) \quad (23)$$

Where k is the crack shape coefficient, for footings $k = 1$ because $cot(\alpha_1) \leq 2$.

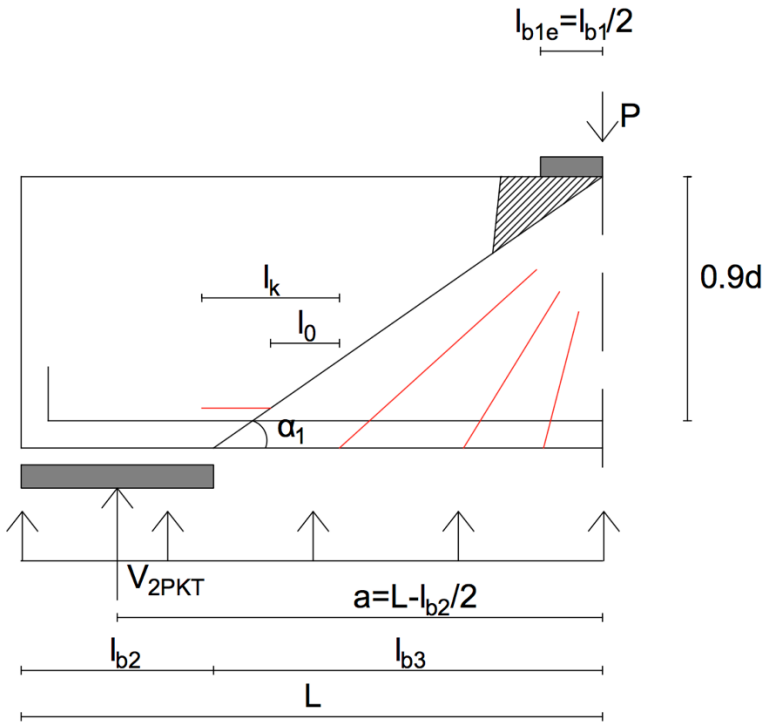

Figure 4.1: Adapted 2PKT for footings

The shear span a is equal to:

$$a = L - \frac{l_{b2}}{2} \quad (24)$$

The procedure of calculations and the formulae are exactly the ones explicated for the 2PKT for beams in paragraph 3.3 Two-Parameter Kinematic Theory (2PKT) for Shear Behaviour. The part above the main diagonal crack of inclination α_1 is considered again a rigid block. Below are shown the formulae that change for the 2PKT for footings compared to the original 2PKT for beams.

$$l_{b2} = L - a \cdot cot\alpha_1 \quad (25)$$

$$tan\alpha_1 = tan\alpha = \frac{1.4d}{\frac{2L}{3} - \frac{l_{b1}}{2}} \rightarrow \alpha_1 = \arctan\left(\frac{1.4d}{\frac{2L}{3} - \frac{l_{b1}}{2}}\right) \quad (26)$$

$$l_k = l_0 + s_{max} \rightarrow \ l_k = 2l_0 = 2s_{max} \tag{27}$$

Where l_{b2} is the length of the part of the uniform soil pressure that affect the 2PKT calculations; $tan\alpha_1$ is derived from footings punching tests [28] and l_k is the length of the bottom reinforcement whose elongation contributes to the width of the diagonal critical crack, l_0 is the length of the heavily cracked zone at the bottom of the critical crack and s_{max} is the spacing of the radial cracks at the bottom of the section.

The extended theory is evaluated for footings without shear reinforcement; thus, the final shear capacity will have two contributions: the shear resisted by aggregate interlock (V_{ci}) and the strength of the Critical Loading Zone (V_{CLZ}). The shear resisted by the dowel action (V_d) was not taken into account: the low amount of reinforcement produces a negligible shear resistance. In fact, in practice the footings are lightly reinforced large beams, therefore, in order to obtain conservative shear predictions, the dowel action effect is not taken into account.

$$V = V_{CLZ} + V_{ci} \tag{28}$$

The procedure calculation is iterative and below the main steps are explicated.

The crack width is computed as follow:

$$w = \Delta_c cos\alpha_1 + \frac{l_k \varepsilon_t}{2sin\alpha_1} \tag{29}$$

Where ε_t is the average between the left $\varepsilon_{r,L}$ and right $\varepsilon_{t,R}$ strain with respect to the diagonal crack side.

$$V_{ci} = \left(\frac{v_{ci}}{tan\alpha_1} + n_{ci}\right) bd \tag{30}$$

Where $v_{ci} = \frac{0.18\sqrt{f_c}}{0.31+\frac{24w}{a_g+16}}$ and $n_{ci} = 0$.

The iterative procedure computes the shear demand at the end of iteration 1:

$$V_m = \frac{E_s A_s \varepsilon_t}{a} z \tag{31}$$

At the end of iteration 1, if $V_m < V$, then the new $\varepsilon_{r,L}$ is equal to ε_t, otherwise $\varepsilon_{r,L}$ does not change; if $V_m < V$, then the new $\varepsilon_{t,R}$ is equal to $\varepsilon_{t,R}$, otherwise ε_t does not change.
The iteration 2 starts again from equation (29) computing w' and the last iteration ends when $V = V_m$ with an error equal to zero ($V - V_m = 0$).

4.3 Solution procedure

As for the general 2PKT for deep beams, also in the extended 2PKT for footings, degree of freedom Δ_c is obtained by assuming that the CLZ is at failure under diagonal compressive stresses, while DOF $\varepsilon_{t,avg}$ is obtained as illustrated in Figure 3.17. The thick black line in the plot shows the relationship between $\varepsilon_{t,avg}$ and the applied shear V, while the red line represents the shear resistance which decreases with increasing strains. In the case of footings, the resistance consists of two components: shear carried in the CLZ (V_{CLZ}) and aggregate interlock component (V_{ci}).

The solution of the equations of the 2PKT correspond to the intersection point of the black and red lines which relates to the equilibrium point for shear forces. This graphical representation of the 2PKT is similar to that used by *Muttoni* in a critical shear crack theory for punching of slabs [29]. As the equations of the model are not suitable for a closed-form solution, the shear strength is found by an iterative solution procedure.

Since V needs to be resisted by the two shear contributions mentioned above, the following equation must be respected:

$$V_{CLZ} + V_{ci} = \frac{T \cdot 0.9d}{a} \tag{32}$$

where T is the tension in the bottom longitudinal reinforcement, $0.9d$ is the assumed lever arm between the compression force C and T, and a is the shear span.

Since this theory aims to predict the shear resistance for any value of displacement, the shear contributions are calculated as function of the two computed DOFs. The shear carried by the Critical Loading Zone (CLZ) is defined as a function of the vertical displacement Δ_c of the CLZ in Figure 4.2. It is necessary to specify that the CLZ has a width that depends on the effective width of the loading plate. The concrete in this zone is subjected to high compressive stresses and fails when the maximum strain reaches the crushing limit of 3.5×10^{-3}. The strain profile in the CLZ is assumed to vary linearly from zero to ε_{max} as shown in Figure 4.2.

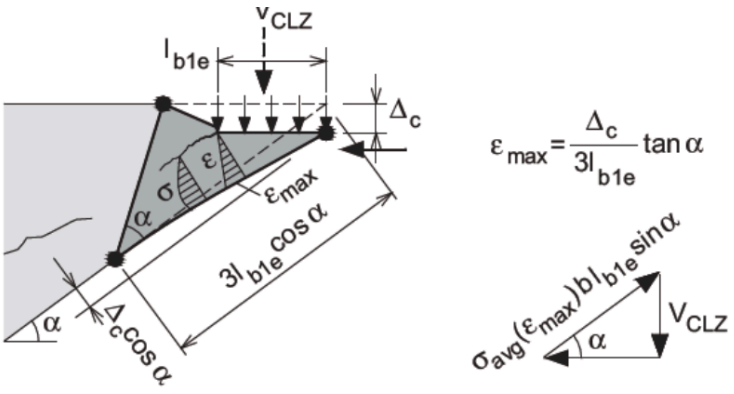

Figure 4.2: Critical Loading Zone [4]

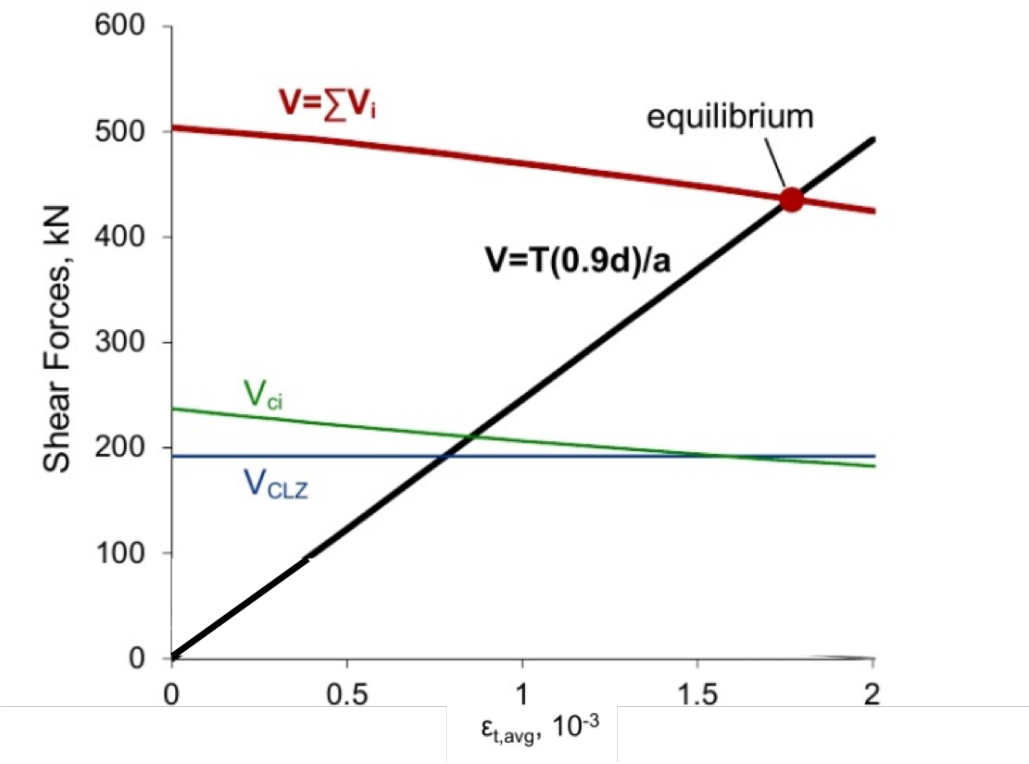

Figure 4.3: Components of shear resistance for footings and equilibrium at peak load

Considering now the two components that will constitute the actual shear strength prediction for footings (Figure 4.3), the aggregate interlock is affected by the strain in the bottom longitudinal reinforcement: by increasing the strain, wider cracks will form. Consequently, wider cracks will also lead to less aggregate interlock forces. Therefore, the curve representing the aggregate interlock decreases with the strain increment.

In Figure 4.3, the thick black line represents the shear obtained from moment equilibrium as derived in equation (32). The curve is bilinear because of the effect of tension stiffening effect. The first part of the curve is stiffer because of the contribution of the concrete matrix around the bars which resists tensile forces. The second part represents the contribution of the reinforcement only since the concrete around the bars has reached its tensile strength. The intersection of the thick black line and the red line, which represents the sum of all the shear contributions, allows to compute the strain and the shear force at equilibrium. The intersection point requires an iterative procedure of calculations.
It is possible to represent the final curve for shear behavior of the footing: it is computed by repeating the calculations for different values of Δ_c and associating each Δ_c to the correspondent value of $\varepsilon_{t,avg}$ after equilibrium.

The shear resistance components, thus Critical Loading Zone and aggregate interlock for footings without shear reinforcement, calculate that, generally, the main shear contribution for footings is principally produced by the aggregate interlock mechanism. In fact, increasing the

dimension of the element, the Critical Loading Zone deforms more, and the diagonal cracks are wider, therefore the shear stresses transmitted throughout the cracks reduces.
Generally, the CLZ provides the second most important shear resistance, therefore, the failure of the element is driven by the failure of the CLZ. This was the basic hypothesis for the 2PKT and the extended 2PKT for footings maintain the same assumption. It means that the concrete in the critical loading zone crushes.

4.4 Flexure

It should be noted that in the 2PKT the flexural reinforcement is assumed to behave linearly, while yielding of the reinforcement can be taken into account by performing a flexural strength calculation based on typical code provisions. The final predicted failure load will be the minimum load obtained from a 2PKT shear calculation and a standard flexural strength calculation.
Therefore, the shear strength predicted by the extended 2PKT must be compared to the flexural calculations. Thus, also the flexural failure should be evaluated and, as consequence, the minimum between the 2PKT shear strength prediction and the flexural strength prediction will be the actual strength. The general procedure for flexural calculations is displayed below.

Calculation of the neutral axis of the section: $x = \frac{A_s f_y}{0.8 f_c b}$ (33)

Calculation of the ultimate bending moment: $M = A_s f_y (d - 0.4x)$ [kNm] (34)

Calculation of the ultimate load: $P = M / \left(\frac{L^2}{4}\right)$ [kN/m] (35)

Check for yielding of the steel: $\frac{\varepsilon_s}{\varepsilon_y} = \frac{-f_{cu} + \frac{f_{cu}}{d} x}{\frac{f_y}{E_s}} > 1$ [-] (36)

4.5 Conclusions

As previously mentioned, the actual strength for concrete footings is given by checking the failure mode, thus, comparing the shear failure load computed with the 2PKT and the flexural strength prediction. The minimum between these two strengths will be the failure load:

$$P_u = min\{P_{2PKT}; P_{flex}\} \quad (37)$$

The scope of this chapter was the development of the 2PKT for footings, adapting the loading conditions and the shear resistance contributions that interest this member with respect to the ones for beams. In fact, the main factors that contribute to shear resistance are the shear forces resisted by the critical loading zone and by aggregate interlock. The stirrups contribute is not

present because one of the main assumptions is to consider footings without shear reinforcement, which in practice is respected. Then, footings have generally low longitudinal reinforcement ratio, therefore, the dowel action is neglected in order to obtain conservative results and remain on safe side. The uniformly distributed load in the bottom part of the footing affects the vertical applied load *P* just for the rigid block above the main diagonal crack; while the uniformly distributed load in the part below the main diagonal crack is not considered by the theory, as it was for the 2PKT for deep beams. With the predicted DOFs, as for the 2PKT for shear behavior in deep beams, the extended 2PKT for concrete footings can also be used to evaluate the deformation patterns of the beam near shear failure, including crack widths, deflections, and the complete displacement field of the footing.

In the next chapter the extended 2PKT for footings is validated thanks to laboratory tests and Finite Element Models validated against real tests. Therefore, the calculations for the database of footings are implemented, the procedure is iterative (the complete last step for the iteration is displayed in the Appendix 3).

5. Validation of models and parametric study

5.1 Introduction

Once the 2PKT has been adapted to shear behavior for large compact footings, the next step is the validation of the theory and the model by means of laboratory tests. Due to the lack of significative and adequate tests in the literature suitable for the made hypothesis, a non-linear finite element analysis is performed. It is important to specify the assumptions adopted for these concrete members: large-scale specimen without stirrups with uniformly distributed soil pressure and a point-load along the geometrical axis coming from the column of the superstructure.
In addition to experimental tests and to the creation of a proper database, it is necessary to develop and deepen the knowledge regarding one-way shear behavior of large compact footings by finding a general trend, varying some characteristic parameters and understanding their influence, then, by proposing an analytical model and comparing the predictions with the results obtained by tests.
First of all, it is necessary to validate the FEM, therefore the *Uzel*'s tests are reproduced using the program VecTor2 and the predicted failure loads are compared with the actual ones. After the validation of the FEM approach, it is possible to compute the shear strength provisions for *Uzel*'s tests by means of the adapted 2PKT. Finally, in order to enlarge the database of footings and further demonstrate the validity and the efficiency of the 2PKT, a parametric study is computed. The objective is to validate the analytical model finding a tendency for the compact footings with the mentioned characteristics, in particular by varying the longitudinal reinforcement ratio, the compressive strength and the length of the footing.

5.2 Strength predictions

5.2.1 FEM strength predictions

Non-linear finite element models of footings subjected to uniformly distributed loads and point-load from the column are modelled by using the program VecTor2 as specified and illustrated in *Chapter 3* (section 3.2.4 General layout of Finite Element Mesh).
The obtained results are shown in Table 5.1, and the experimental-to-predicted strength is computed in the last column. As it is possible to observe the mean value is 1.02 and the coefficient of variation (CoV) is 6%. Thus, the achieved results are reliable, and the FEM approach is validated. Consequently, it is possible to create, starting from these models based on real tests, other samples changing some parameters.
For *Uzel*'s tests, also load-displacement charts are produced and the comparison of FEM prediction with respect to the experiment results is shown in Appendix 4.

Uzel	Test Total Load (kN)	FEM (kN)	Ratio Exp/Pred (-)
UN100	1186	**1149**	1,03
AF3	541	**494**	1,09
AF6	1298	**1398**	0,93
AF7	713	**739**	0,96
AF11	2645	**2448**	1,08
AF11-r1	1408	**1335**	1,05
AF13	1857	**1848**	1,00
		Avg	1,02
		CoV	0,06

Table 5.1: FEM strength prediction for Uzel's tests

5.2.2 2PKT strength predictions

The 2PKT predictions for the *Uzel*'s tests (2003) are shown in Table 5.2 and the experimental-to-predicted strength is displayed in the last column. It is necessary to specify that in the following chart, only shear is taken into account, obviously the sample may failure in flexure therefore in next paragraph (5.2.3 Flexural calculations), flexure is evaluated and then in section 5.2.4 Comparison of results), the failure mode is determined taking the smallest computed failure load between shear and flexure. The 2PKT predictions are calculated by following the prescriptions in *Chapter 4* for extended 2PKT for concrete footings.
The results obtained by 2PKT predictions are quite good except for the sample AF11-r1 which fails in flexure, as it is stated by *Uzel*, during the laboratory tests. For four of the considered samples the prediction is conservative, thus on safe side. For AF13 the prediction is quite far from the measured strength during the test, even if it is conservative, it is necessary to analyze this value because it is too conservative. Sample AF13 has longitudinal reinforcement ratio almost three times with respect to the other considered specimens, therefore the dowel action might be a non-negligible component. More detailed calculations and explanations regarding AF13 are developed in Appendix 3.

The same procedure is performed also for the previously mentioned Richardt's tests (2.3 Tests in the literature), again only the shear failure is evaluated applying the 2PKT method, but observing the results, the failure loads is largely overestimated, thus probably the flexural load will be smaller in those cases and the flexural calculations will produce better results. The 2PKT overestimates the actual test load. It is necessary to repeat that *Richart*'s tests are not properly large-scale tests. In Table 5.3, all the tests are presented, but not always they are suitable with the conducted analysis of the shear behavior of footings, this is why the obtained results are not reliable in this case.

The complete chart with data of the specimens is displayed in Appendix 1 and the 2PKT calculations are shown in Appendix 2.

Uzel	Test Total Load (kN)	2PKT (kN)	Ratio Exp/Pred (-)
UN100	1186	**1203**	0,99
AF3	541	**497**	1,09
AF6	1298	**1515**	0,86
AF7	713	**609**	1,17
AF11	2645	**2492**	1,06
AF11-r1	1408	**2492**	0,56
AF13	1857	**1124**	1,65
		Avg	1,05
		CoV	0,31

Table 5.2: 2PKT strength prediction for Uzel's tests

Richart	Test Total Load (kN/m)	2PKT (kN/m)	Ratio Exp/Pred (-)
501a	639	**751**	0,85
501b	616	**756**	0,81
502a	898	**2109**	0,43
502b	937	**2002**	0,47
503a	950	**2116**	0,45
503b	892	**2087**	0,43
504a	474	**456**	1,04
504b	511	**468**	1,09
505a	800	**1391**	0,57
505b	766	**1405**	0,55
506a	730	**1300**	0,56
506b	730	**1428**	0,51
		Avg	0,65
		CoV	0,37

Table 5.3: 2PKT strength prediction for Richart's tests

5.2.3 Flexural calculations

In this section, the flexural calculations are performed following the section 4.4 Flexure. In Table 5.4 and Table 5.5 the flexural results for *Uzel*'s tests and *Richart*'s tests are presented. Then they must be compared to the 2PKT prediction for shear failure.

Uzel	Test Total Load (kN)	Flexural Calculations (kN)	Ratio Exp/Pred (-)
UN100	1186	**1356**	0,87
AF3	541	**511**	1,06
AF6	1298	**1523**	0,85
AF7	713	**681**	1,05
AF11	2645	**2055**	1,29
AF11-r1	1408	**2055**	0,69
AF13	1857	**2627**	0,71
		Avg	0,93
		CoV	0,23

Table 5.4: Flexural prediction for Uzel's tests

Richart	Test Total Load (kN/m)	Flexural Calculations (kN/m)	Ratio Exp/Pred (-)
501a	639	**650**	0,98
501b	616	**651**	0,95
502a	898	**692**	1,30
502b	937	**689**	1,36
503a	950	**692**	1,37
503b	892	**691**	1,29
504a	474	**626**	0,76
504b	511	**631**	0,81
505a	800	**589**	1,36
505b	766	**589**	1,30
506a	730	**585**	1,25
506b	730	**590**	1,24
		Avg	1,16
		CoV	0,19

Table 5.5: Flexural prediction for Richart's tests

5.2.4 Comparison of results

In order to check the failure mode, as previously mentioned, the shear failure load computed with the 2PKT is compared with the flexural calculation and the minimum one is taken as failure load:

$$P_u = min\{P_{2PKT}; P_{flex}\} \tag{37}$$

Applying this to the previous results tables, it is possible to observe in Table 5.6 and Table 5.7 the comparison of experimental results and 2PKT (including flexural calculations comparison) predictions for *Uzel*'s tests and *Richart*'s tests, respectively.
Generally, the achieved results reproduce in a realistic way the actual load and the 2PKT very well reproduce the shear failure load and the global test trend.
As it is possible to observe by comparing the results, the 2PKT well reproduce *Uzel*'s tests and most of the specimens fail in shear; while *Richart*'s tests are better reproduced by the flexural calculations, apart from the series 501 and 504, which are, referring to *Richart* [2] the only ones that fails under diagonal tension, for which in fact the 2PKT predictions are quite precise.

More specific comments are necessary for *Uzel*'s tests: the strength predictions of the 2PKT approach are generally conservative because the average value of the experimental-to-predicted ratio is 1.10, but specimen AF11r1 is largely overestimated and AF13 underestimated. Specifically, AF11r1 presented some problems during the test and it fails in flexure. On the other hand, AF13 has longitudinal reinforcement ratio almost three times with respect to the other considered specimens, therefore the dowel action might be a non-negligible component (in Appendix 3 this aspect is investigated).

Uzel	Test Total Load (kN)	FEM (kN)	Flexural Calculations (kN)	2PKT (kN)	Final (kN)	Ratio Exp/Pred (-)
UN100	1186	1149	1356	1203	**1203**	0,99
AF3	541	494	511	497	**497**	1,09
AF6	1298	1398	1523	1515	**1515**	0,86
AF7	713	739	681	609	**609**	1,17
AF11	2645	2448	2055	2492	**2055**	1,29
AF11-r1	1408	1335	2055	2492	**2055**	0,69
AF13	1857	1848	2627	1124	**1124**	1,65
					Avg	1,10
					CoV	0,28

Table 5.6: Final summarizing table for Uzel's tests

Richart	Test Total Load (kN/m)	2PKT (kN/m)	Flexural Calculations (kN/m)	Final (kN/m)	Ratio Exp/Pred (-)
501a	639	**758**	**650**	**650**	0,98
501b	616	**763**	**651**	**651**	0,95
502a	898	**2109**	**692**	**692**	1,30
502b	937	**2002**	**689**	**689**	1,36
503a	950	**2116**	**692**	**692**	1,37
503b	892	**2087**	**691**	**691**	1,29
504a	474	**505**	**626**	**505**	0,94
504b	511	**516**	**631**	**516**	0,99
505a	800	**1391**	**589**	**589**	1,36
505b	766	**1405**	**589**	**589**	1,30
506a	730	**1300**	**585**	**585**	1,25
506b	730	**1428**	**590**	**590**	1,24
				Avg	1,19
				CoV	0,15

Table 5.7: Final summarizing table for Richart's tests

It can be seen that the 2PKT method well reproduce the observation and the measurements during the large-scale laboratory tests. In particular, in Figure 5.1, it is possible to observe the experimental-to-predicted 2PKT strength for *Uzel*'s tests, and in Figure 5.2 for the FEM modelled tests with different *L/d* ratios. Apart from AF11r1 and AF13, for what has been explained before, the other tests are well reproduced, and the prediction is conservative. In fact, the average experimental-to-predicted ratio obtained with the 2PKT calculations is 1.10 and the Coefficient of Variation is 28% (Figure 5.1). Similarly, in Figure 5.2, the experimental-to-predicted ratios for FEM provisions are plotted for *Uzel*'s tests. It is possible to observe that the results are a good approximation of the actual test shear strength, in fact, the values are all around 1 (as presented in section 5.2.1 FEM strength predictions).
The shear resistance components, thus critical loading zone and aggregate interlock for footings without shear reinforcement, calculate that the size effect for deep concrete footings is principally produced by the aggregate interlock mechanism. In fact, increasing the dimension of the element, the critical loading zone deforms more, and the diagonal cracks are wider, therefore the shear stresses transmitted throughout the cracks reduces.

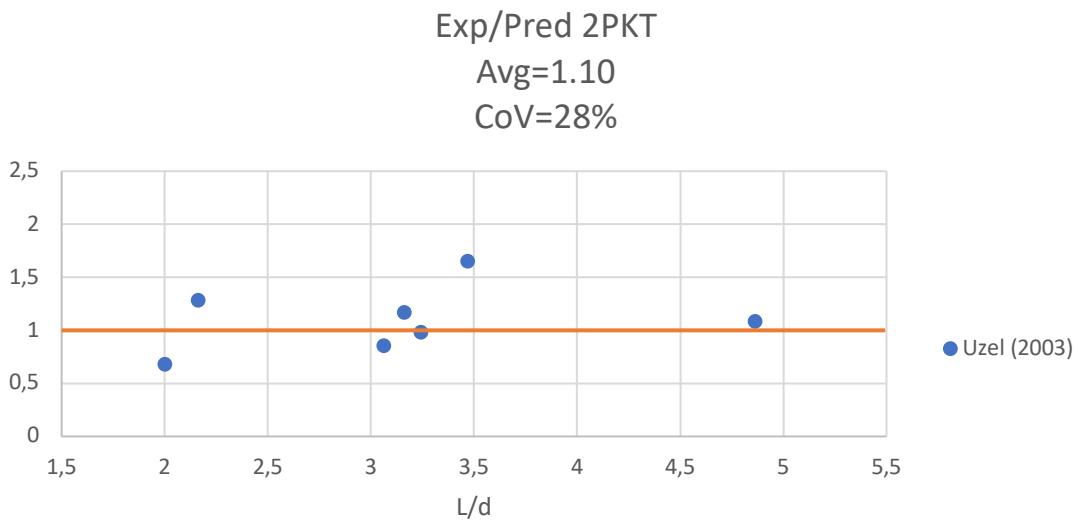

Figure 5.1: Experimental-to-predicted 2PKT strength provisions

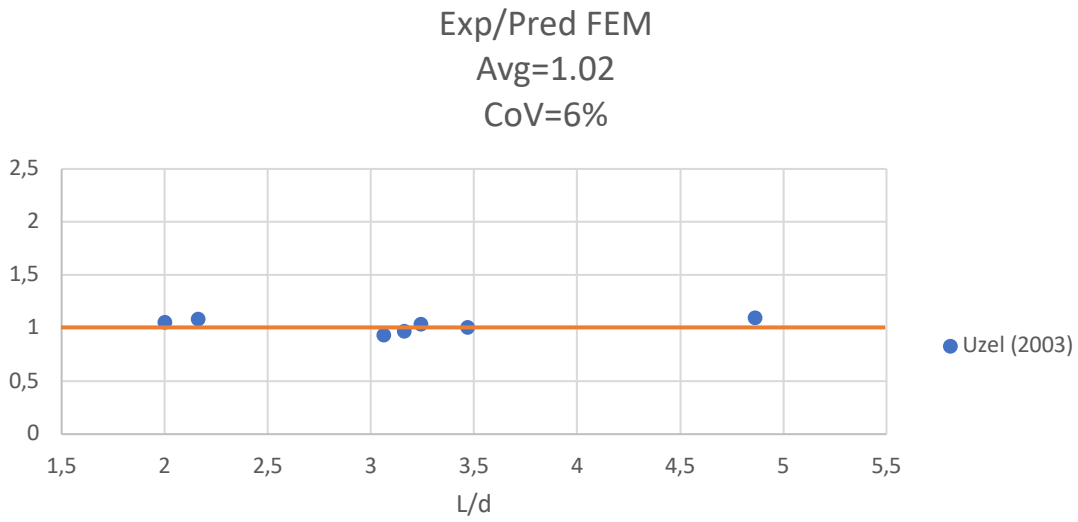

Figure 5.2: Experimental-to-predicted FEM strength provisions

5.3 Deformation patterns near failure

A further comparison between the real information obtained during *Uzel*'s tests and the 2PKT provisions is treated in this section. Specifically, it is possible also to compare the deformation patterns at failure for the specimens between the actual displacement measured during laboratory tests and the 2PKT predictions.

By using the *Principle of Virtual Work (PVW)*, it is possible to predict the displacement of the compact footing imagining it as a truss composed of vertical, horizontal and diagonal elements. In fact, during the laboratory tests performed by *Uzel* (2003) Zurich Targets were placed in precise and calculated position along the face of the tested footing. It is possible to observe the position of those targets from Figure 2.6 to Figure 2.10. The vertical, horizontal and diagonal

distances between the Zurich Targets were measured by the specific gauges. Furthermore, surface deformations were measured by means of gauges on the created grid of Zurich Targets. The vertical and the lateral strains were then calculated based on the change in distance between vertically and horizontally placed targets. The diagonal strains were computed in the change of diagonal distance between the targets.
Knowing the strain at each target, it is possible to compute the displacement, a MatLab code [*Mihaylov*] is created in order to visually observe the displacement of each element of the truss and globally note the behavior of the compact footing under each load stage. In the code it is necessary to introduce the Scale Factor (SF) in order to be able to observe the displacement of each element of the truss system.

The input data for the code are:

- the coordinates of the Zurich Targets supposing the 2D reference system centred in the midpoint of the bottom side of the concrete member;
- the numbering of each square component of the truss;
- the triad of numbers clockwise per each triangular element per each row of targets (as show in Figure 5.3 and Table 5.8);
- the restraint condition (1 means no displacement along *x*-axis and 2 no displacement along *y*-axis) in the matrix of Boundary Condition (BC);
- the column vector F containing the forces per each load stage (LS);
- the data collected and measured by strain gauges during the real laboratory test at the end of each load stage.

As the *PVW* states, the displacement Δ_i can be computed as follow:

$$\Delta_i = \sum \frac{N_i \cdot N_i^*}{EA} L_i = \sum N_i^* \cdot \delta_i$$

Where N_i is the axial load applied to the real system, N_i^* is the unitary axial load applied to the virtual system, A is the cross-sectional area, E is the Young Module and L_i is the length of the element i. In particular, $\frac{EA}{L}$ is the stiffness of the element i.
It is assumed that the displacements are small compared to the dimension of the element.

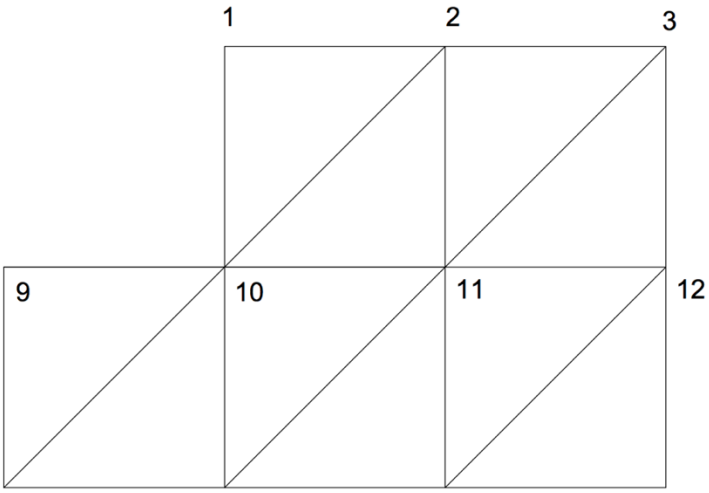

Figure 5.3: Example of mesh and nomenclature

2	11	10
10	1	2
3	12	11
11	2	3

Table 5.8: Example of meshing

First of all, the actual test displacements per each point of the constructed truss are plotted, in Figure 5.4 sample AF11 is displayed with respect to the original position of the truss element. A Scale Factor (SF) equal to 30 is used in order to make the deformations visible. A similar procedure is done also for AF1 UN 100 (Figure 5.7).

The extended two-Parameter Kinematic Theory (2PKT) for compact concrete footings is a kinematic model depending on two parameters, two degrees of freedom: the average strain in the bottom reinforcement, $\varepsilon_{t,avg}$, and the vertical displacement of the critical loading zone, Δ_c. With the predicted DOFs, the extended 2PKT can also be used to evaluate the deformation patterns of the beam near shear failure, including crack widths, deflections, and the complete displacement field.

Therfore, the previously mentioned Matlab code is implemented in order to compare the predicted displacement at failure by the 2PKT and the real test displacement by means of the Zurich Targets. The calculation of the predicted displacements is done by following the equation from (1) to (4) regarding the position of each point with respect to the main diagonal crack, displayed in Figure 5.6 for AF11 and simplified as a straight line.

For sample AF11, the comparison between the actual displacement measured during the test and the 2PKT predictions, represented by blue dots, is shown in Figure 5.5. While for specimen AF1 UN100 the procedure is similar and the comparison between test and 2PKT provisions is displayed in Figure 5.8.

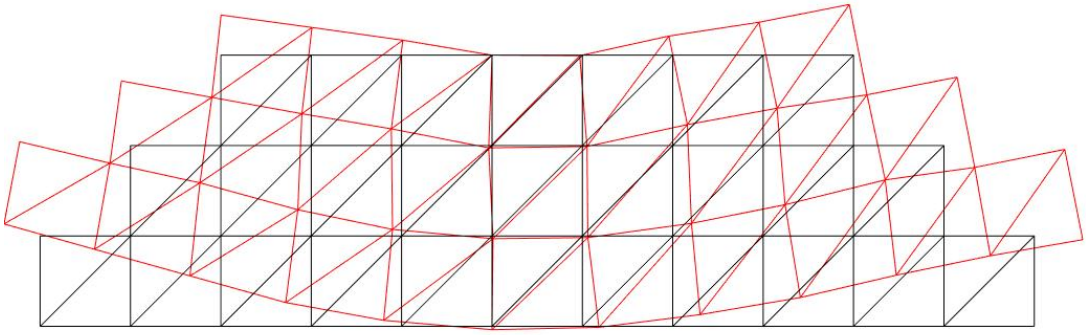

Figure 5.4: Test displacements for specimen AF11 (SF=30)

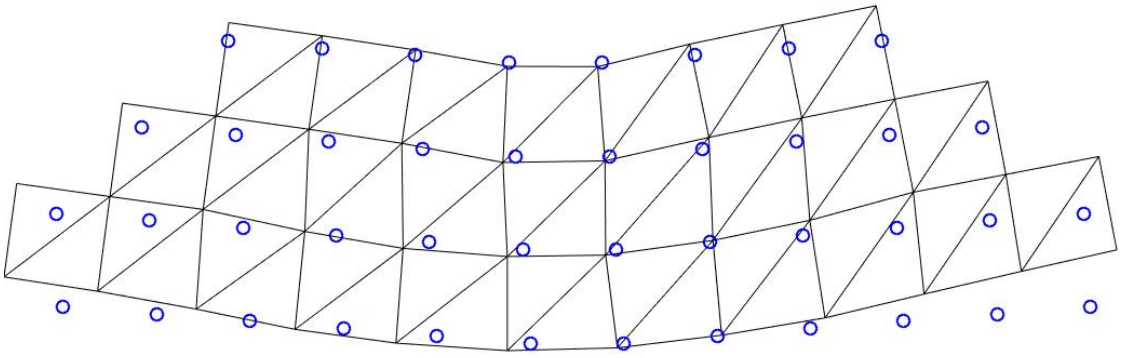

Figure 5.5: Comparison between actual test displacement and 2PKT predictions for AF11 (SF=30)

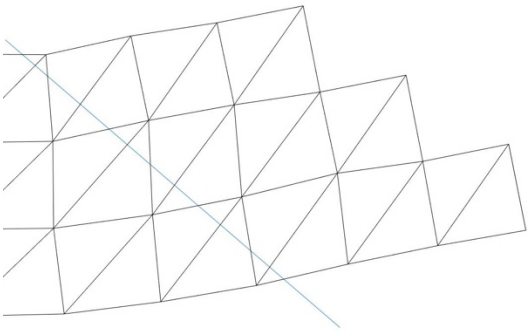

Figure 5.6: Main diagonal crack (simplified as a straight line)

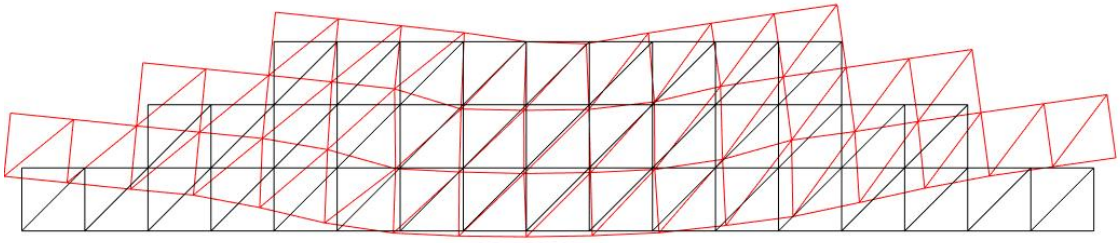

Figure 5.7: Test displacements for specimen AF1 UN100 (SF=30)

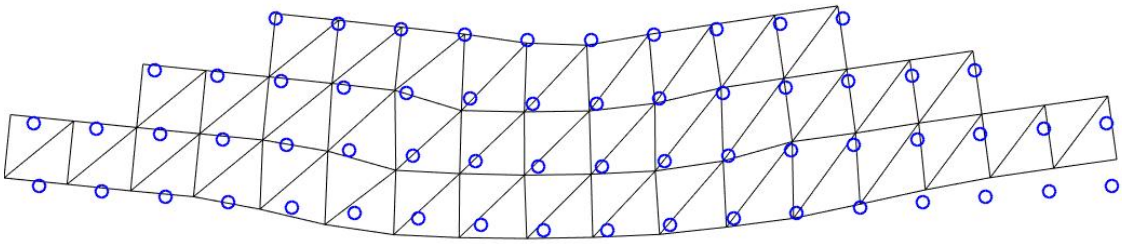

Figure 5.8: Comparison between actual test displacement and 2PKT predictions for AF1 UN100 (SF=30)

By observing Figure 5.5 and Figure 5.8, it is immediately visible the 2PKT predictions for displacements at failure. The global trend and displacement behavior are well reproduced by the 2PKT. The blue dots are not exactly overlapped to the shape of the real displacement tendency, especially for specimen AF11 which is properly called compact footing. The theory predicts better AF1 UN100 which is slightly slenderer. Thus, the 2PKT could be improved regarding the displacement aspect.
It is possible to extend the code for each of *Uzel*'s specimens in order to directly and visually compare the results of the 2PKT. In fact, the comparisons between the actual test displacement and the 2PKT predictions for samples AF3, AF6, AF11r1 and AF13 are shown below.
For specimen AF13 it is necessary to specify that the grid of Zurich Targets was not placed symmetrically during the laboratory test, thus, Figure 5.12 presents a particular shape.

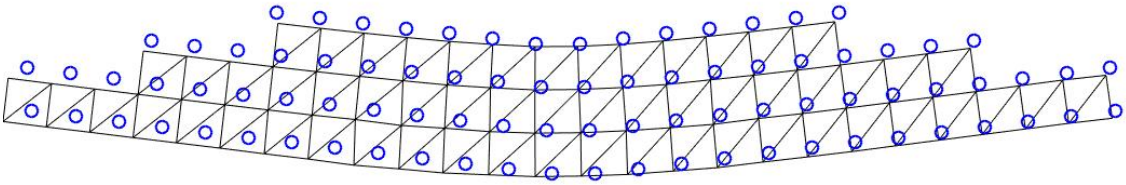

Figure 5.9: Comparison between actual test displacement and 2PKT predictions for AF3 (SF=30)

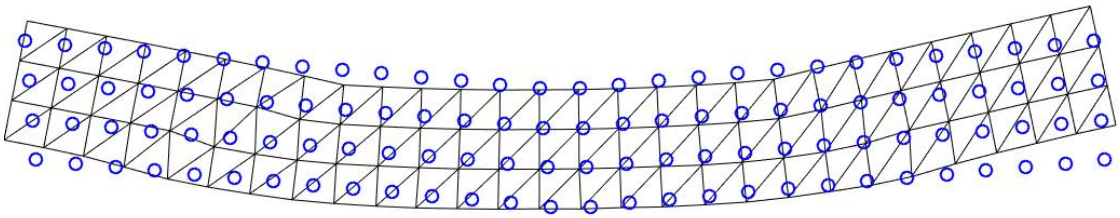

Figure 5.10: Comparison between actual test displacement and 2PKT predictions for AF6 (SF=30)

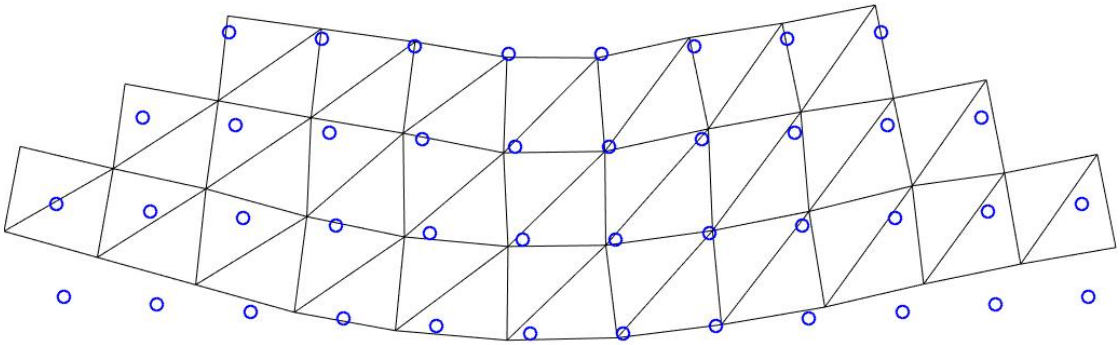

Figure 5.11: Comparison between actual test displacement and 2PKT predictions for AF11-r1 (SF=30)

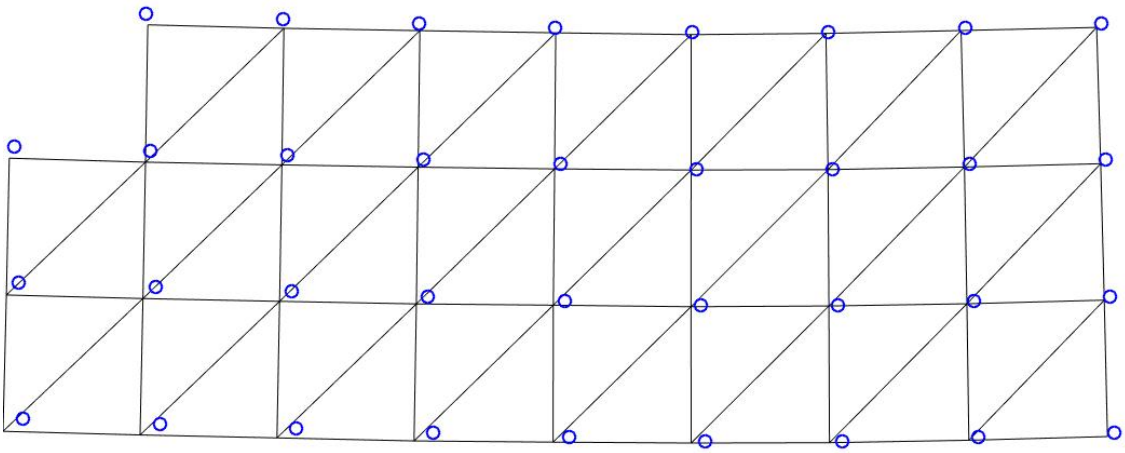

Figure 5.12: Comparison between actual test displacement and 2PKT predictions for AF13 (SF=30)

Strain analysis

Moreover using the MatLab code (implemented in 5.3 Deformation patterns near failure), it is possible to plot the measured strain within two different target, for example in Figure 5.13 the strain measured at the two farther elements versus the load is displayed for sample AF11. The strain at failure measured during the test and displayed in the figure is 2.8 and it is exactly the same as the one predicted by the 2PKT in the last computational iteration for AF11, as it is shown in Table A.3 in Appendix 2: 2PTK Calculations. Therefore, the same comparison between measured strain and predicted one is possible by associating Table A.1 containing test

data and Table A.3 with the predictions computed by the 2PKT. Also, in terms of strain the 2PKT very well reproduce the test results, in fact, it is well estimated, a part for specimen AF13 which is the only *Uzel*'s test with longitudinal reinforcement ratio almost three times the others. In fact, the 2PKT predictions for AF13 are the least accurate and probably this is due to the large amount of longitudinal reinforcement which makes not negligible the dowel action contribution for shear resistance. Regarding this last topic, more considerations are done in Appendix 2: 2PTK Calculations, trying to consider the dowel action for AF13 and for the other high reinforced tests used in the following parametric analysis by varying the reinforcement ratio.

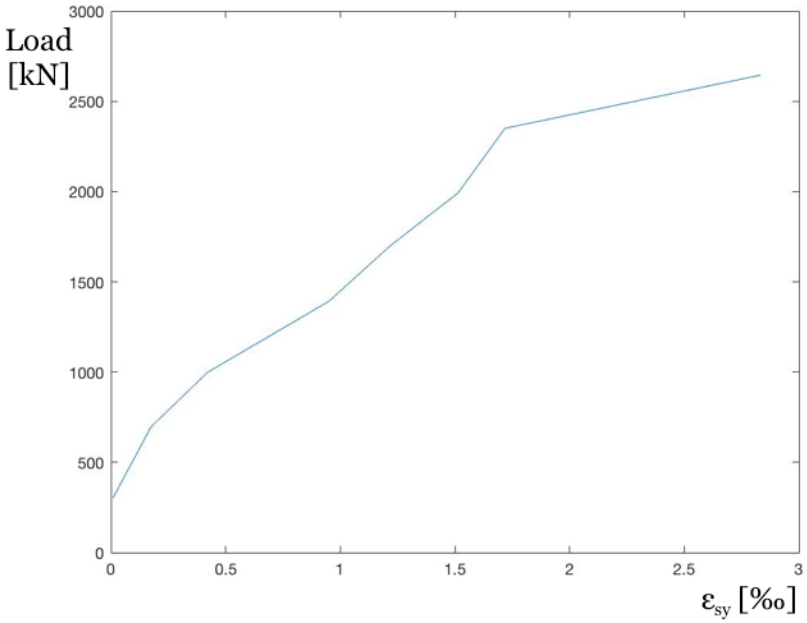

Figure 5.13:Measured strain with respect to total load for AF11

5.4 Parametric Analysis

The extended two-Parameter Kinematic Theory (2PKT) for concrete footings is a kinematic model depending on two parameters, two degrees of freedom: the average strain in the bottom reinforcement, $\varepsilon_{t,avg}$, and the vertical displacement of the critical loading zone, Δ_c. By combining the theory with the equilibrium equations and the stress-strain relationships, it is possible to predict the shear strength (paragraph 5.2.2 2PKT strength predictions for *Uzel*'s tests), the deformation patterns at shear failure (paragraph 5.3 Deformation patterns near failure shows the comparison between tests and 2PKT predictions in terms of displacements and deformation configurations), crack width and maximum deflection.
In order to validate the 2PKT for footings, a parametric analysis is performed. The study is introduced with the aim of demonstrating the validity of the Model by varying one parameter while keeping constant all the other factors. After the adaptation of the theory to compact footings, the parameters included in the parametric study are: the concrete strength f_c, the

longitudinal reinforcement ratio ρ_l and the length of the footing L (keeping d, the effective depth, constant). The tests contained into the parametric analysis are the ones that follow the simple hypothesis of one vertical load coming from the superstructure applied along the symmetry axis of the footings and uniformly distributed load along the whole length of the footing in the bottom side which reproduces the soil pressure. The details of the considered tests are displayed in Table 2.1. In particular, the most interesting samples are AF1 UN100 and AF11 due to their similar characteristics regarding the materials, but different L/d ratio and therefore peculiar for the analysis of deep compact footings. In fact, sample AF1 has L_0/d (shear length to effective depth) equal to 3.2 and sample AF11 has L_0/d equal to 2.0. For each of the specified remarkable sample, the parametric study is achieved. The range of variation of the longitudinal reinforcement ratio is from 0.5% to 2%; the range of variation of the concrete strength is from 20 MPa to 70 MPa and the L/d deviation is from 0.5 to 4.9. Then, in the same chart, the test results from *Uzel* (2003), the parametric study performed with the non-linear finite element models (produced with VecTor2, as illustrated in paragraph 3.2.4 General layout of Finite Element Mesh) and the 2PKT results per each FEM model (computed by iterations, see the last iteration in Table A.3 in the Appendix 2: 2PTK Calculations) are compared for both AF1-UN100 and AF11. The obtained results are three curves for each of the two considered specimens in which only one parameter varies, and the other are kept constant. Therefore, the parametric analysis is based on the use of non-linear finite element calculations validated against experimental results, due to the lack of an extended database for footings in the literature. Only by performing this analysis it is possible to validate the 2PKT extended to concrete compact footings.
Generally, the 2PKT well adapt to the test result and to the FEM prevision, but a detailed discussion for each parametric study is developed below the graphs.

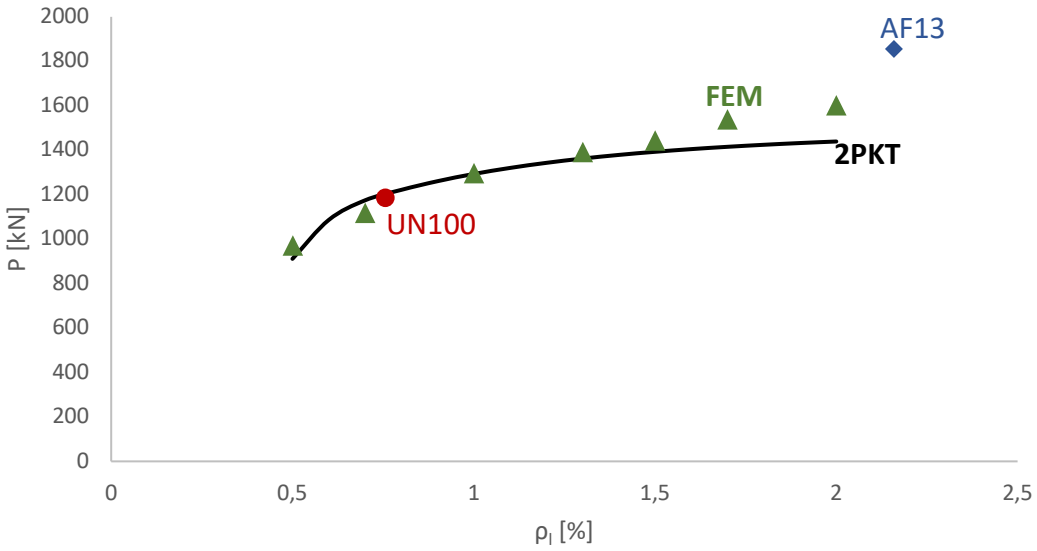

Figure 5.14: Parametric study varying the longitudinal reinforcement ratio using test UN100 as model

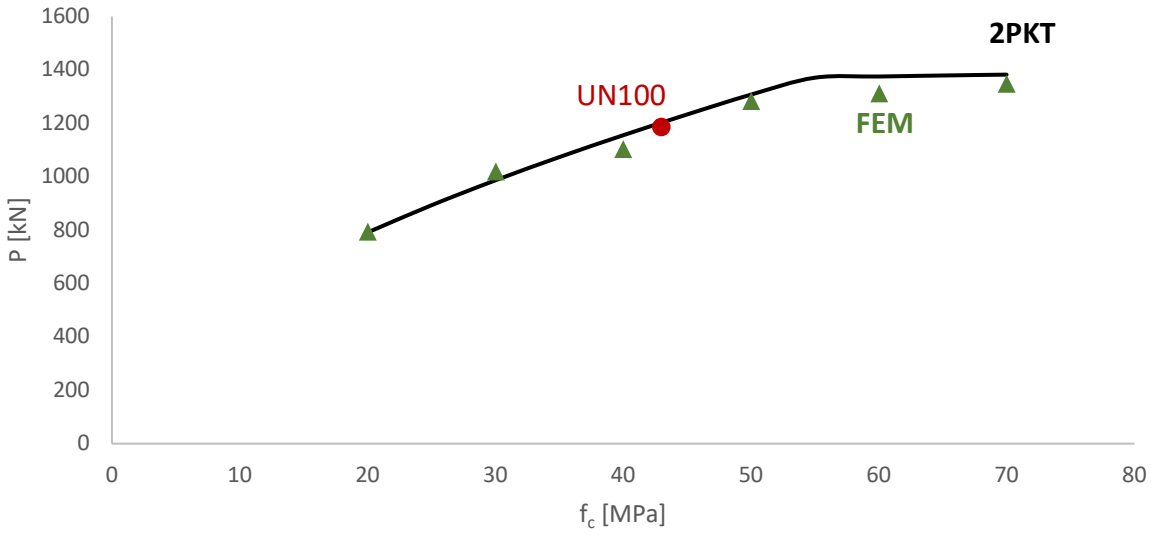

Figure 5.15: Parametric study varying the concrete strength using test UN100 as model

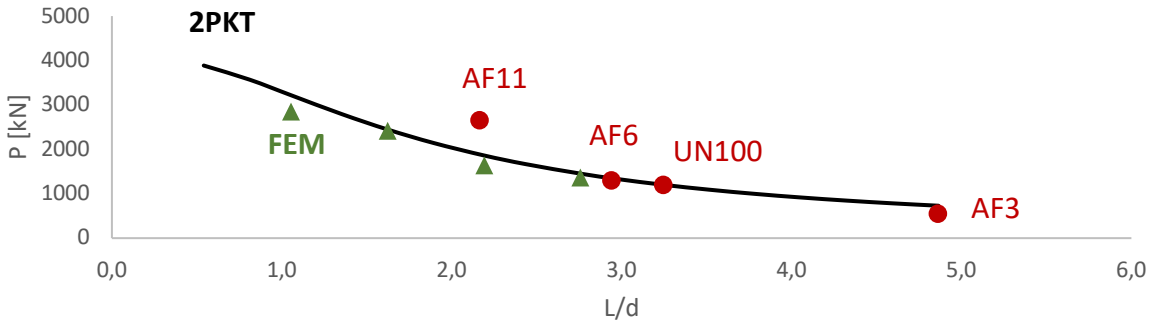

Figure 5.16: Parametric study varying the L/d ratio using test UN100 as model

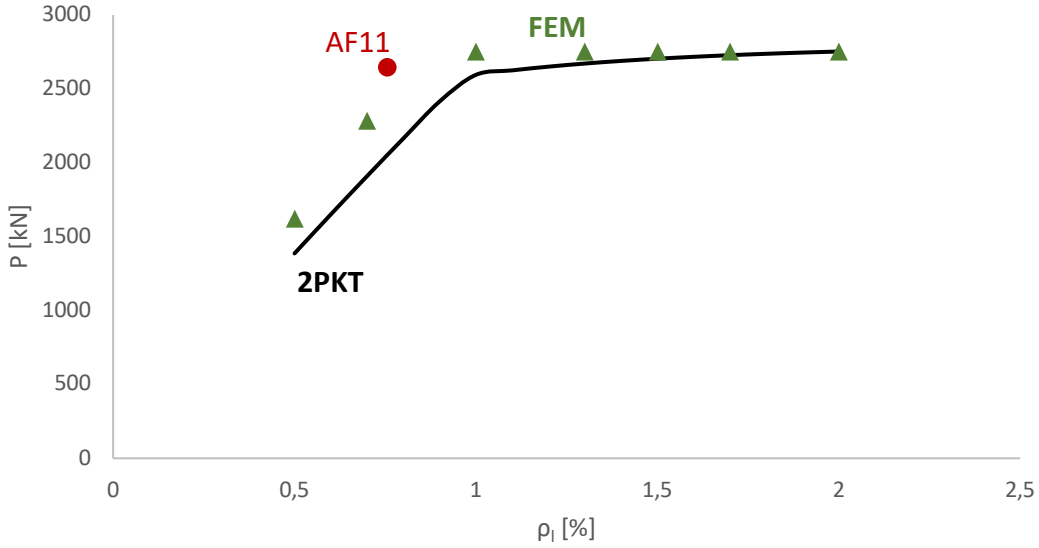

Figure 5.17: Parametric study varying the longitudinal reinforcement ratio using test AF11 as model

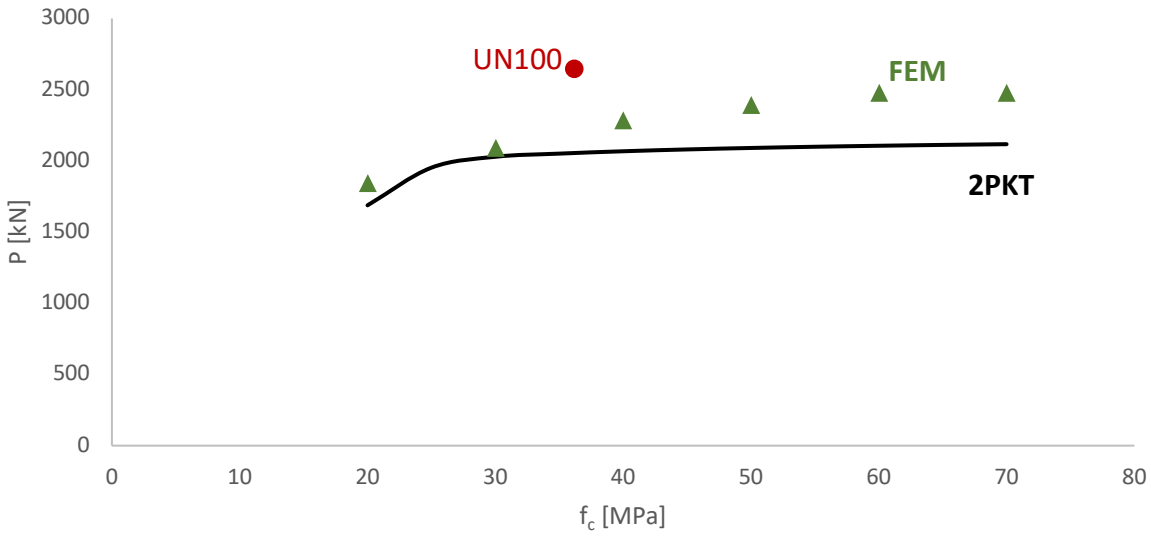

Figure 5.18: Parametric study varying the concrete strength using test AF11 as model

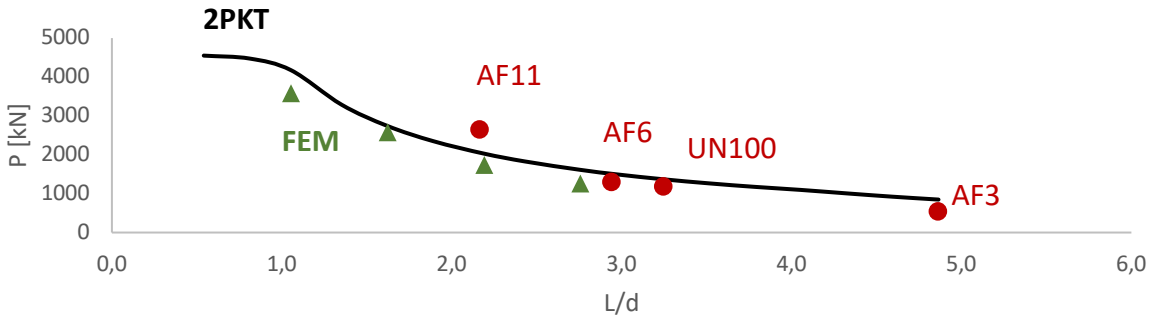

Figure 5.19: Parametric study varying the L/d ratio using test AF11 as model

The parametric analysis based on the specimen AF1 UN100 as model is illustrated in Figure 5.14, Figure 5.15 and Figure 5.16. In the first image it is possible to observe that the FEM models and the 2PKT predictions have a similar trend and the test AF1 UN100 belongs to the 2PKT prevision. Furthermore, in the figure it is represented also the test AF13 because it has similar *L/d* ratio (3.5 instead of 3.2 of UN100 specimen), but very different longitudinal reinforcement ratio (2.16% instead of 0.76% of UN100 sample), the parameter which in this case is requested to vary. The test result of AF13 is far from the 2PKT and FEM prevision, the fact is quite unexpected also considering the concrete strength which is smaller with respect the model used for the parametric study (35.7 MPa instead of 43 MPa for the model). The test provides a surprising result which was not predicted by none of the models; a deepen discussion regarding the sample AF13 will be developed in the Appendix 2: 2PTK Calculations.

In Figure 5.15 the models, 2PKT and FEM, are perfectly overlapped and the result from test experiment belongs to the 2PKT curve.
In Figure 5.16, again, the 2PKT and the FEM models are coincident and the test results UN100 belongs to the 2PKT curve. Furthermore, the specimens AF3, AF6 and AF11 are added because

they have different *L/d*, same longitudinal reinforcement ratio and similar concrete strength; the sample AF11, among the considered ones, is the only one which is far from the models' curves. Varying the *L/d* ratio, the sample AF13 is not considered due to its different reinforcement ratio (2.16%). Generally, form the graph it is evident that the strength decreases by increasing *L/d* ratio.

The parametric analysis based on specimen AF11 as model is illustrated in Figure 5.17, Figure 5.18 and Figure 5.19. In the first picture, the longitudinal reinforcement ratio is the parameter that is varying and, FEM and 2PKT produce quite similar predictions, but the test results are better reproduced by the FEM analysis with respect to the 2PKT. In this case the sample AF13 is not plotted due to the dissimilar value for the *L/d* ratio (it is equal to 2.2 for AF11 and 3.5 for AF13).
In Figure 5.18 it is possible to observe the results of the parametric study varying the concrete strength, the FEM and 2PKT models are quite similar at the beginning, then by increasing the concrete strength they assume a different trend and the average gap between the two predictions is 400 kN. The test result for AF11 is unexpectedly higher with respect both forecasts.
In Figure 5.19 the curves of FEM and 2PKT analysis are overlapped and the compatible test results belong to the curves, therefore in this case the calculations adapt the results obtained by the performed large-scale tests.

In both Figure 5.15 and Figure 5.18, thus the P-f_c curves, it is possible to notice the plateau due to the passage from shear failure to the flexural failure. Using AF1 UN100 as model, increasing the concrete strength after 55 MPa, the ultimate capacity load remains approximately constant. While, using AF11 as model, the flat part of the curve is visible only for the 2PKT and starting from lower values of concrete strength, around 40 MPa.

For AF1 UN100 and AF11 models, by increasing the reinforcement ratio from 0.5% to 2%, the footing tests fail in shear and the Finite Element Modellings of VecTor2 reproduce very well the 2PKT predictions. When the sample has a very low amount of reinforcement, it fails under flexure. Then, by varying the concrete strength, it is possible to observe that, by increasing f_c from 20 MPa to 70 MPa, the tests fail in shear up to a certain point and then the dominant failure mode is the flexural one.

Generally, it is observed an increment in the shear stress at failure when the shear span to effective depth (*a/d*) decreases. For elements with low *a/d* ratio, the internal forces redistribute, after the formation of the main diagonal crack. The formation of flexural cracks is followed by the development of inclined shear cracks along which a shear deformation occurs, resulting into high compression stresses in the concrete strut carrying shear; crushing of the concrete strut activates a redistribution of internal forces which eventually leads to failure.
When *a/d* is greater than 1.5, the elements develop the main diagonal crack and the stress at which it arises is function of the total member depth (compare also Figure A.13 and A.16, then Figure A.31 with A.34 in the Appendix 3).

The specimens used as model and FEM specimens created for the parametric analysis are summarized in Table 5.9. Only the main data are shown, for detailed database of footings it is necessary to consult the Appendix 1.
Furthermore, in the Appendix 2: 2PTK Calculations, a detailed 2PKT calculations and the last iterative step are shown; while in the Appendix 3: FEM results from the parametric study, some examples of footings modeled with VecTor2 and some plots are displayed in order to compare the results for high and low concrete strength specimens, for high and low reinforcement ratio tests, and for slender and deep footings.

Specimen	**Reinforcement**	**Concrete**	**Geometry**		
	ρ *[%]*	f_c' [MPa]	L_0 [mm]	d [mm]	L_0/d
AF1 UN100	0.76	43	2925	925	3.16
Parametric study	0.76	20-70	2925	925	3.16
Parametric study	0.5-2	43	2925	925	3.16
Parametric study	0.76	43	850-8850	925	0.5-4.8
AF11	0.76	36.2	1850	925	2.00
Parametric study	0.76	20-70	1850	925	2.00
Parametric study	0.5-2	36.2	1850	925	2.00
Parametric study	0.76	36.2	850-8850	925	0.5-4.8

Table 5.9: Summarizing table for the parametric study

Similarly to what was previously done for the 2PKT and FEM strength provisions for *Uzel*'s tests, the experimental-to-predicted ratio is computed and plotted in Figure 5.20 for *Uzel*'s tests and for the finite element models created for the parametric study varying the length of the specimens. Generally, the samples crated by varying the *L/d* parameter are quite overestimated by the 2PKT, these values are not far from 1, but they are not on the safe side. Globally the average experimental-to-predicted ratio for these specimens is 1.00 and the coefficient of variation is 22.3%.
Finally, the average of the experimental-to-predicted ratio is equal to 1.08 and the coefficient of variation is 15.3% considering now the whole non-linear finite element models analysis and the experimental results (thus including also *Richart*'s tests). Moreover, considering only the *Uzel*'s tests predictions and the parametric study by means of the FEA (thus without *Richart*'s tests, by observing the results in Table A.2 in Appendix 2: 2PTK Calculations), the average of experimental-to-predicted is 1.04 and the coefficient of variation is 14.2%. The obtained product means that the 2PKT precisely reproduce the test results and, in particular, for large-scale specimens the size effect is taken into account and the results are more accurate with respect to code's shear provisions.

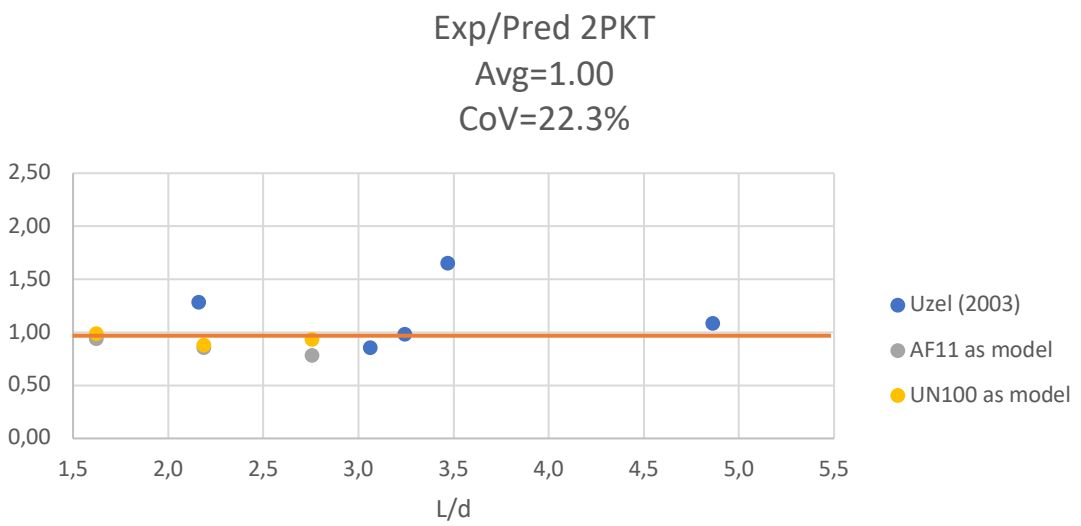

Figure 5.20: Experimental-to-predicted 2PKT strength provisions for Uzel's tests and models created for the parametric study

6. Conclusions

6.1 General overview

This thesis work presents a general overview of concrete compact footings, their possible failure modes with special regarding to one-way shear failure (beam action shear), thus, considering a strip of the element. The foundations have in fact the purpose to transfer the load of the superstructure and its weight to the soil layers. In order to accomplish this, in practice, reinforced concrete footings are designed without shear reinforcement (stirrups); therefore, these elements are predisposed to brittle failure according to the amount of diagonal cracking due to excessive local shear stresses. Then, the footings are analyzed using as starting point *Uzel*'s laboratory tests (the full-scale series) data. It is known that there is a significant size effect on shear strength of lightly reinforced slender members without shear reinforcement. Thus, it is important to simulate during the test the real size of this kind of elements in order to correctly evaluate the influence of the size on the shear behavior of large footings. The size effect is generally neglected by codes provision, such as ACI shear provisions, therefore the failure shear stress for slender members without shear reinforcement decreases as the thickness of the structural member increases; this may be very unconservative for thick members. Due to the absence of shear reinforcement, the resistance of the footing is often governed by the concrete contribution to shear strength. In fact, the ratio of shear length L_0 to the effective depth d is typically not very large, when it is low, an alternate force-resisting mechanism consisting of diagonal struts and tension ties can create, and this may provide adequate shear resistance even for very thick footings. The used tests are loaded by a set of hydraulic jacks which simulates the uniformly distributed loads from the soil. It is necessary to denote that the soil pressure is assumed uniformly distributed below the footing even though, its pressure is not uniform, but it is function of the type of the soil. Specifically, if the foundation soil layers is a non-cohesive material (i.e. sand), the soil pressure is maximum at the mid span of the footing and minimum at the ends; while, if the soil foundation is composed of cohesive materials (i.e. clays), the pressure will be maximum at the extremities and minimum in correspondence of the geometrical mid span section. This specification is made in order to clarify that *Uzel*'s tests were modelled to represent a strip of a footing member subjected to point load (simulating the load coming from the column footing) and uniformly distributed loads (simplifying the soil pressure).

6.2 Results and comparison

After the understanding of the performed tests and the obtained results, non-linear finite element models of the previously mentioned laboratory tests were performed by *Uzel* (using the program VecTor2) in order to obtain reliable and accurate predictions and reproductions. This was a necessary step in order to prove the validity of FEM results and enlarge the database of footings. In fact, in the literature, few suitable tests for the presented purpose are available.

Therefore, the Finite Element Analysis by using VecTor2 software, was essential after the demonstration of its reliability and efficiency with the precedent models of *Uzel*'s tests, to produce other possible footing samples following *Uzel*'s suggestions and recommendations.

Simultaneously, the understanding of the 2PKT (two-Parameter Kinematic Theory) for shear behavior in beams represented the main objective for this research. By means of the 2PKT it is possible to predict the shear failure load, the crack widths near failure, and the complete deformed shapes of diagonally cracked point-loaded deep beams subjected to single curvature. The two parameters involved in the models are: the ultimate vertical displacement of Critical Loading Zone (CLZ) and the average tensile strain in the longitudinal reinforcement on the flexural tension side. The theory allows to consider the size effect for deep beams the obtained shear provisions are more accurate with respect to code's ones. In fact, the beam's mechanism of shear resistance strictly depends on the size of the element itself. A slender beam is a structural member with a shear span-depth ratio, *a/d*, greater than 2.3 and its behavior is consistent with "*plane sections remain plane*" and shear resistance is attributed to the ability of the cross section to transfer shear across a diagonal crack. While for deep beams the statement is no more valid, the shear strain becomes dominant and the deformation pattern becomes more complex. Shear resistance is attributable to stirrups contribute, aggregate interlock of concrete of the primary diagonal crack, dowel action of longitudinal reinforcement and shear capacity of the CLZ.

Then, the scope was the development of the 2PKT for footings, adapting the loading conditions and the shear resistance contributions that interest this member with respect to the beams. In fact, the main factors that contribute to shear resistance are the shear forces resisted by the critical loading zone and by aggregate interlock. The stirrups contribute is not present because the specimens are without shear reinforcement and the dowel action is neglected in order to obtain conservative results. In practice, in fact, concrete compact footings are designed without shear reinforcement and with light longitudinal reinforcement. The uniformly distributed load in the bottom part of the footing affects the vertical applied load *P* just for the remaining rigid block above the main diagonal crack; while the uniformly distributed load in the part below the main diagonal crack remains not considered by the theory. After the extension of the theory for footings, the following step was the validation of the theory by means of real tests and FEM analysis. The average strength predictions by 2PKT for *Uzel*'s tests is conservative, the average value of experimental-to-predicted ratio is 1.10 and the coefficient of variation is 28%. Apart AF11r1 and AF13, the other tests are well reproduced, and the prediction is conservative. The peculiarity of AF11r1 is that it fails in flexure and, regarding AF13, it has almost three times the longitudinal amount of reinforcement with respect to the other samples. Thus, for AF13 sample the predictions are too conservative, and the dowel action contribution might not be neglected. For *Richart*'s tests experimental-to-predicted ratio is 1.19 and the coefficient of variation is 15%.
In order to validate the extended 2PKT, starting with the FEM models of the actual tests, some parameters are modified, and a parametric study is developed. The parametric analysis by varying one of the considered factors per time and keeping constant the others. Precisely, the

parameters included in the parametric study are: the concrete strength f_c, the longitudinal reinforcement ratio ρ_l and the length of the footing L (keeping d, the effective depth, constant). Again, the tests contained into the parametric analysis are the ones that follow the simple hypothesis of one vertical load coming from the superstructure and applied along the symmetry axis of the footings and uniformly distributed loads along the whole length of the footings in the bottom side which reproduce the soil pressure. The parametric study offers reliable results thanks to the consistent results obtained by the FEM of *Uzel*'s tests in which the average experimental-to-predicted strength is 1.02 and the Coefficient of Variation is 6%. Considering these coherent models as starting point, it is possible to proceed with the parametric analysis.
Considering AF1 UN100 and AF11 as models for the parametric study, by increasing the reinforcement ratio from 0.5% to 2%, the footing tests fail in shear and the Finite Element Modellings of VecTor2 reproduce very well the 2PKT predictions. When the sample has a low amount of reinforcement, it fails under flexure. Then, by varying the concrete strength, it is possible to observe that, by increasing f_c from 20 MPa to 70 MPa, the tests fail in shear up to a certain point and then the dominant failure mode is the flexural one.
Then, it is seen an increment in the shear strength at failure when the shear span to effective depth ratio decreases. For elements with low shear span-to-effective depth ratio, the internal forces redistribute, after the formation of the main diagonal crack. The formation of flexural cracks is followed by the development of inclined shear cracks along which a shear deformation occurs, resulting into high compression stresses in the concrete strut carrying shear; crushing of the concrete strut activates a redistribution of internal forces which eventually leads to failure. The developing of the main diagonal crack and the stress at which it arises are function of the total member depth.

Based on the use of non-linear finite element calculations proved against experimental results, it is possible to validate the 2PKT extended to concrete compact footings. It can be seen that the 2PKT method well reproduces the observation and the measurements obtained during the large-scale laboratory tests. In fact, the average experimental-to-predicted ratio obtained with the 2PKT calculations is 1.04 and the coefficient of variation (CoV) is 14.2% (considering only the *Uzel*'s tests predictions and the parametric study by means of the FEA, thus without *Richart*'s tests).
Also, in terms of strain the 2PKT very well reproduce test results, apart AF13 which is the only *Uzel*'s test with longitudinal reinforcement ratio almost three times the others. In fact, the 2PKT predictions for AF13 are the least accurate and probably this is due to the large amount of longitudinal reinforcement which might makes not negligible the dowel action effect for shear resistance.
Furthermore, in order to compare the predicted displacement at failure by the 2PKT and the real test displacement by means of the Zurich Targets, a Matlab code is implemented. Also, from this side, the global deformation pattern at failure and displacement behavior are well reproduced and captured by the 2PKT. The displacement predictions do not exactly overlap to the shape of the real test displacement, thus the 2PKT could be improved regarding the displacement aspect.
Finally, it is possible to state that, globally, the obtained results validate the extended 2PKT, in particular, for large-scale specimens with respect to medium-scale samples (*Richart*'s tests).

6.3 Future research

Due to the fact that in practice footings may be of substantial thickness and are generally constructed without shear reinforcement, the safety of these large members is based on the accuracy of shear design provisions. For that reason, this thesis work is just the starting point for the validation of the 2PKT because the database based on real tests' data is composed by few specimens. Therefore, the samples obtained by FEM models could be in future real laboratory large-scale tests and their results could further demonstrate the shear predictions of the theory and, thus, enlarge its validity.

Another interesting topic to develop is the study of non-uniformly distributed load in the bottom part of the footing, thus a more realistic approach regarding the pressure given by the soil in the contact zone. The study could be related to both, sand and clay type of soil, but, since the uniform pressure distribution will result slightly unsafe for rigid footings on clays, most attention should be payed to this last kind of soil. *Uzel* tested some specimens in such a way that they were subjected to pressure distribution only in a portion of the footing in order to simulate the behavior of footings on cohesive soil (clay). Therefore, it could be interesting to develop and study the 2PKT changing the loading configuration in order to take into account the real behavior of the contact zone and the not uniformly distributed pressure.

Moreover, since the 2PKT predictions are not good in the same manner for all the specimens, it could be interesting in the future to develop the theory taking into account also the deliamination along the bottom reinforcement. In fact, in tests by *Uzel* it is observed that in some cases (AF6 and AF13 especially) the main diagonal crack extends to the ends of the footings, probably due a not prober anchor of the rebar. The 2PKT does not take into account the development of the main diagonal crack in this way, thus could be interesting elaborate on this behavior.

Concluding, future research regarding shear behavior of concrete compact footings and the extension of the 2PKT should be developed in terms of real laboratory large-scale tests in order to prove it and compare its predictions against a greater amount of footing samples that will increase the database for this kind of member and, therefore, will confirm, or not, the validity of the theory. The real tests should help also in the understanding of the dowel action effect, if it is negligible in general or, for a certain amount of longitudinal reinforcement, it plays an important and significative role.

Bibliography & References

1. MACGREGOR J. G., WIGHT, J. K., Reinforced concrete mechanics and design, Pearson, 6th ed. (2011);
2. RICHART F. E., Reinforced Concrete Wall and Column Footings (1948);
3. UZEL A., Shear design of large footings, PhD Thesis, University of Toronto (2003);
4. MIHAYLOV B., Two-Parameter Kinematic Theory for shear behaviour in deep beams, ACI Structural Journal/May-June (2013);
5. Eurocode 2: Design of Concrete Structures, Part 1.1: General Rules and Rules for Buildings;
6. ACI Committee 318, Building Code Requirements for Structural Concrete (ACI 318-02-11) and Commentary (318R-02), Farmington Hills: American Concrete Institute (2007);
7. VecTor2 Manual;
8. BENTZ E. C., VECCHIO F. J., COLLINS M. P., Simplified Modified Compression Field Theory for Calculating Shear Strength of Reinforced Concrete Elements, ACI Structural Journal, Volume 103, No. 4, July-August (2006);
9. VECCHIO F. J., COLLINS M. P., Modified Compression Field Theory for Reinforced Concrete Elements subjected to Shear, ACI Structural Journal, March-April (1986);
10. UZEL A., PODGORNIAK B., BENTZ E. C., COLLINS M. P., Design of Large Footings for One-Way Shear, ACI Structural Journal, Volume 108, No. 2, March-April (2011);
11. Theconstructor.org;
12. BAEK K. R., Response of Reinforced Concrete Beams with Indirect Loading, McGill University - Quebec, (2016);
13. COLLINS, M. P., BENTZ, E., SHERWOOD, E., XIE, L., An adequate theory for the shear strength of reinforced concrete structures (2007);
14. KANI, G., Basic facts concerning shear failure, ACI Journal, 675-692 (1966);
15. KANI, G., How safe are our large reinforced concrete beams, ACI Journal, 128-141 (1997);
16. KANI, G., The Riddle of Shear Failure and Its Solutions, ACI Journal, 441- 467 (1964);
17. ZIARA, M. M., The influence of confining the compression zone in the design of structural concrete beams, Heriot-Watt University (1993);
18. BRAESTRUP, M., Structural Concrete Beam Shear - Still a Riddle?, ACI Special Publication, 327-344 (2009);
19. COLLINS M. P., KUCHMA D., How Safe Are Our Large, Lightly Reinforced Concrete Beams, Slabs, and Footings?, ACI Structural Journal, Volume 96, No. 4, (1999);
20. RUSSO G., ZINGONE G., PULERI G.; Flexure-shear interaction model for longitudinally reinforced beams, ACI Structural Journal, Volume 88 (1991);
21. UZEL A., BENTZ E. C., COLLINS M. P., Design of indirectly loaded large footings for one-way shear, ACI Structural Journal, Volume 113, No. 3, May-June (2016);

22. BENTZ E. C., COLLINS M. P., Simplified modified compression field theory for calculating shear strength of reinforced concrete elements, ACI Structural Journal, Volume 103, No. 4, July-Aug. (2006);
23. COLLINS M. P., MITCHELL D., BENTZ E. C., Shear design of concrete structures, The Structural Engineer, Volume 86, No. 10, May (2008);
24. SMITH K. N., FEREIG S. M., Effect of loading and supporting conditions on the shear strength of deep beams, Shear in Reinforce Concrete, Farmington Hills: American Concrete Institute (1974);
25. TUCHSCHERER R. G., BIRRCHER D. B., BAYARAK O., Reducing Discrepancy between Deep Beam and Sectional Shear-Strength Predictions, ACI Structural Journal, Volume 113, No. 1, Jan.-Feb. (2016);
26. BENTZ E. C., Sectional analysis of reinforced concrete members, PhD Thesis, University of Toronto (2000);
27. BIRGISSON S. R., Shear resistance of reinforced concrete beams without stirrups, PhD Thesis, University of Reykjavik (2011);
28. KUERES D., Two-parameter kinematic theory for punching shear in reinforced concrete slabs, Aauflage Aachen Eigenverlag, Heft 52, Lehrstuhl un Institit fur Massivbau (2018);
29. MUTTONI A., SCHWARTZ J., Behaviour of beams and punching in slabs without shear reinforcement, IABSE Colloquium (1991);
30. MUTTONI A., FERNANDEZ RUIZ M., Shear strength of members without transverse reinforcement as function of critical shear crack width, American Concrete Institute (2008);
31. PODGORNIAK-STANIK B., The influence of concrete strength, distribution of longitudinal reinforcement, amount of transverse reinforcement and member size on shear strength of reinforced concrete members, PhD Thesis, University of Toronto (1998);
32. SCHLAICH J., SCHÄFER K, JENNEWEN M., Towards a consistent design of reinforced concrete structures, PCI Journal (1987);
33. SCHLAICH J., SCHÄFER K, Design and detailing of structural concrete using strut-and-tie models, The Structural Engineer, Volume 69, No. 6 (19 March 1991);
34. ADEBAR P., ZHOU Z. L., Design of Deep Pile Caps by Strut-and-Tie Models, ACI Structural Journal, Volume 93, No. 4, July-August (1996).

Appendix 1: Database of footings

Ref.	Name	b	h	a	L	d	d_s	A_s	ρ	f_{sy}	ε_{sy}	f_{tk}	a_g	f_c	Failure type
		mm	mm	mm	mm	mm	mm	mm²	%	MPa	‰	MPa	mm	MPa	-
Richardt (1948a, 1948b)	501a	1829	304,8	356	2743	254	16	6400	1,38	425	2,1	721	25,4	25,4	DT
	501b	1829	304,8	356	2743	254	16	6400	1,38	425	2,1	721	25,4	25,7	DT
	502a	1829	457,2	356	2743	406,4	13	3999	0,54	420	2,1	639	25,4	24,3	T/DT
	502b	1829	457,2	356	2743	406,4	13	3999	0,54	420	2,1	639	25,4	22,7	T/DT
	503a	1829	457,2	356	2743	406,4	13	3999	0,54	420	2,1	639	25,4	24,4	T/DT
	503b	1828	457,2	356	2743	406,4	13	3999	0,54	420	2,1	639	25,4	24	T/DT
	504a	1524	304,8	356	3048	254	19	6852	1,77	510	2,6	765	25,4	24,9	DT
	504b	1524	304,8	356	3048	254	19	6852	1,77	510	2,6	765	25,4	25,8	DT
	505a	1524	457,2	356	3048	406,4	16	4200	0,68	425	2,1	721	25,4	25,4	T/DT
	505b	1524	457,2	356	3048	406,4	16	4200	0,68	425	2,1	721	25,4	25,7	T/DT
	506a	1524	457,2	356	3048	406,4	16	4200	0,68	425	2,1	721	25,4	23,1	T/DT
	506b	1524	457,2	356	3048	406,4	16	4200	0,68	425	2,1	721	25,4	26,3	T/DT
Uzel et al., (2003)	UN100	300	1000	150	6000	925	30	2100	0,76	550	2,8	750	10	43	S
	AF3	300	670	150	6000	617	30	1400	0,76	475	2,4	621	19	27,3	S
	AF6	300	670	150	6000	617	30	1400	0,76	562	2,8	710	19	32,2	S
	AF7	300	1000	150	6000	925	30	2100	0,76	562	2,8	710	19	33,8	S
	AF11	300	1000	300	4000	925	30	2100	0,76	562	2,8	710	19	36,2	F
	AF11r1	300	1000	300	4000	925	30	2100	0,76	562	2,8	710	19	36,2	
	AF13	300	1000	150	6000	865	30	5600	2,16	475	2,4	621	19	35,7	S
Varying ρ	UN100	300	1000	150	6000	925	30	1388	0,5	550	2,8	750	10	43	F
	UN100	300	1000	150	6000	925	30	1665	0,6	550	2,8	750	10	43	
	UN100	300	1000	150	6000	925	30	1943	0,7	550	2,8	750	10	43	S
	UN100	300	1000	150	6000	925	30	2220	0,8	550	2,8	750	10	43	
	UN100	300	1000	150	6000	925	30	2498	0,9	550	2,8	750	10	43	
	UN100	300	1000	150	6000	925	30	2775	1	550	2,8	750	10	43	S
	UN100	300	1000	150	6000	925	30	3053	1,1	550	2,8	750	10	43	
	UN100	300	1000	150	6000	925	30	3330	1,2	550	2,8	750	10	43	
	UN100	300	1000	150	6000	925	30	3608	1,3	550	2,8	750	10	43	S
	UN100	300	1000	150	6000	925	30	3885	1,4	550	2,8	750	10	43	
	UN100	300	1000	150	6000	925	30	4163	1,5	550	2,8	750	10	43	S
	UN100	300	1000	150	6000	925	30	4440	1,6	550	2,8	750	10	43	
	UN100	300	1000	150	6000	925	30	4718	1,7	550	2,8	750	10	43	S
	UN100	300	1000	150	6000	925	30	4995	1,8	550	2,8	750	10	43	
	UN100	300	1000	150	6000	925	30	5273	1,9	550	2,8	750	10	43	
	UN100	300	1000	150	6000	925	30	5550	2	550	2,8	750	10	43	S
Varying f_c	UN100	300	1000	150	6000	925	30	2100	0,76	550	2,8	750	10	20	S
	UN100	300	1000	150	6000	925	30	2100	0,76	550	2,8	750	10	25	
	UN100	300	1000	150	6000	925	30	2100	0,76	550	2,8	750	10	30	S

Ref.	Name	b	h	a	L	d	d_s	A_s	ρ	f_{sy}	ε_{sy}	f_{tk}	a_g	f_c	Failure type
		mm	mm	mm	mm	mm	mm	mm²	%	MPa	‰	MPa	mm	MPa	-
	UN100	300	1000	150	6000	925	30	2100	0,76	550	2,8	750	10	35	
	UN100	300	1000	150	6000	925	30	2100	0,76	550	2,8	750	10	40	S
	UN100	300	1000	150	6000	925	30	2100	0,76	550	2,8	750	10	45	
	UN100	300	1000	150	6000	925	30	2100	0,76	550	2,8	750	10	50	S
	UN100	300	1000	150	6000	925	30	2100	0,76	550	2,8	750	10	55	
	UN100	300	1000	150	6000	925	30	2100	0,76	550	2,8	750	10	60	F
	UN100	300	1000	150	6000	925	30	2100	0,76	550	2,8	750	10	65	
	UN100	300	1000	150	6000	925	30	2100	0,76	550	2,8	750	10	70	F
Varying L	UN100	300	1000	150	1000	925	30	2100	0,76	550	2,8	750	10	43	
	UN100	300	1000	150	1500	925	30	2100	0,76	550	2,8	750	10	43	
	UN100	300	1000	150	1950	925	30	2100	0,76	550	2,8	750	10	43	F
	UN100	300	1000	150	2500	925	30	2100	0,76	550	2,8	750	10	43	
	UN100	300	1000	150	3000	925	30	2100	0,76	550	2,8	750	10	43	F
	UN100	300	1000	150	3500	925	30	2100	0,76	550	2,8	750	10	43	
	UN100	300	1000	150	4050	925	30	2100	0,76	550	2,8	750	10	43	F
	UN100	300	1000	150	4500	925	30	2100	0,76	550	2,8	750	10	43	
	UN100	300	1000	150	5100	925	30	2100	0,76	550	2,8	750	10	43	F
	UN100	300	1000	150	5500	925	30	2100	0,76	550	2,8	750	10	43	
	UN100	300	1000	150	6000	925	30	2100	0,76	550	2,8	750	10	43	
	UN100	300	1000	150	6500	925	30	2100	0,76	550	2,8	750	10	43	
	UN100	300	1000	150	7000	925	30	2100	0,76	550	2,8	750	10	43	
	UN100	300	1000	150	7500	925	30	2100	0,76	550	2,8	750	10	43	
	UN100	300	1000	150	8000	925	30	2100	0,76	550	2,8	750	10	43	
	UN100	300	1000	150	8500	925	30	2100	0,76	550	2,8	750	10	43	
	UN100	300	1000	150	9000	925	30	2100	0,76	550	2,8	750	10	43	
Varying ρ	AF11	300	1000	300	4000	925	30	1388	0,5	562	2,8	710	19	36,2	F
	AF11	300	1000	300	4000	925	30	1665	0,6	562	2,8	710	19	36,2	
	AF11	300	1000	300	4000	925	30	1943	0,7	562	2,8	710	19	36,2	F
	AF11	300	1000	300	4000	925	30	2220	0,8	562	2,8	710	19	36,2	
	AF11	300	1000	300	4000	925	30	2498	0,9	562	2,8	710	19	36,2	
	AF11	300	1000	300	4000	925	30	2775	1	562	2,8	710	19	36,2	F
	AF11	300	1000	300	4000	925	30	3053	1,1	562	2,8	710	19	36,2	
	AF11	300	1000	300	4000	925	30	3330	1,2	562	2,8	710	19	36,2	
	AF11	300	1000	300	4000	925	30	3608	1,3	562	2,8	710	19	36,2	F
	AF11	300	1000	300	4000	925	30	3885	1,4	562	2,8	710	19	36,2	
	AF11	300	1000	300	4000	925	30	4163	1,5	562	2,8	710	19	36,2	F
	AF11	300	1000	300	4000	925	30	4440	1,6	562	2,8	710	19	36,2	
	AF11	300	1000	300	4000	925	30	4718	1,7	562	2,8	710	19	36,2	S
	AF11	300	1000	300	4000	925	30	4995	1,8	562	2,8	710	19	36,2	
	AF11	300	1000	300	4000	925	30	5273	1,9	562	2,8	710	19	36,2	
	AF11	300	1000	300	4000	925	30	5550	2	562	2,8	710	19	36,2	S

Ref.	Name	b	h	a	L	d	d_s	A_s	ρ	f_{sy}	ε_{sy}	f_{tk}	a_g	f_c	Failure type
		mm	mm	mm	mm	mm	mm	mm²	%	MPa	‰	MPa	mm	MPa	-
Varying f_c	AF11	300	1000	300	4000	925	30	2100	0,76	562	2,8	710	19	20	S
	AF11	300	1000	300	4000	925	30	2100	0,76	562	2,8	710	19	25	
	AF11	300	1000	300	4000	925	30	2100	0,76	562	2,8	710	19	30	F
	AF11	300	1000	300	4000	925	30	2100	0,76	562	2,8	710	19	35	
	AF11	300	1000	300	4000	925	30	2100	0,76	562	2,8	710	19	40	F
	AF11	300	1000	300	4000	925	30	2100	0,76	562	2,8	710	19	45	
	AF11	300	1000	300	4000	925	30	2100	0,76	562	2,8	710	19	50	F
	AF11	300	1000	300	4000	925	30	2100	0,76	562	2,8	710	19	55	
	AF11	300	1000	300	4000	925	30	2100	0,76	562	2,8	710	19	60	F
	AF11	300	1000	300	4000	925	30	2100	0,76	562	2,8	710	19	65	
	AF11	300	1000	300	4000	925	30	2100	0,76	562	2,8	710	19	70	F
Varying L	AF11	300	1000	300	1000	925	30	2100	0,76	562	2,8	710	19	36,2	
	AF11	300	1000	300	1500	925	30	2100	0,76	562	2,8	710	19	36,2	
	AF11	300	1000	300	1950	925	30	2100	0,76	562	2,8	710	19	36,2	S
	AF11	300	1000	300	2500	925	30	2100	0,76	562	2,8	710	19	36,2	
	AF11	300	1000	300	3000	925	30	2100	0,76	562	2,8	710	19	36,2	F
	AF11	300	1000	300	3500	925	30	2100	0,76	562	2,8	710	19	36,2	
	AF11	300	1000	300	4050	925	30	2100	0,76	562	2,8	710	19	36,2	F
	AF11	300	1000	300	4500	925	30	2100	0,76	562	2,8	710	19	36,2	
	AF11	300	1000	300	5100	925	30	2100	0,76	562	2,8	710	19	36,2	F
	AF11	300	1000	300	5500	925	30	2100	0,76	562	2,8	710	19	36,2	
	AF11	300	1000	300	6000	925	30	2100	0,76	562	2,8	710	19	36,2	
	AF11	300	1000	300	6500	925	30	2100	0,76	562	2,8	710	19	36,2	
	AF11	300	1000	300	7000	925	30	2100	0,76	562	2,8	710	19	36,2	
	AF11	300	1000	300	7500	925	30	2100	0,76	562	2,8	710	19	36,2	
	AF11	300	1000	300	8000	925	30	2100	0,76	562	2,8	710	19	36,2	
	AF11	300	1000	300	8500	925	30	2100	0,76	562	2,8	710	19	36,2	
	AF11	300	1000	300	9000	925	30	2100	0,76	562	2,8	710	19	36,2	

Table A.1: Database of footings (tests and parametric study)

Legend for the failure mode:

T = tension failure [2]
DT = diagonal tension [2]

F = flexural failure
S = shear failure

Appendix 2: 2PTK Calculations

Ref.	Name	L/d	l_{b1}	P_{exp}	P_{FEM}	P	P_{2PKT}	P_{sect}	P_{flex}	Exp/Pred	α_1	α	l_{b1e}	V_{clz}	Δ_c	s_{max}	$V_{d,cr}$	V_{sh}
			mm	kN	kN	kN	kN	kN	kN	(2PKT)	°	Rad	mm	kN	mm	mm	kN	kN
Richardt (1948a, 1948b)	501a	5,4	356	1753		1782	2060	1426	1782	0,98	26	0,27	178	455	6,6	161	101	556
	501b	5,4	356	1690		1785	2075	1430	1785	0,95	26	0,27	178	459	6,6	161	101	560
	502a	3,4	356	2464		1898	5786	2093	1898	1,30	38	0,51	178	1419	3,3	207	86	1644
	502b	3,4	356	2571		1891	5493	2044	1891	1,36	38	0,51	178	1339	3,3	207	84	1561
	503a	3,4	356	2607		1899	5803	2096	1899	1,37	38	0,51	178	1424	3,3	207	86	1649
	503b	3,4	356	2446		1897	5726	2083	1897	1,29	38	0,51	178	1403	3,3	207	86	1628
	504a	6,0	356	1446		1390	1390	1180	1908	1,04	23	0,24	178	292	7,5	151	97	367
	504b	6,0	356	1557		1427	1427	1194	1922	1,09	23	0,24	178	301	7,5	151	98	377
	505a	3,8	356	2438		1795	4241	1725	1795	1,36	34	0,46	178	998	3,8	205	91	1183
	505b	3,8	356	2335		1797	4282	1733	1797	1,30	34	0,46	178	1009	3,8	205	91	1195
	506a	3,8	356	2224		1785	3964	1672	1785	1,25	34	0,46	178	926	3,8	205	88	1106
	506b	3,8	356	2224		1799	4352	1745	1799	1,24	34	0,46	178	1027	3,8	205	92	1214
Uzel et al., (2003)	UN100	3,2	150	1186	1149	1203	1203	641	1356	0,99	34	0,50	75	150	1,4	224	36	303
	AF3	4,9	150	541	494	497	497	353	511	1,09	24	0,35	75	52	2,2	237	35	125
	AF6	3,1	150	1298	1398	1515	1515	820	1523	0,86	36	0,53	75	132	1,3	237	37	245
	AF11	2,2	300	2645	2448	2055	2493	1076	2055	1,29	48	0,73	150	502	1,8	224	34	677
	AF13	3,5	150	1857	1848	1124	1124	817	2627	1,65	32	0,39	75	83	1,9	151	10	264
Varying ρ	UN100	3,2	150		972	911	1049	559	911	1,07	34	0,50	75	150	1,4	341	42	265
	UN100	3,2	150			1086	1117	595	1086		34	0,50	75	150	1,4	284	40	282
	UN100	3,2	150		1119	1174	1174	626	1259	0,95	34	0,50	75	150	1,4	243	37	296
	UN100	3,2	150			1221	1221	652	1429		34	0,50	75	150	1,4	213	35	308
	UN100	3,2	150			1260	1260	676	1597		34	0,50	75	150	1,4	189	33	318
	UN100	3,2	150		1296	1293	1293	697	1762	1,00	34	0,50	75	150	1,4	170	31	326
	UN100	3,2	150			1320	1320	717	1925		34	0,50	75	150	1,4	155	29	333
	UN100	3,2	150			1343	1343	734	2085		34	0,50	75	150	1,4	142	27	339
	UN100	3,2	150		1393	1362	1362	750	2244	1,02	34	0,50	75	150	1,4	131	25	344
	UN100	3,2	150			1379	1379	765	2399		34	0,50	75	150	1,4	122	23	348
	UN100	3,2	150		1443	1393	1393	779	2553	1,04	34	0,50	75	150	1,4	114	21	351
	UN100	3,2	150			1405	1405	792	2704		34	0,50	75	150	1,4	106	19	354
	UN100	3,2	150		1539	1415	1415	803	2852	1,09	34	0,50	75	150	1,4	100	17	357
	UN100	3,2	150			1424	1424	814	2998		34	0,50	75	150	1,4	95	15	359
	UN100	3,2	150			1432	1432	825	3142		34	0,50	75	150	1,4	90	13	361
	UN100	3,2	150		1604	1439	1439	835	3283	1,11	34	0,50	75	150	1,4	85	11	363
Varying f_c	UN100	3,2	150		794	791	791	490	1276	1,00	34	0,50	75	81	1,4	225	28	200
	UN100	3,2	150			893	893	531	1306		34	0,50	75	97	1,4	225	30	225
	UN100	3,2	150		1021	986	986	566	1326	1,03	34	0,50	75	112	1,4	225	32	249
	UN100	3,2	150			1073	1073	597	1340		34	0,50	75	127	1,4	225	34	271
	UN100	3,2	150		1103	1155	1155	625	1350	0,96	34	0,50	75	142	1,4	225	35	291
	UN100	3,2	150			1233	1233	651	1359		34	0,50	75	156	1,4	225	37	311

Ref.	Name	L/d	l_{b1}	P_{exp}	P_{FEM}	P	P_{2PKT}	P_{sect}	P_{flex}	Exp/Pred	α_1	α	l_{b1e}	V_{clz}	Δ_c	s_{max}	$V_{d,cr}$	V_{sh}
			mm	kN	kN	kN	kN	kN	kN	(2PKT)	°	Rad	mm	kN	mm	mm	kN	kN
	UN100	3,2	150		1284	1307	1307	675	1365	0,98	34	0,50	75	169	1,4	225	38	330
	UN100	3,2	150			1371	1379	697	1371		34	0,50	75	183	1,4	225	39	348
	UN100	3,2	150		1312	1375	1447	718	1375	0,95	34	0,50	75	196	1,4	225	41	365
	UN100	3,2	150			1379	1514	674	1379		34	0,50	75	209	1,4	225	42	382
	UN100	3,2	150		1348	1382	1579	595	1382	0,98	34	0,50	75	222	1,4	225	43	398
Varying L	UN100	0,5	150			3887	3887	-578	8133		79	1,33	75	615	0,2	225	36	1168
	UN100	0,8	150			3568	3568	-1661	5422		72	1,19	75	561	0,3	225	36	1003
	UN100	1,1	150		2844	3218	3218	-20861	4171	0,88	66	1,07	75	502	0,4	225	36	876
	UN100	1,4	150			2795	2795	2573	3253		60	0,95	75	429	0,6	225	36	743
	UN100	1,6	150		2417	2447	2447	1495	2711	0,99	54	0,85	75	368	0,7	225	36	641
	UN100	1,9	150			2144	2144	1128	2324		50	0,77	75	314	0,8	225	36	556
	UN100	2,2	150		1638	1863	1863	927	2008	0,88	45	0,69	75	264	1,0	225	36	479
	UN100	2,4	150			1669	1669	825	1807		42	0,64	75	230	1,1	225	36	426
	UN100	2,8	150		1359	1453	1453	732	1595	0,94	39	0,57	75	193	1,2	225	36	369
	UN100	3,0	150			1332	1332	687	1479		36	0,54	75	172	1,3	225	36	337
	UN100	3,2	150			1202	1202	641	1356		34	0,50	75	150	1,4	225	36	303
	UN100	3,5	150			1092	1092	605	1251		32	0,47	75	132	1,6	225	36	275
	UN100	3,8	150			997	997	575	1162		30	0,44	75	116	1,7	225	36	250
	UN100	4,1	150			916	916	549	1084		28	0,41	75	103	1,8	225	36	229
	UN100	4,3	150			845	845	527	1017		27	0,39	75	92	1,9	225	36	211
	UN100	4,6	150			784	784	508	957		25	0,36	75	83	2,1	225	36	196
	UN100	4,9	150			730	730	491	904		24	0,35	75	75	2,2	225	36	182
Varying ρ	AF11	2,2	300		1622	1387	2312	947	1387	1,17	48	0,73	150	502	1,8	341	39	628
	AF11	2,2	300			1650	2393	1004	1650		48	0,73	150	502	1,8	284	37	650
	AF11	2,2	300		2282	1910	2459	1052	1910	1,20	48	0,73	150	502	1,8	243	35	668
	AF11	2,2	300			2165	2514	1093	2165		48	0,73	150	502	1,8	213	33	683
	AF11	2,2	300			2415	2558	1130	2415		48	0,73	150	502	1,8	189	32	695
	AF11	2,2	300		2750	2595	2595	1163	2661	1,06	48	0,73	150	502	1,8	170	30	705
	AF11	2,2	300			2625	2625	1192	2903		48	0,73	150	502	1,8	155	28	713
	AF11	2,2	300			2650	2650	1218	3140		48	0,73	150	502	1,8	142	26	720
	AF11	2,2	300		2750	2671	2671	1242	3372	1,03	48	0,73	150	502	1,8	131	24	725
	AF11	2,2	300			2689	2689	1264	3600		48	0,73	150	502	1,8	122	22	730
	AF11	2,2	300		2750	2704	2704	1285	3824	1,02	48	0,73	150	502	1,8	114	20	734
	AF11	2,2	300			2717	2717	1303	4043		48	0,73	150	502	1,8	106	18	738
	AF11	2,2	300		2750	2728	2728	1321	4258	1,01	48	0,73	150	502	1,8	100	16	741
	AF11	2,2	300			2737	2737	1337	4468		48	0,73	150	502	1,8	95	14	743
	AF11	2,2	300			2746	2746	1352	4673		48	0,73	150	502	1,8	90	12	746
	AF11	2,2	300		2750	2753	2753	1366	4874	1,00	48	0,73	150	502	1,8	85	10	748
Varying f_c	AF11	2,2	300		1842	1688	1688	868	1951	1,09	48	0,73	150	312	1,8	225	28	458
	AF11	2,2	300			1952	1952	942	1998		48	0,73	150	373	1,8	225	30	530
	AF11	2,2	300		2090	2029	2201	1006	2029	1,03	48	0,73	150	432	1,8	225	32	598
	AF11	2,2	300			2051	2437	1063	2051		48	0,73	150	488	1,8	225	34	662

Ref.	Name	L/d	l_{b1}	P_{exp}	P_{FEM}	P	P_{2PKT}	P_{sect}	P_{flex}	Exp/Pred	α_1	α	l_{b1e}	V_{clz}	Δ_c	s_{max}	$V_{d,cr}$	V_{sh}
			mm	kN	kN	kN	kN	kN	kN	(2PKT)	°	Rad	mm	kN	mm	mm	kN	kN
	AF11	2,2	300		2283	2067	2663	1115	2067	1,10	48	0,73	150	543	1,8	225	35	723
	AF11	2,2	300			2080	2881	1162	2080		48	0,73	150	597	1,8	225	37	782
	AF11	2,2	300		2392	2091	3091	1205	2091	1,14	48	0,73	150	650	1,8	225	38	840
	AF11	2,2	300			2099	3297	1246	2099		48	0,73	150	701	1,8	225	39	895
	AF11	2,2	300		2475	2106	3496	1284	2106	1,18	48	0,73	150	752	1,8	225	41	949
	AF11	2,2	300			2112	3692	1171	2112		48	0,73	150	801	1,8	225	42	1003
	AF11	2,2	300		2475	2117	3883	949	2117	1,17	48	0,73	150	850	1,8	225	43	1054
Varying L	AF11	0,5	300			4549	4549	-538	8220		82	1,40	150	1103	0,3	225	34	1631
	AF11	0,8	300			4474	4474	-1363	5480		75	1,25	150	1023	0,5	225	34	1431
	AF11	1,1	300		3597	4174	4174	-5552	4216	0,86	69	1,13	150	927	0,7	225	34	1261
	AF11	1,4	300			3288	3702	3905	3288		62	0,99	150	799	1,0	225	34	1070
	AF11	1,6	300		2577	2740	3261	1865	2740	0,94	57	0,89	150	688	1,3	225	34	917
	AF11	1,9	300			2349	2852	1328	2349		52	0,80	150	588	1,5	225	34	786
	AF11	2,2	300		1741	2030	2458	1058	2030	0,86	47	0,72	150	494	1,8	225	34	667
	AF11	2,4	300			1827	2182	927	1827		44	0,66	150	429	2,0	225	34	586
	AF11	2,8	300		1265	1612	1873	812	1612	0,78	40	0,60	150	358	2,3	225	34	497
	AF11	3,0	300			1495	1699	757	1495		38	0,56	150	319	2,5	225	34	448
	AF11	3,2	300			1370	1512	702	1370		35	0,52	150	278	2,8	225	34	396
	AF11	3,5	300			1265	1354	659	1265		33	0,48	150	243	3,0	225	34	353
	AF11	3,8	300			1174	1220	624	1174		31	0,45	150	214	3,3	225	34	316
	AF11	4,1	300			1096	1105	594	1096		29	0,42	150	190	3,5	225	34	285
	AF11	4,3	300			1007	1007	569	1028		27	0,40	150	169	3,8	225	34	259
	AF11	4,6	300			922	922	547	967		26	0,37	150	151	4,0	225	34	236
	AF11	4,9	300			848	848	528	913		24	0,35	150	136	4,3	225	34	217
									Avg.	**1,04**								
									COV	**14,2%**								

Table A.2: 2PKT calculations

It is necessary to specify that considering only the *Uzel*'s tests predictions and the parametric study by means of the FEA (thus without *Richart*'s tests), the average of experimental-to-predicted is 1.04 and the Coefficient of Variation is 14.2%. While considering also *Richart*'s tests the average is 1.08 and the CoV is 15.3%.

Note that the Coefficient of Variation represents the ratio of the standard deviation to the mean, and it is a useful statistic element for comparing the degree of variation from one data series to another, even if the means are drastically different from one another.

Ref.	Name	L/d	f_c	ρ	ε_t	w	n_{ci}	v_{ci}	V_{ci}	V_d	V_{sh}
			MPa	%	‰	mm	MPa	MPa	kN	kN	kN
Richardt (1948a, 1948b)	501a	5,4	25,4	1,38	1,9	6,7	0,00	0,22	101	0	556
	501b	5,4	25,7	1,38	1,9	6,7	0,00	0,22	101	0	560
	502a	3,4	24,3	0,54	5,5	4,5	0,00	0,30	226	0	1644
	502b	3,4	22,7	0,54	5,2	4,4	0,00	0,30	222	0	1561
	503a	3,4	24,4	0,54	5,5	4,5	0,00	0,30	226	0	1649
	503b	3,4	24	0,54	5,5	4,5	0,00	0,30	225	0	1628
	504a	6,0	24,9	1,77	1,3	7,5	0,00	0,19	75	0	367
	504b	6,0	25,8	1,77	1,3	7,5	0,00	0,20	76	0	377
	505a	3,8	25,4	0,68	4,2	4,7	0,00	0,30	185	0	1183
	505b	3,8	25,7	0,68	4,3	4,7	0,00	0,30	186	0	1195
	506a	3,8	23,1	0,68	4,0	4,6	0,00	0,29	180	0	1106
	506b	3,8	26,3	0,68	4,3	4,7	0,00	0,30	187	0	1214
Uzel et al., (2003)	UN100	3,2	43	0,76	1,9	2,0	0,00	0,55	153	0	303
	AF3	4,9	27,3	0,76	1,8	3,0	0,00	0,39	73	0	125
	AF6	3,1	32,2	0,76	2,2	2,0	0,00	0,61	113	0	245
	AF11	2,2	36,2	0,76	2,8	2,1	0,00	0,63	175	0	677
	AF13	3,5	35,7	2,16	0,7	1,8	0,00	0,70	181	0	264
Varying ρ	UN100	3,2	43	0,5	2,6	2,8	0,00	0,41	115	0	265
	UN100	3,2	43	0,6	2,3	2,4	0,00	0,48	132	0	282
	UN100	3,2	43	0,7	2,1	2,1	0,00	0,53	146	0	296
	UN100	3,2	43	0,8	1,9	1,9	0,00	0,57	158	0	308
	UN100	3,2	43	0,9	1,7	1,8	0,00	0,61	168	0	318
	UN100	3,2	43	1	1,6	1,7	0,00	0,63	176	0	326
	UN100	3,2	43	1,1	1,5	1,6	0,00	0,66	183	0	333
	UN100	3,2	43	1,2	1,4	1,5	0,00	0,68	189	0	339
	UN100	3,2	43	1,3	1,3	1,5	0,00	0,70	194	0	344
	UN100	3,2	43	1,4	1,2	1,5	0,00	0,71	198	0	348
	UN100	3,2	43	1,5	1,1	1,4	0,00	0,73	201	0	351
	UN100	3,2	43	1,6	1,1	1,4	0,00	0,74	204	0	354
	UN100	3,2	43	1,7	1,0	1,4	0,00	0,75	207	0	357
	UN100	3,2	43	1,8	1,0	1,4	0,00	0,75	209	0	359
	UN100	3,2	43	1,9	0,9	1,3	0,00	0,76	211	0	361
	UN100	3,2	43	2	0,9	1,3	0,00	0,77	213	0	363
Varying f_c	UN100	3,2	20	0,76	1,3	1,7	0,00	0,43	118	0	200
	UN100	3,2	25	0,76	1,4	1,8	0,00	0,46	128	0	225
	UN100	3,2	30	0,76	1,6	1,8	0,00	0,49	136	0	249
	UN100	3,2	35	0,76	1,7	1,9	0,00	0,52	143	0	271
	UN100	3,2	40	0,76	1,9	1,9	0,00	0,54	150	0	291
	UN100	3,2	45	0,76	2,0	2,0	0,00	0,56	155	0	311
	UN100	3,2	50	0,76	2,1	2,0	0,00	0,58	161	0	330
	UN100	3,2	55	0,76	2,2	2,1	0,00	0,59	165	0	348
	UN100	3,2	60	0,76	2,3	2,1	0,00	0,61	169	0	365

Ref.	Name	L/d	f_c	ρ	ε_t	w	n_{ci}	v_{ci}	V_{ci}	V_d	V_{sh}
			MPa	%	‰	mm	MPa	MPa	kN	kN	kN
	UN100	3,2	65	0,76	2,5	2,2	0,00	0,62	173	0	382
	UN100	3,2	70	0,76	2,6	2,2	0,00	0,64	177	0	398
Varying L	UN100	0,5	43	0,76	1,2	0,3	0,00	1,99	553	0	1168
	UN100	0,8	43	0,76	1,5	0,5	0,00	1,60	443	0	1003
	UN100	1,1	43	0,76	1,8	0,6	0,00	1,35	374	0	876
	UN100	1,4	43	0,76	1,9	0,8	0,00	1,13	314	0	743
	UN100	1,6	43	0,76	2,0	1,0	0,00	0,98	273	0	641
	UN100	1,9	43	0,76	2,1	1,1	0,00	0,87	242	0	556
	UN100	2,2	43	0,76	2,1	1,3	0,00	0,77	214	0	479
	UN100	2,4	43	0,76	2,0	1,5	0,00	0,71	196	0	426
	UN100	2,8	43	0,76	2,0	1,7	0,00	0,64	176	0	369
	UN100	3,0	43	0,76	2,0	1,8	0,00	0,60	165	0	337
	UN100	3,2	43	0,76	1,9	2,0	0,00	0,55	153	0	303
	UN100	3,5	43	0,76	1,9	2,1	0,00	0,51	143	0	275
	UN100	3,8	43	0,76	1,9	2,3	0,00	0,48	134	0	250
	UN100	4,1	43	0,76	1,8	2,5	0,00	0,45	126	0	229
	UN100	4,3	43	0,76	1,8	2,6	0,00	0,43	119	0	211
	UN100	4,6	43	0,76	1,8	2,8	0,00	0,41	113	0	196
	UN100	4,9	43	0,76	1,8	3,0	0,00	0,39	107	0	182
Varying ρ	AF11	2,2	36,2	0,5	4,0	3,0	0,00	0,45	126	0	628
	AF11	2,2	36,2	0,6	3,4	2,5	0,00	0,53	148	0	650
	AF11	2,2	36,2	0,7	3,0	2,2	0,00	0,60	166	0	668
	AF11	2,2	36,2	0,8	2,7	2,0	0,00	0,65	181	0	683
	AF11	2,2	36,2	0,9	2,4	1,8	0,00	0,70	193	0	695
	AF11	2,2	36,2	1	2,2	1,7	0,00	0,73	203	0	705
	AF11	2,2	36,2	1,1	2,0	1,6	0,00	0,76	211	0	713
	AF11	2,2	36,2	1,2	1,9	1,6	0,00	0,79	218	0	720
	AF11	2,2	36,2	1,3	1,8	1,5	0,00	0,81	224	0	725
	AF11	2,2	36,2	1,4	1,6	1,5	0,00	0,82	229	0	730
	AF11	2,2	36,2	1,5	1,5	1,4	0,00	0,84	233	0	734
	AF11	2,2	36,2	1,6	1,5	1,4	0,00	0,85	236	0	738
	AF11	2,2	36,2	1,7	1,4	1,4	0,00	0,86	239	0	741
	AF11	2,2	36,2	1,8	1,3	1,4	0,00	0,87	242	0	743
	AF11	2,2	36,2	1,9	1,2	1,3	0,00	0,88	244	0	746
	AF11	2,2	36,2	2	1,2	1,3	0,00	0,89	246	0	748
Varying f_c	AF11	2,2	20	0,76	1,9	1,8	0,00	0,53	146	0	458
	AF11	2,2	25	0,76	2,2	1,9	0,00	0,57	157	0	530
	AF11	2,2	30	0,76	2,5	2,0	0,00	0,60	166	0	598
	AF11	2,2	35	0,76	2,8	2,0	0,00	0,62	173	0	662
	AF11	2,2	40	0,76	3,0	2,1	0,00	0,65	180	0	723
	AF11	2,2	45	0,76	3,3	2,2	0,00	0,67	185	0	782
	AF11	2,2	50	0,76	3,5	2,3	0,00	0,68	190	0	840
	AF11	2,2	55	0,76	3,7	2,3	0,00	0,70	194	0	895

Ref.	Name	L/d	f_c	ρ	ε_t	w	n_{ci}	v_{ci}	V_{ci}	V_d	V_{sh}
			MPa	%	‰	mm	MPa	MPa	kN	kN	kN
	AF11	2,2	60	0,76	4,0	2,4	0,00	0,71	198	0	949
	AF11	2,2	65	0,76	4,2	2,5	0,00	0,72	201	0	1003
	AF11	2,2	70	0,76	4,4	2,5	0,00	0,74	204	0	1054
Varying L	AF11	0,5	36,2	0,76	1,5	0,4	0,00	1,90	528	0	1631
	AF11	0,8	36,2	0,76	2,1	0,6	0,00	1,47	408	0	1431
	AF11	1,1	36,2	0,76	2,5	0,9	0,00	1,20	334	0	1261
	AF11	1,4	36,2	0,76	2,7	1,2	0,00	0,97	270	0	1070
	AF11	1,6	36,2	0,76	2,8	1,5	0,00	0,83	229	0	917
	AF11	1,9	36,2	0,76	2,9	1,8	0,00	0,72	199	0	786
	AF11	2,2	36,2	0,76	2,8	2,1	0,00	0,62	173	0	667
	AF11	2,4	36,2	0,76	2,8	2,4	0,00	0,56	156	0	586
	AF11	2,8	36,2	0,76	2,7	2,7	0,00	0,50	138	0	497
	AF11	3,0	36,2	0,76	2,6	3,0	0,00	0,46	129	0	448
	AF11	3,2	36,2	0,76	2,5	3,3	0,00	0,43	118	0	396
	AF11	3,5	36,2	0,76	2,4	3,5	0,00	0,39	110	0	353
	AF11	3,8	36,2	0,76	2,3	3,8	0,00	0,37	102	0	316
	AF11	4,1	36,2	0,76	2,3	4,1	0,00	0,34	95	0	285
	AF11	4,3	36,2	0,76	2,2	4,4	0,00	0,32	90	0	259
	AF11	4,6	36,2	0,76	2,1	4,7	0,00	0,31	85	0	236
	AF11	4,9	36,2	0,76	2,1	5,0	0,00	0,29	80	0	217

Table A.3: Last iteration of the 2PKT method

Ref.	Name	ρ	Exp/Pred	Exp/Pred	P_{exp}	P_{FEM}	P_{pred}
		%	(2PKT) With dowel action	(2PKT) Without dowel action	kN	kN	kN With dowel action
	AF13	2,16	1,32	1,65	1857	1848	181
Varying ρ	UN100	0,5	1,07	1,07		972	911
	UN100	0,7	0,94	0,95		1119	1197
	UN100	1	0,95	1,00		1296	1371
	UN100	1,3	0,91	1,02		1393	1529
	UN100	1,5	0,88	1,04		1443	1637
	UN100	1,7	0,88	1,09		1539	1749
	UN100	2	0,83	1,11		1604	1932
Varying ρ	AF11	0,5	1,17	1,17		1622	1387
	AF11	0,7	1,20	1,20		2282	1910
	AF11	1	1,04	1,06		2750	2635
	AF11	1,3	0,99	1,03		2750	2791
	AF11	1,5	0,95	1,02		2750	2896
	AF11	1,7	0,92	1,01		2750	3005
	AF11	2	0,86	1,00		2750	3184

Table A.4: Effect of dowel action increasing the amount of longitudinal reinforcement

In this section of the Appendix, Table A.4, it is possible to analyze the effect of dowel action in the tests in which the reinforcement ratio is particularly high. Specifically, it is the case for AF13, in which the amount of longitudinal reinforcement is almost three times with respect to the other *Uzel*'s footing tests, and for the FEM models in which the longitudinal reinforcement ratio is the parameter that varies. In Table A.4 the comparison between taking into account the dowel action or not is displayed. The results show that neglecting the dowel action contribute is possible to obtain more precise prediction just for the specific case of specimen AF13. In fact, for FEM samples the 2PKT, considering also the dowel action contribute, produces an overestimation of the shear strength. Therefore, this is also why the dowel action contribution is not taken into account for footing's strength predictions. Concluding, it might be possible that large strength underestimation by the 2PKT for AF13 is a cause inherent in the test itself.

Appendix 3: FEM results from the parametric study

In this part of the thesis, the FEM results from the parametric analysis are elaborated and discussed deeply.
For both model AF1 UN100 and AF11, crack pattern at failure and stresses in the longitudinal reinforcement at failure produced as result of the FEM analysis by VecTor2 are plotted below for the limit cases of each parameter. For limit cases it is meant the minimum and maximum reinforcement ratio evaluated, the minimum and maximum value for the concrete strength and for *L/d* ratio equal to 1.5 and 3. Moreover, also the curve load-displacement at the end section of the footing is illustrated for the same considered specimens. These last graphs can reproduce accurately the real laboratory test under the same hypothesis and conditions (as it is possible to see in the comparison with the model and the real tests in Appendix 4).
Analyzing AF1 UN100 as model, from Figures A.1 and A.2, the failure mode of the specimen with 0.5% of reinforcement ratio is flexural failure due to under-reinforced footing, in fact the longitudinal reinforcement yields excessively resulting in failure in the concrete compression zone. While for the specimen with 2% of reinforcement ratio, in Figures A.4 and A.5, the visible failure type is shear diagonal failure (the bar is not yielded).
Similarly, for model AF11, in Figures A.19, A.20, A.22 and A.23, the specimen with low reinforcement ratio fails under flexure condition due to the yielding of the under-dimensioned reinforcement; while the specimen with higher reinforcement ratio shows the typical shear failure (for footings with low *L/d* ratio).
Proceeding into the analysis of the second parameter, the concrete strength, from Figures A.7, A.8, A.10 and A.11 for model AF1 UN100 and from Figures A.25, A.26, A.28 and A.29, for model AF11, it is possible to observe that in the tests with low concrete strength the failure is in shear (diagonal tension failure for AF1 and shear tension failure for AF11); while the samples with high concrete strength present flexural failure in AF11 also because the reinforcement are yielded, but probably a mix of shear failure and flexural failure in AF11 because the main diagonal crack is evident and the bars are not yielded at failure.
Examining the last parameter, the slenderness (*L/d* ratio), for model AF1 UN100 the failure modes are under shear; while for model AF1 the stocky element presents a mix of shear and flexural failure due to both the yielding of the reinforcement and the shear diagonal crack, the slender element shows the typical diagonal shear failure.

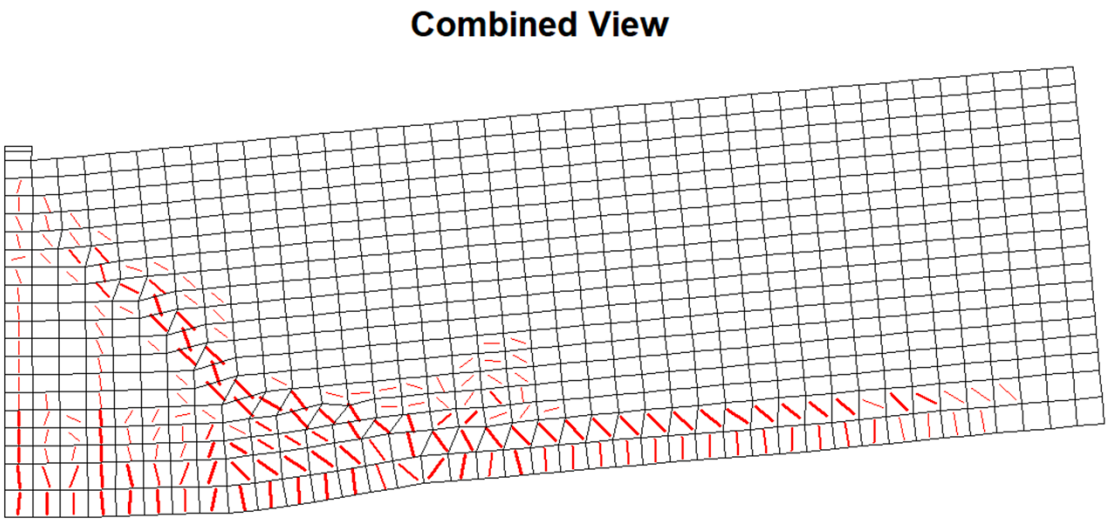

A.1: Combined view of cracks at failure – AF1 UN100 with $\rho_l = 0.5\%$

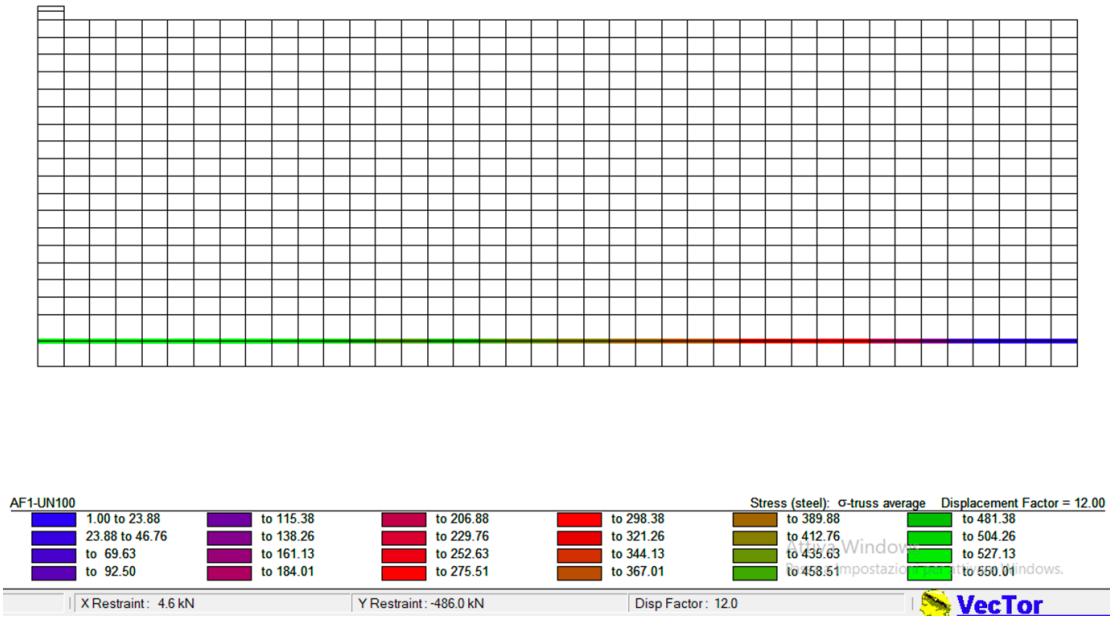

A.2: Stresses in the reinforcement at failure – AF1 UN100 with $\rho_l = 0.5\%$

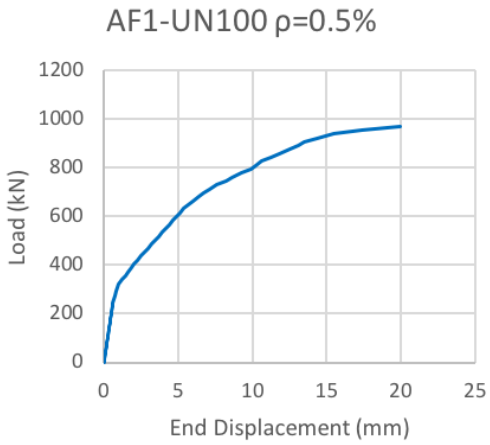

A.3: Load-Displacement plot for AF1 UN100 with $\rho_l = 0.5\%$

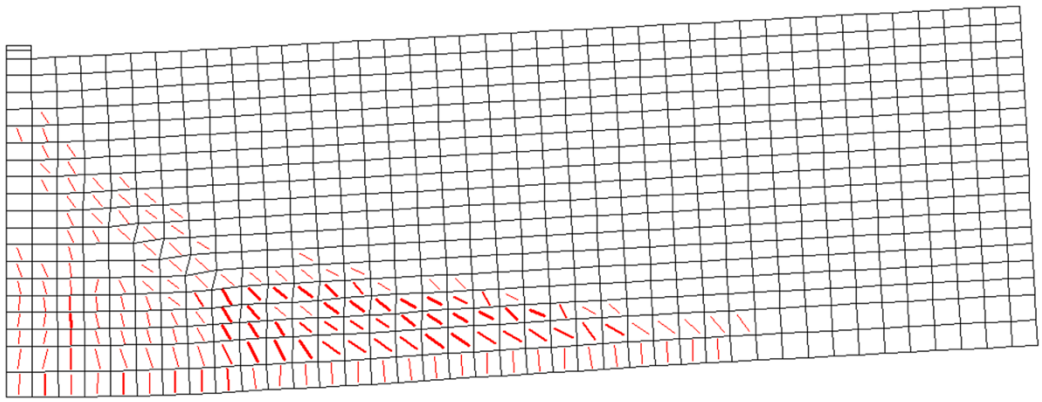

A.4: Combined view of cracks at failure – AF1 UN100 with $\rho_l = 2\%$

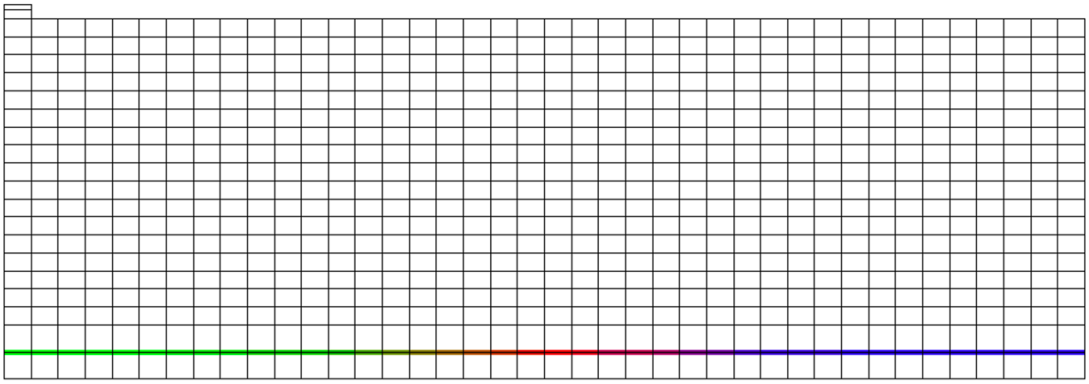

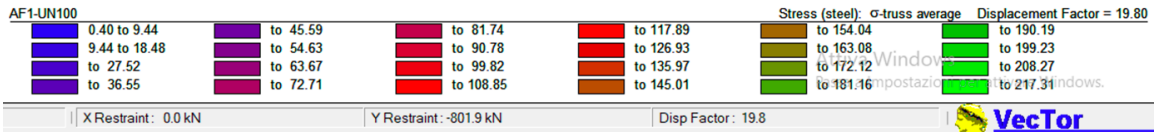

A.5: Stresses in the reinforcement at failure – AF1 UN100 with $\rho_l = 2\%$

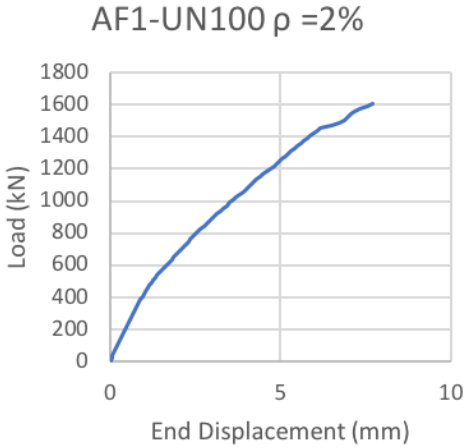

A.6: Load-Displacement plot for AF1 UN100 with $\rho_l = 2\%$

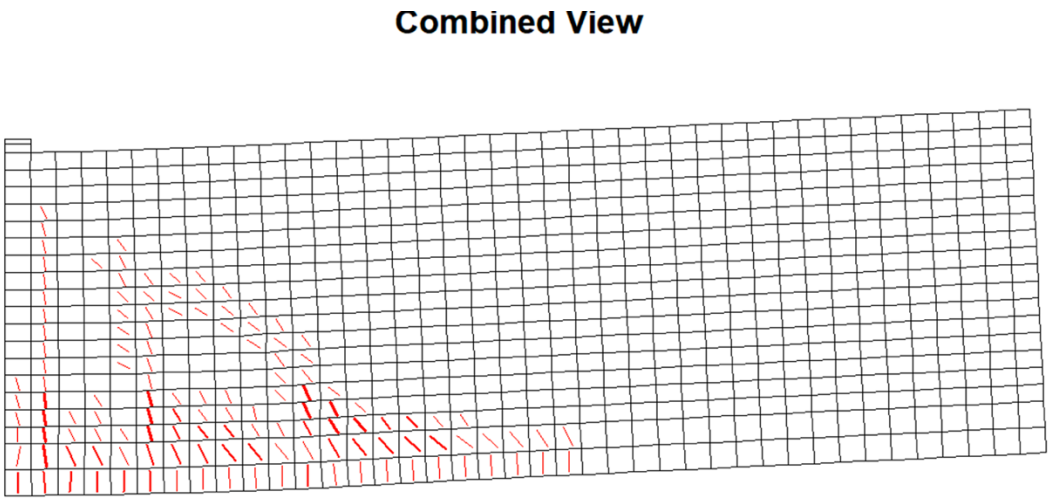

A.7: Combined view of cracks at failure – AF1 UN100 with $f_c = 20\ MPa$

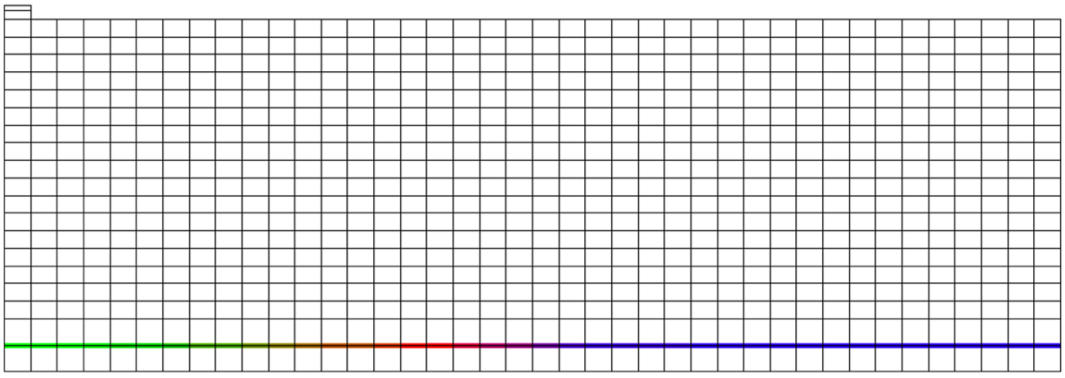

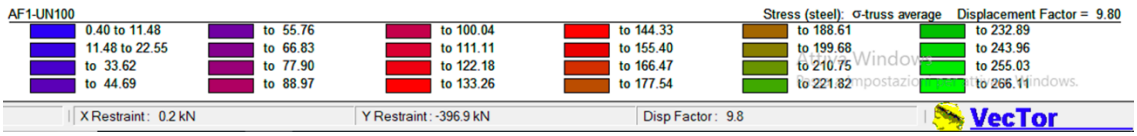

A.8: Stresses in the reinforcement at failure – AF1 UN100 with $f_c = 20\ MPa$

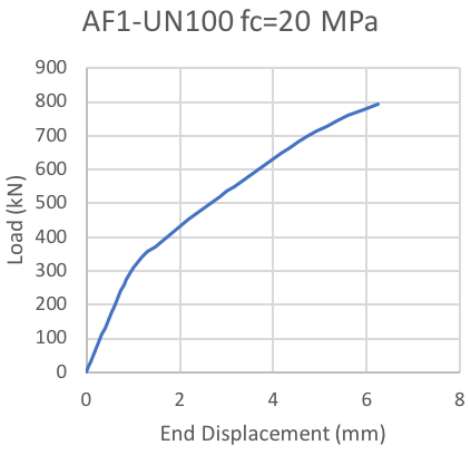

A.9: Load-Displacement plot for AF1 UN100 with $f_c = 20\ MPa$

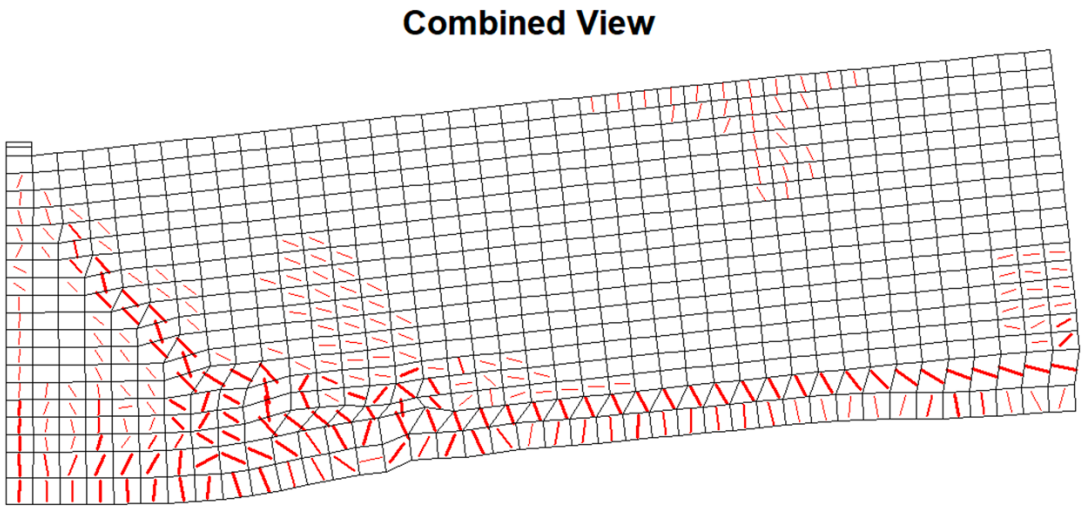

A.10: Combined view of cracks at failure – AF1 UN100 with $f_c = 70\ MPa$

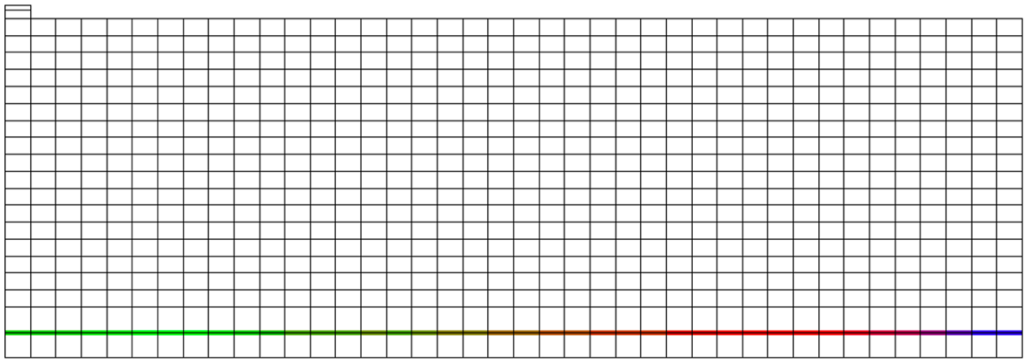

A.11: Stresses in the reinforcement at failure – AF1 UN100 with $f_c = 70\ MPa$

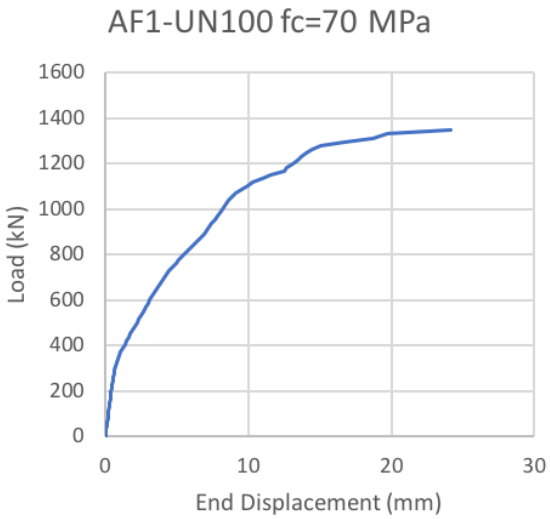

A.12: Load-Displacement plot for AF1 UN100 with $f_c = 70\ MPa$

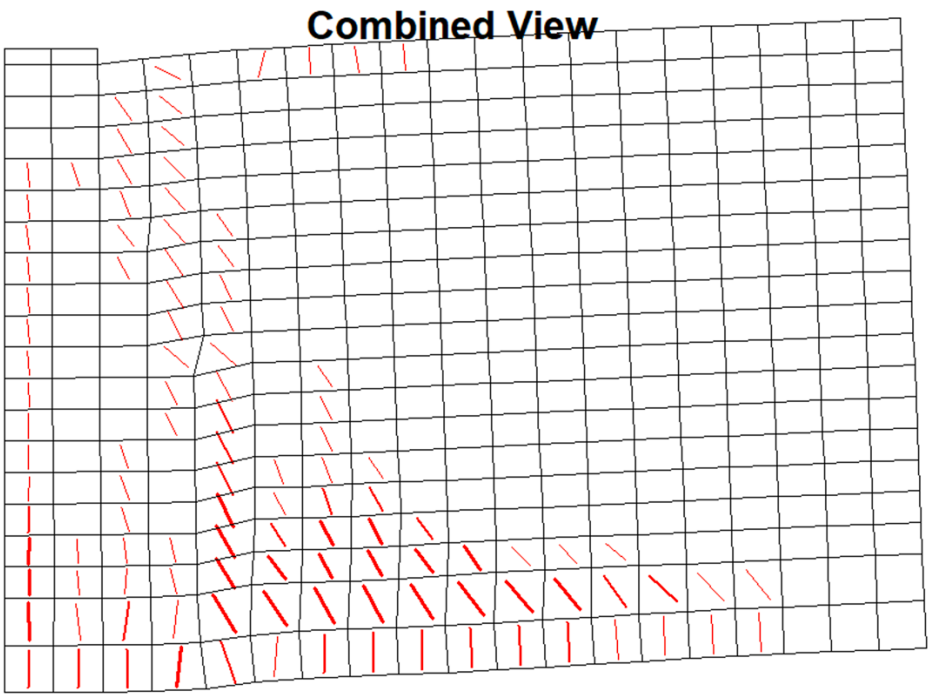

A.13: Combined view of cracks at failure – AF1 UN100 with $\frac{L}{d} = 1.5$

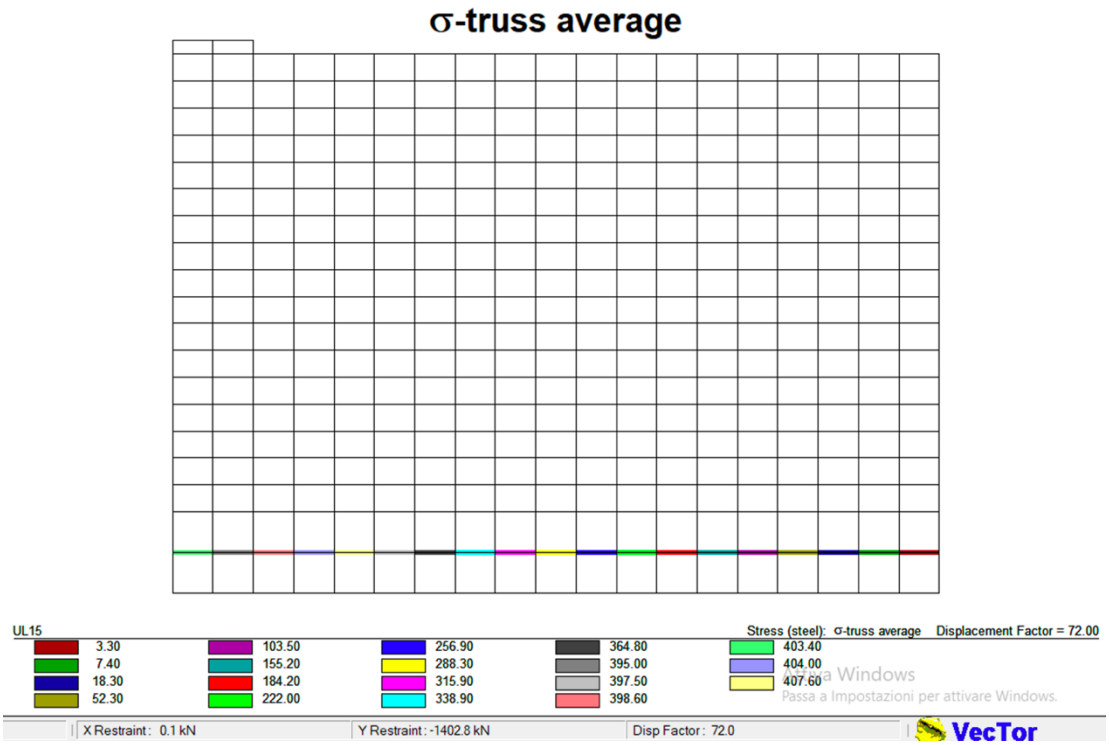

A.14: Stresses in the reinforcement at failure – AF1 UN100 with $\frac{L}{d} = 1.5$

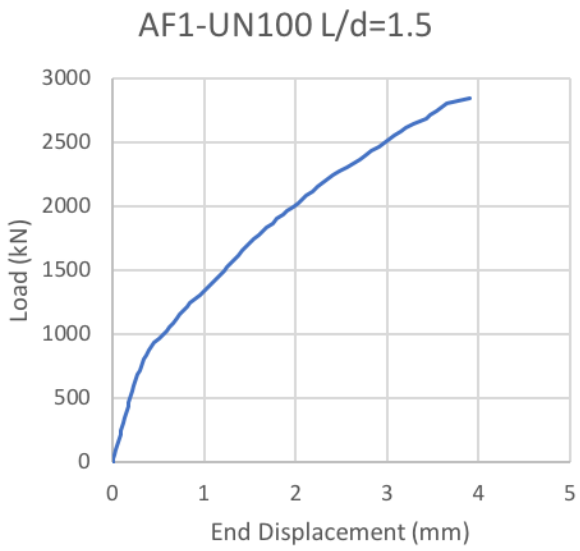

A.15: Load-Displacement plot for AF1 UN100 with $\frac{L}{d} = 1.5$

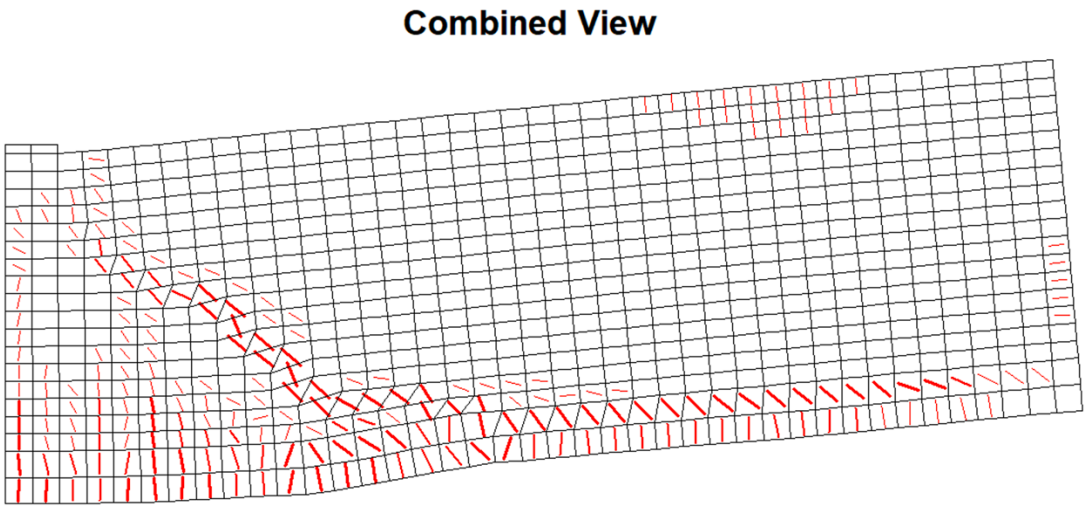

A.16: Combined view of cracks at failure – AF1 UN100 with $\frac{L}{d} = 3$

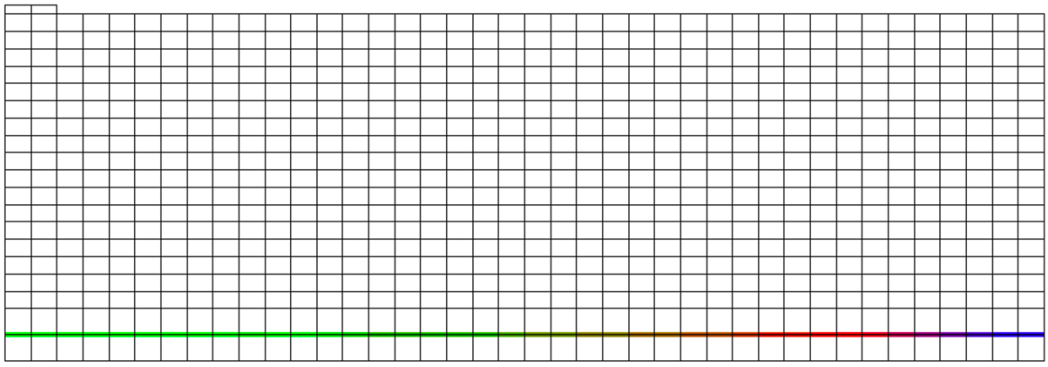

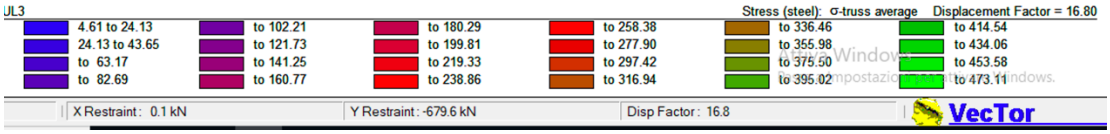

A.17: Stresses in the reinforcement at failure – AF1 UN100 with $\frac{L}{d} = 3$

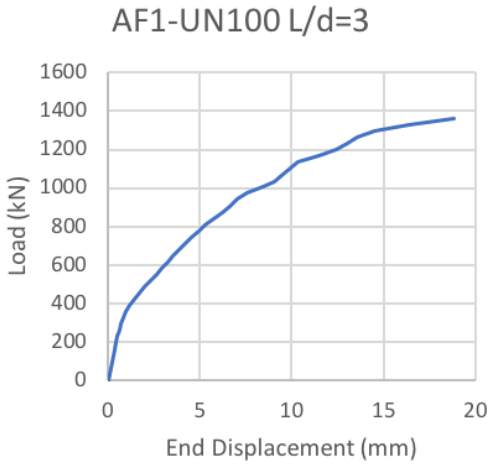

A.18: Load-Displacement plot for AF1 UN100 with $\frac{L}{d} = 3$

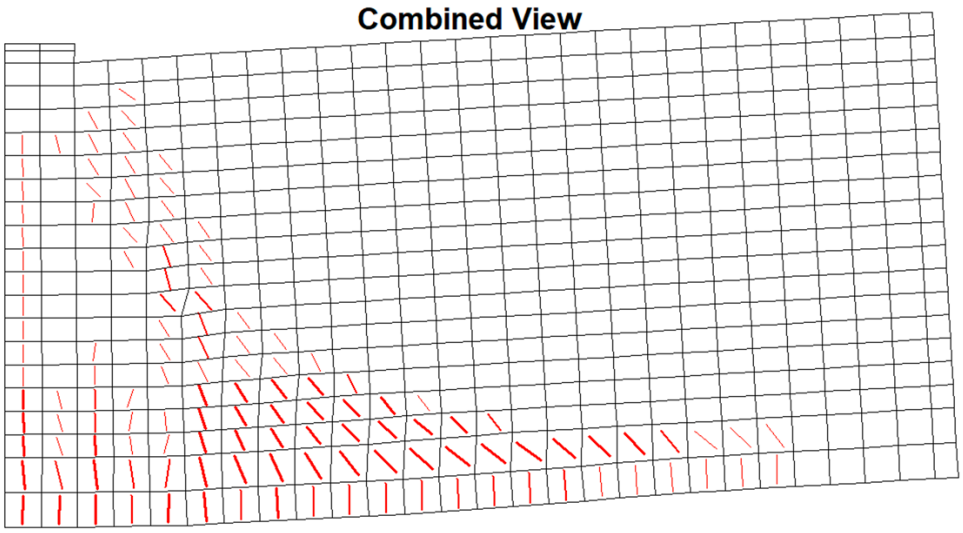

A.19: Combined view of cracks at failure – AF11 with $\rho_l = 0.5\%$

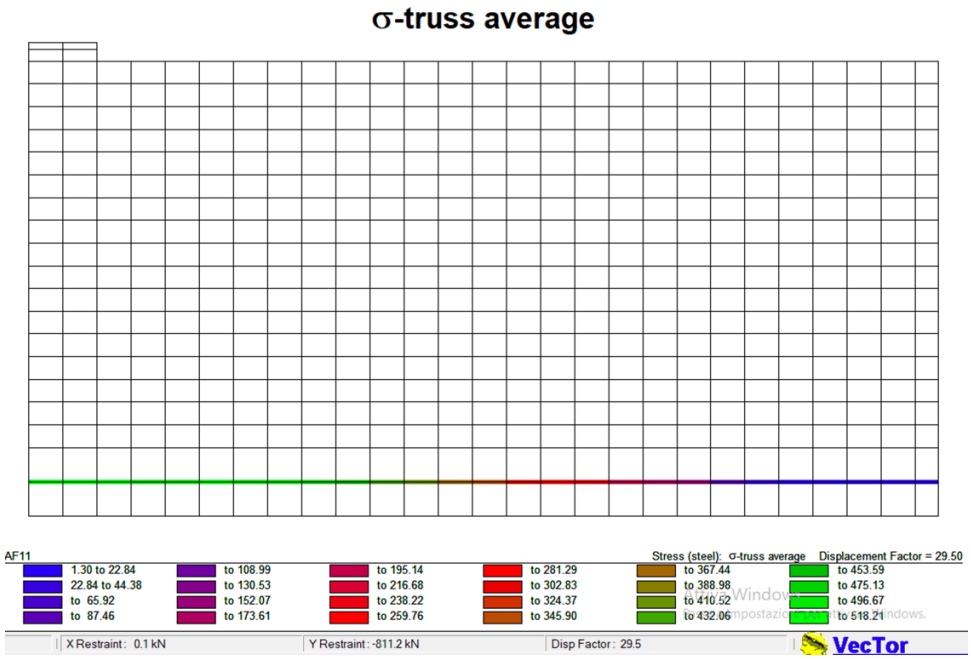

A.20: Stresses in the reinforcement at failure – AF11 with $\rho_l = 0.5\%$

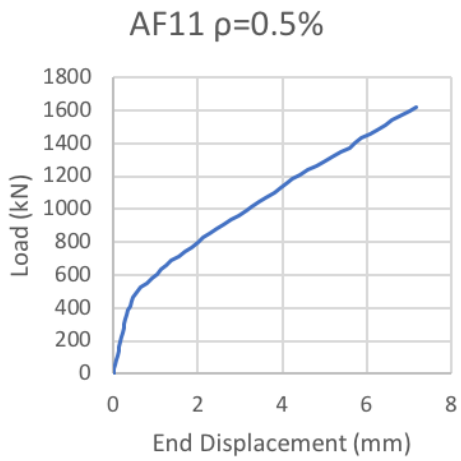

A.21: Load-Displacement plot for AF11 with $\rho_l = 0.5\%$

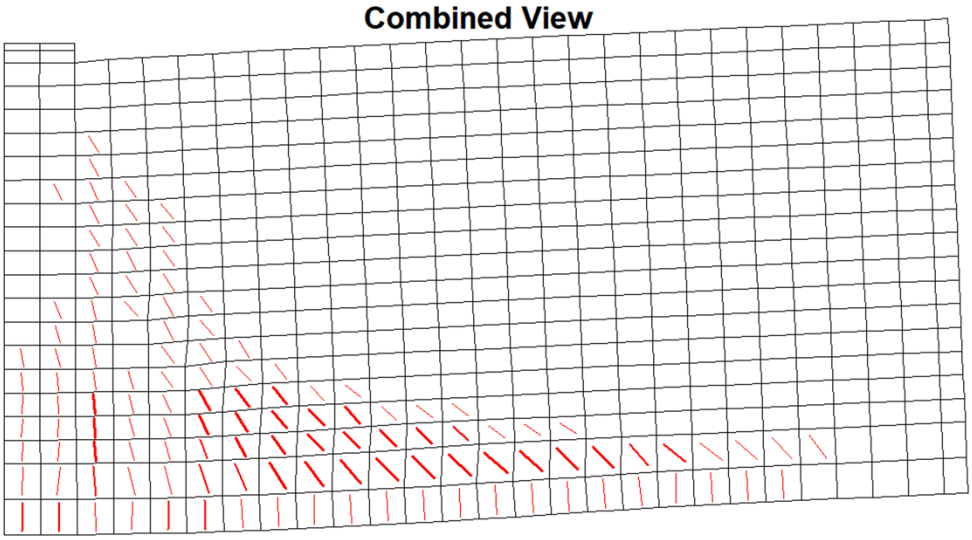

A.22: Combined view of cracks at failure – AF11 with $\rho_l = 2\%$

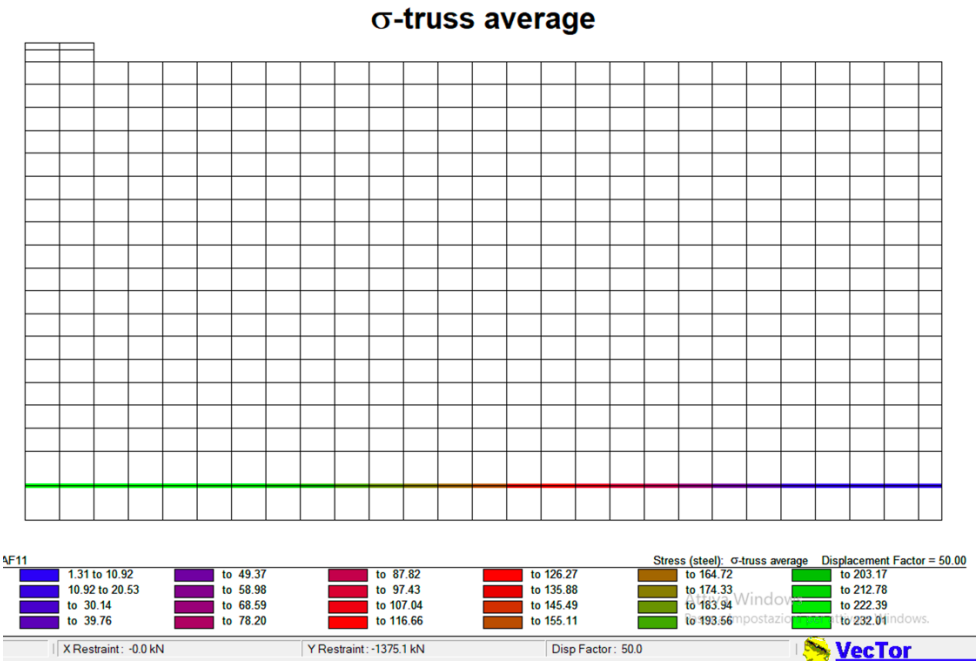

A.23: Stresses in the reinforcement at failure – AF11 with $\rho_l = 2\%$

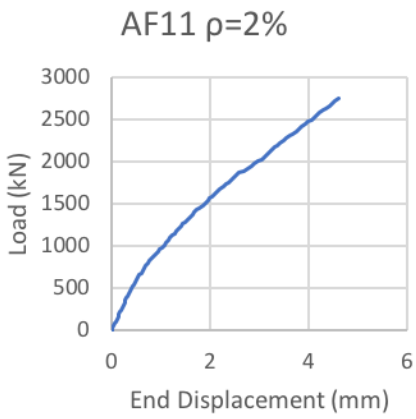

A.24: Load-Displacement plot for AF11 with $\rho_l = 2\%$

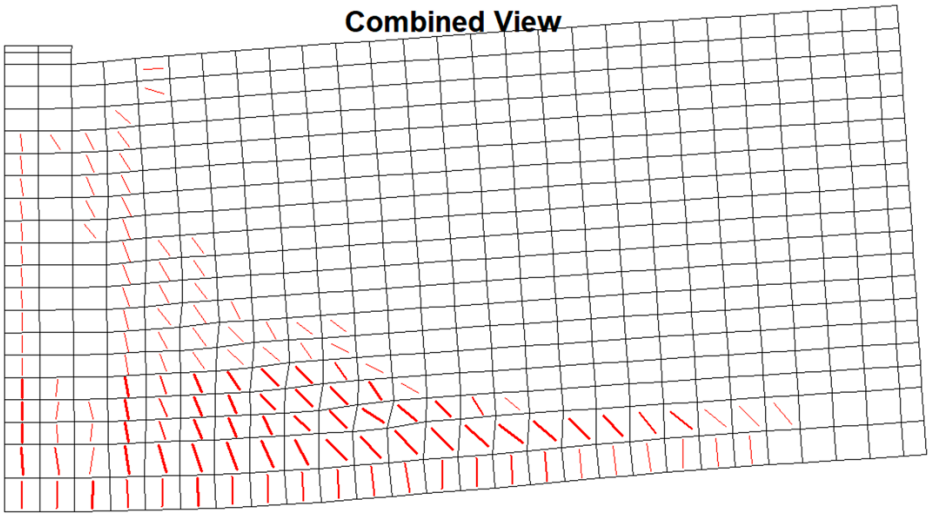

A.25: Combined view of cracks at failure – AF11 with $f_c = 20\ MPa$

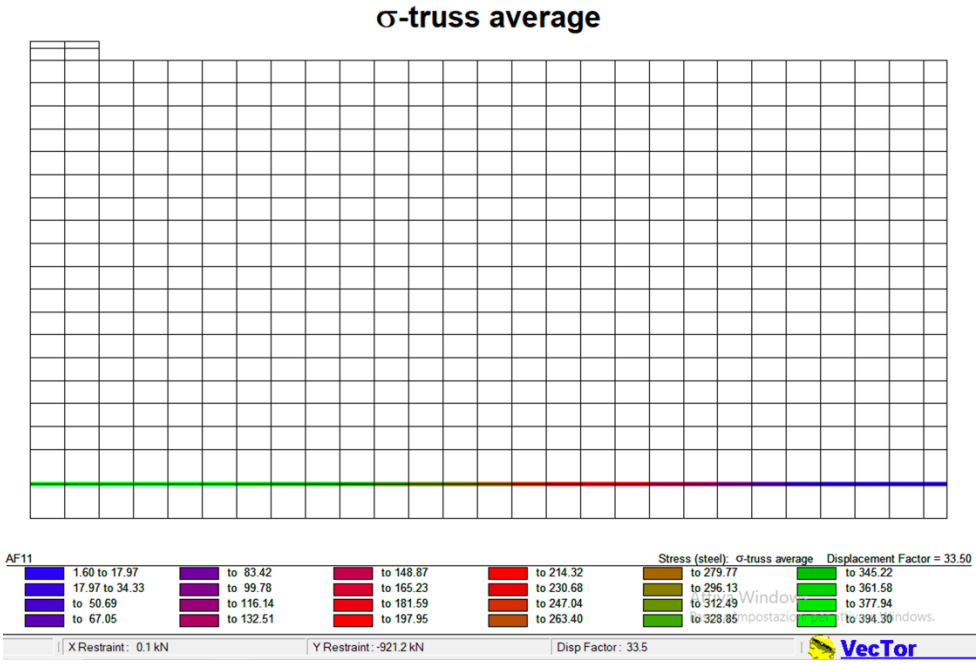

A.26: Stresses in the reinforcement at failure – AF11 with $f_c = 20\ MPa$

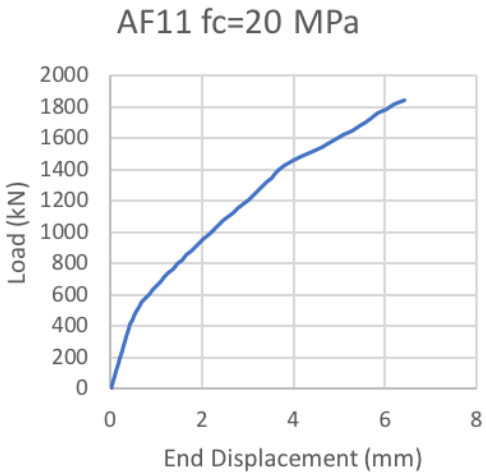

A.27: Load-Displacement plot for AF11 with $f_c = 20\ MPa$

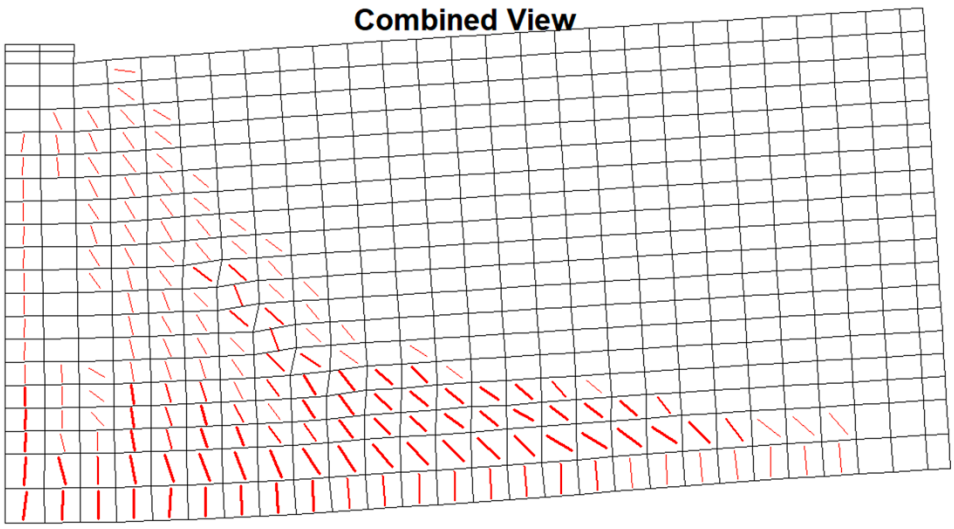

A.28: Combined view of cracks at failure – AF11 with $f_c = 70\ MPa$

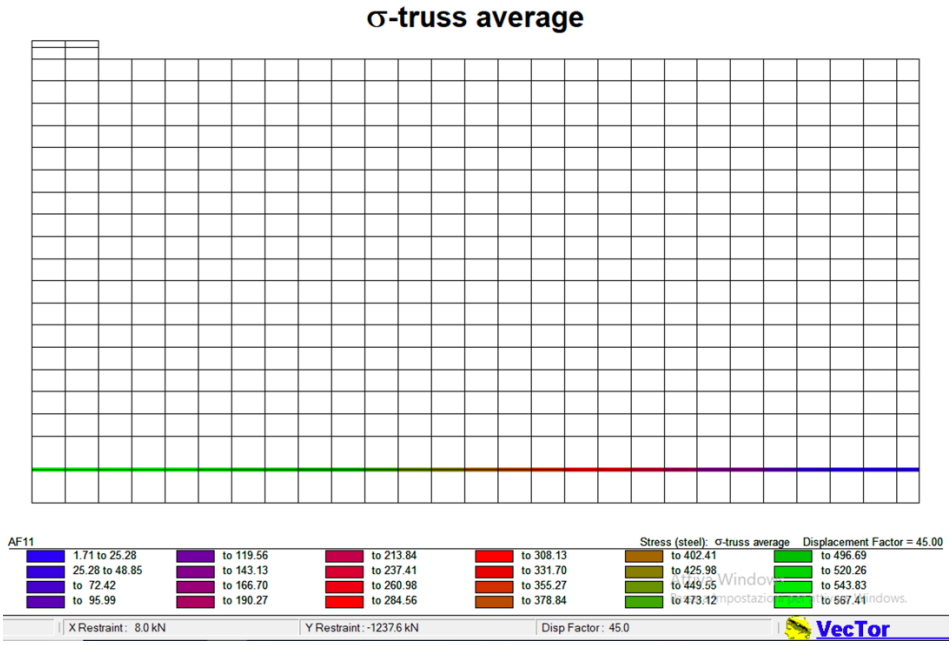

A.29: Stresses in the reinforcement at failure – AF11 with $f_c = 70\ MPa$

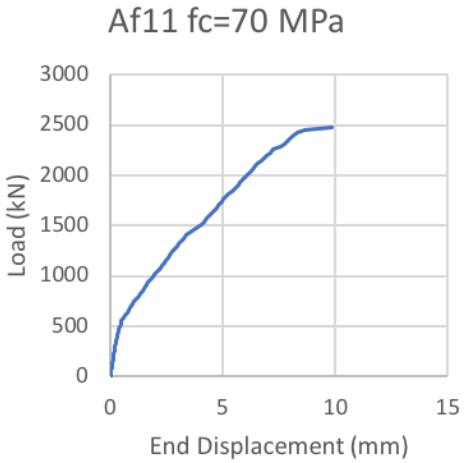

A.30: Load-Displacement plot for AF11 with $f_c = 70\ MPa$

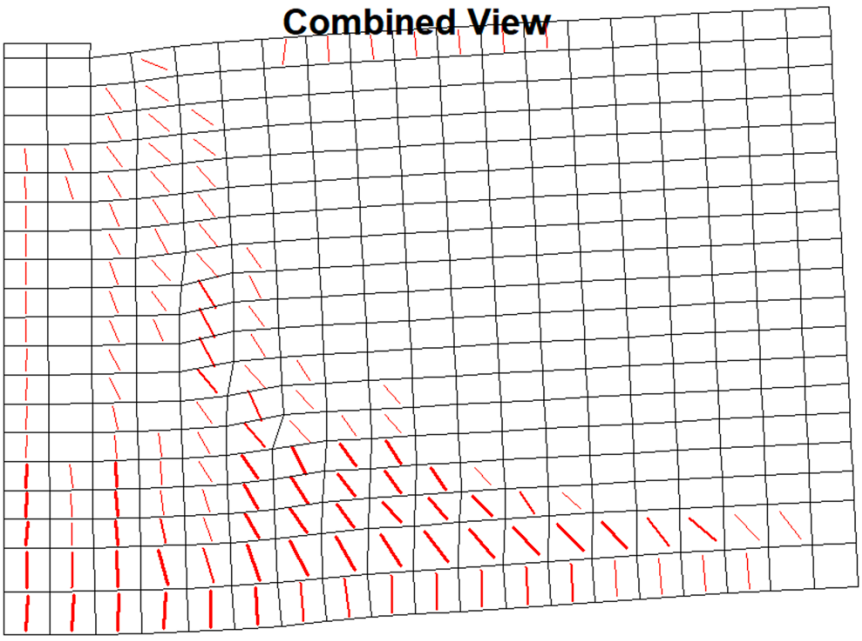

A.31: Combined view of cracks at failure – AF11 with $\frac{L}{d} = 1.5$

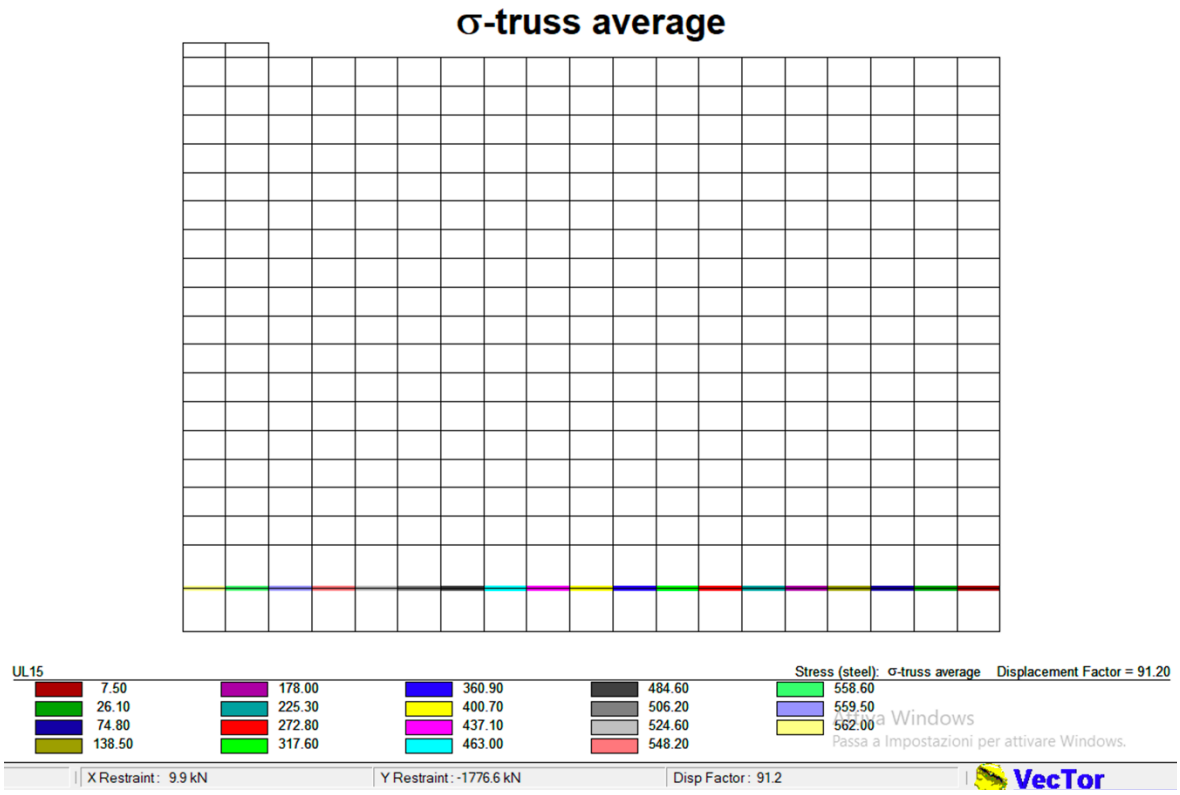

A.32: Stresses in the reinforcement at failure – AF11 with $\frac{L}{d} = 1.5$

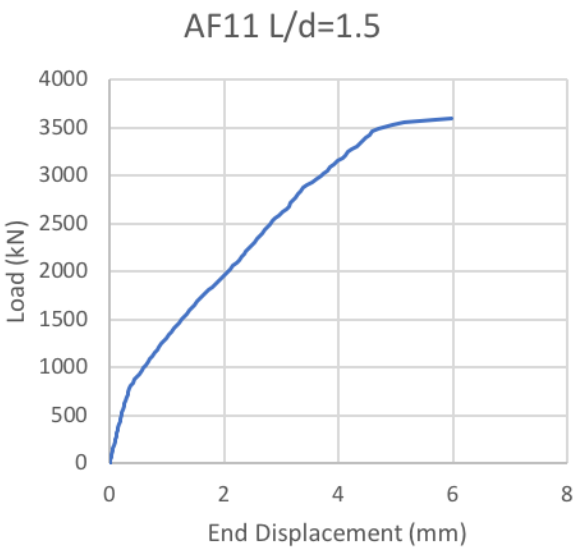

A.33: Load-Displacement plot for AF11 with $\frac{L}{d} = 1.5$

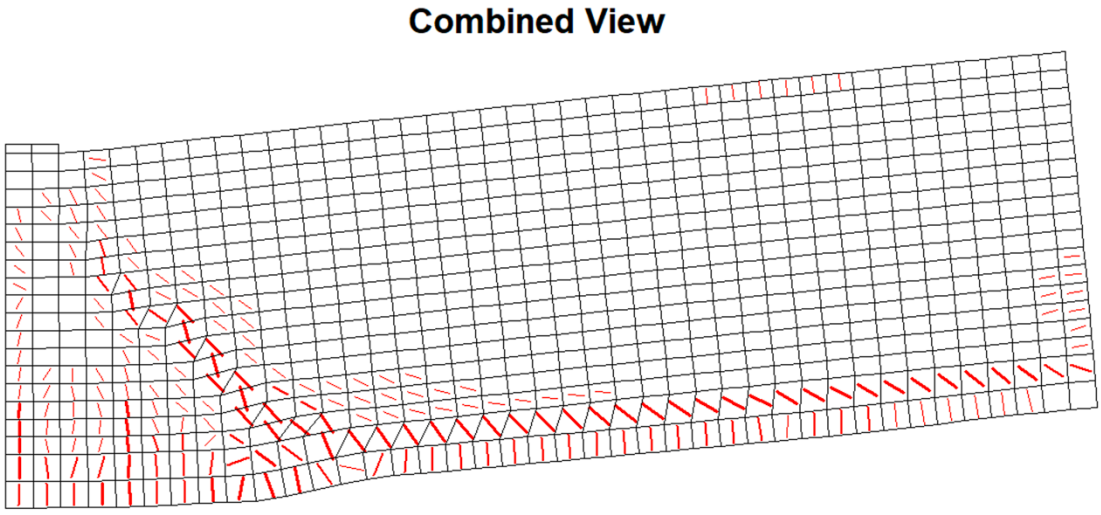

A.34: Combined view of cracks at failure – AF1 UN100 with $\frac{L}{d} = 3$

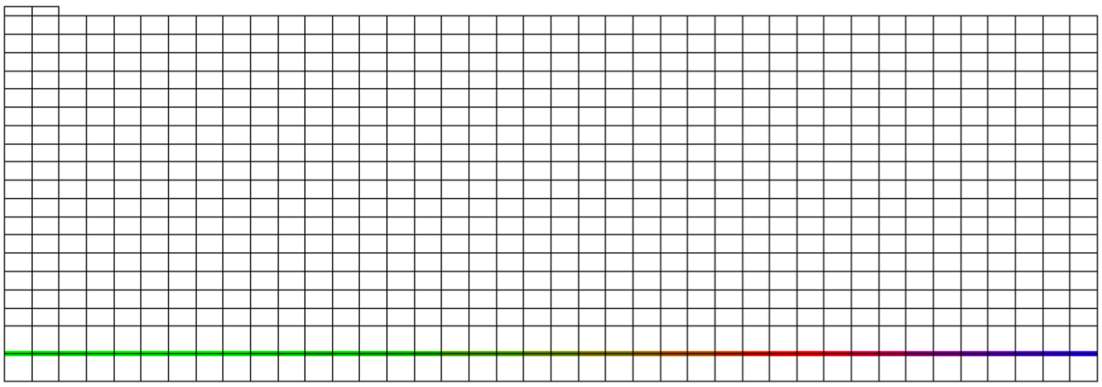

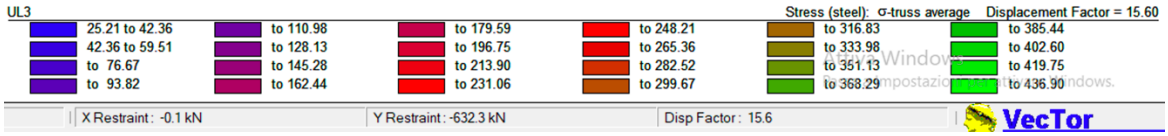

A.35: Stresses in the reinforcement at failure – AF1 UN100 with $\frac{L}{d} = 3$

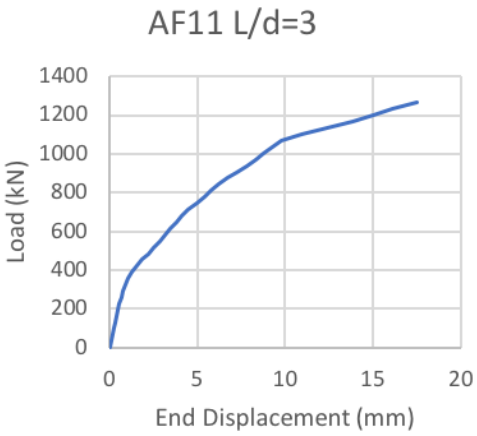

A.36: Load-Displacement plot for AF1 UN100 with $\frac{L}{d} = 3$

Appendix 4: Load-Displacement Charts

In order to validate the parametric study conducted by simulating tests with Non-Linear Finite Element Analysis, the load-displacements plots for the *Uzel*'s tests are shown below. The red curve represents the result from the FEM model of the test and the blue one indicates the real charge-discharge behavior of the test per each load stage. Generally, it is possible to observe that the FEM model well reproduces the global trend of the test during the loading phases, thus these graphs represent an additional evidence of the reliability of FEM. Therefore, the parametric study conducted by modifying the basic model for the test for just one parameter per time, assumes validity and represents many possible real laboratory tests.

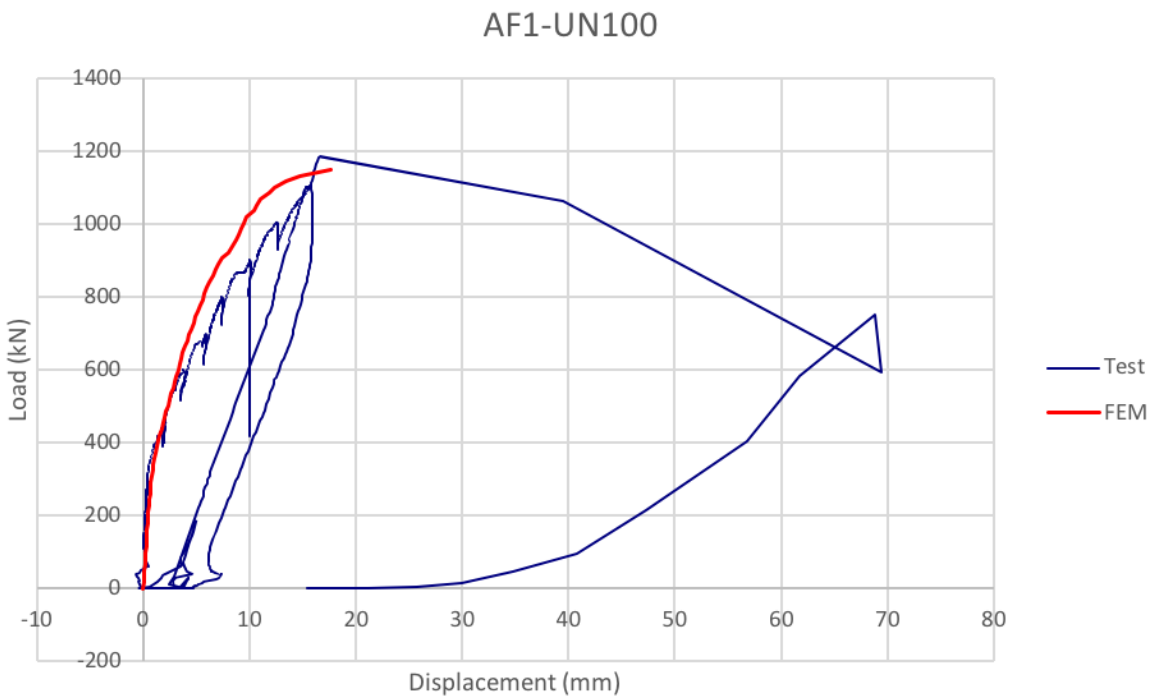

A.37: Load-Displacement plot for specimen AF1 UN100

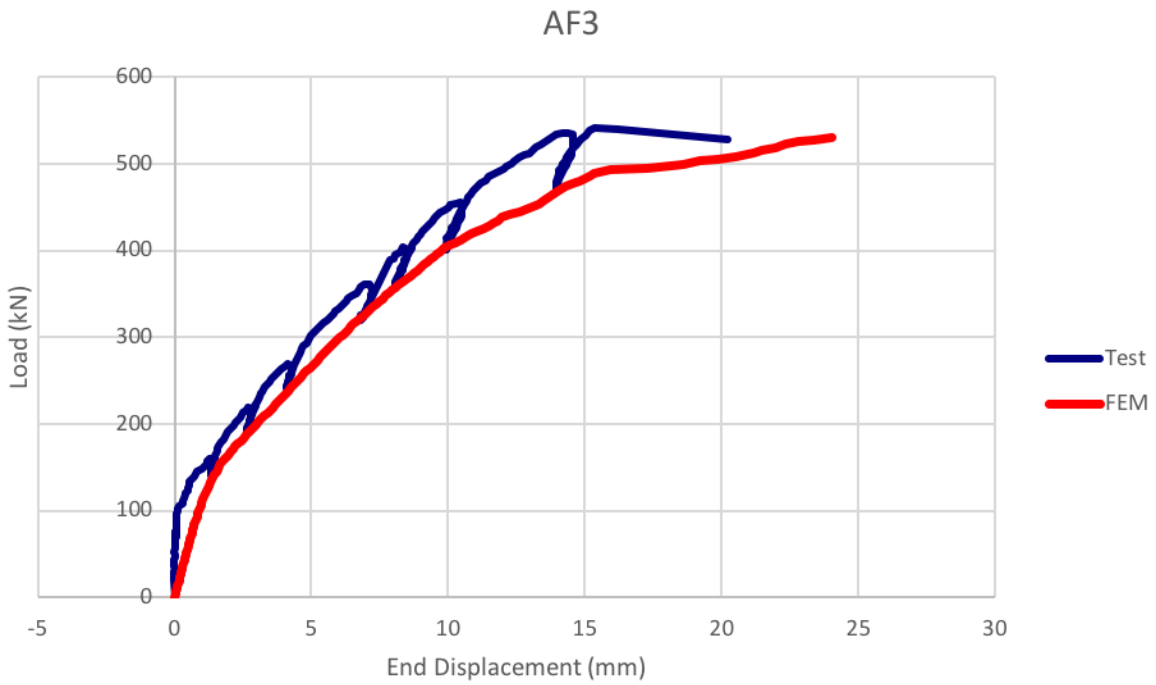

A.38: Load-Displacement plot for specimen AF3

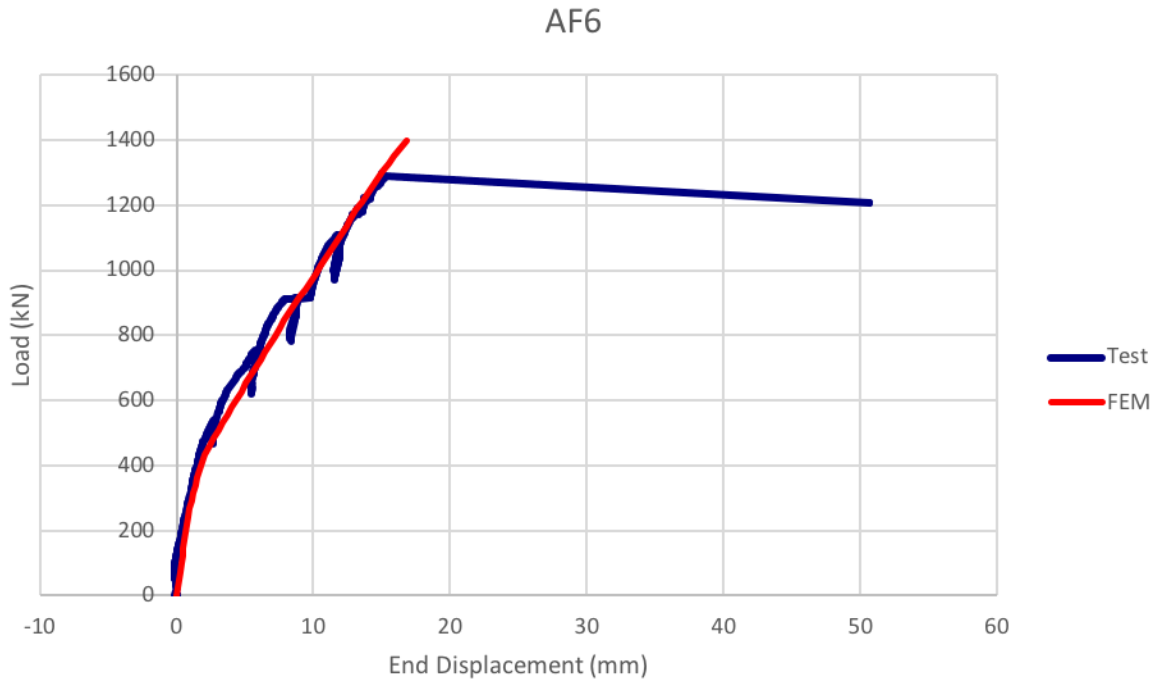

A.39: Load-Displacement plot for specimen AF6

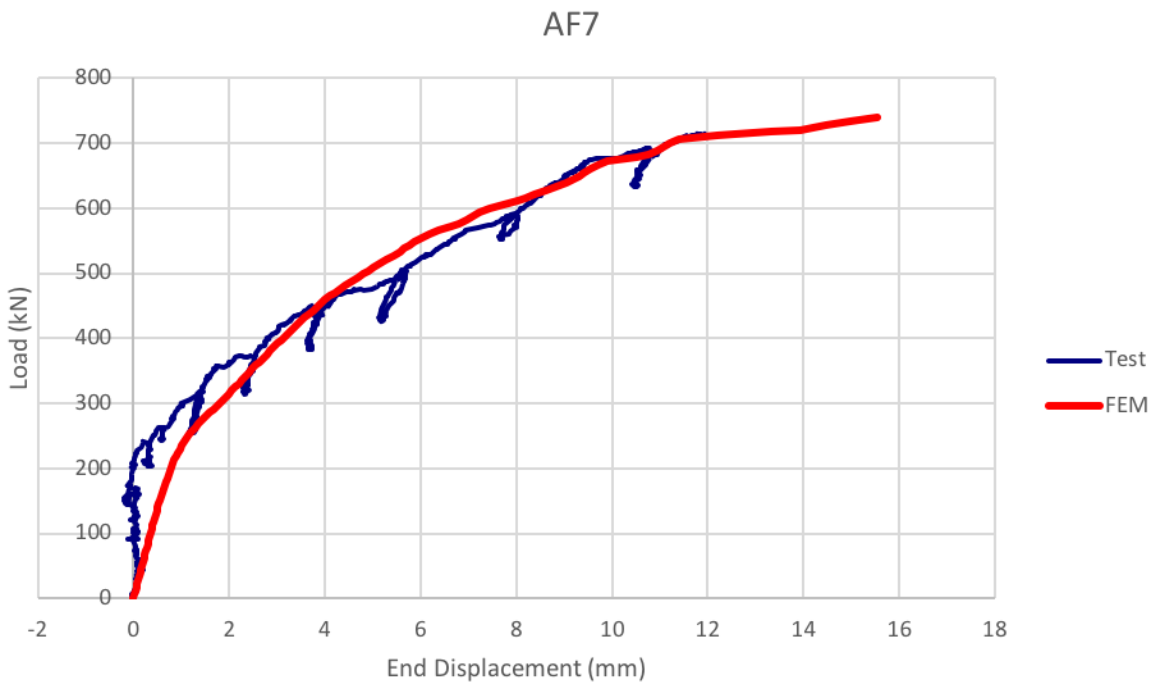

A.40: Load-Displacement plot for specimen AF7

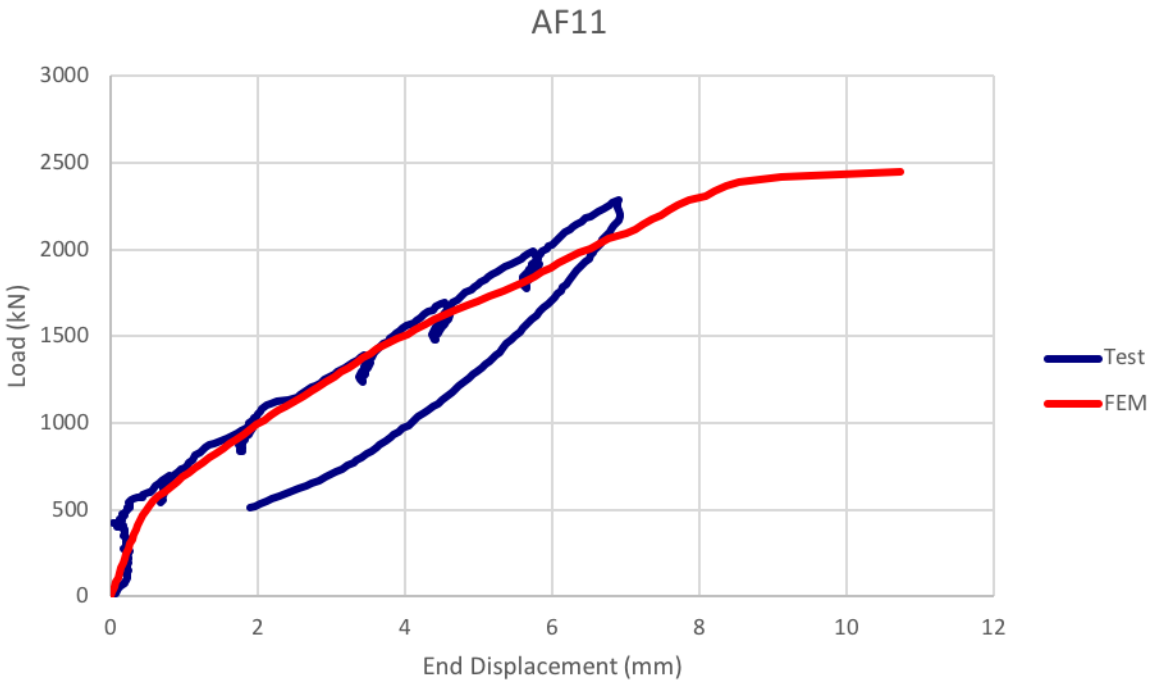

A.41: Load-Displacement plot for specimen AF11

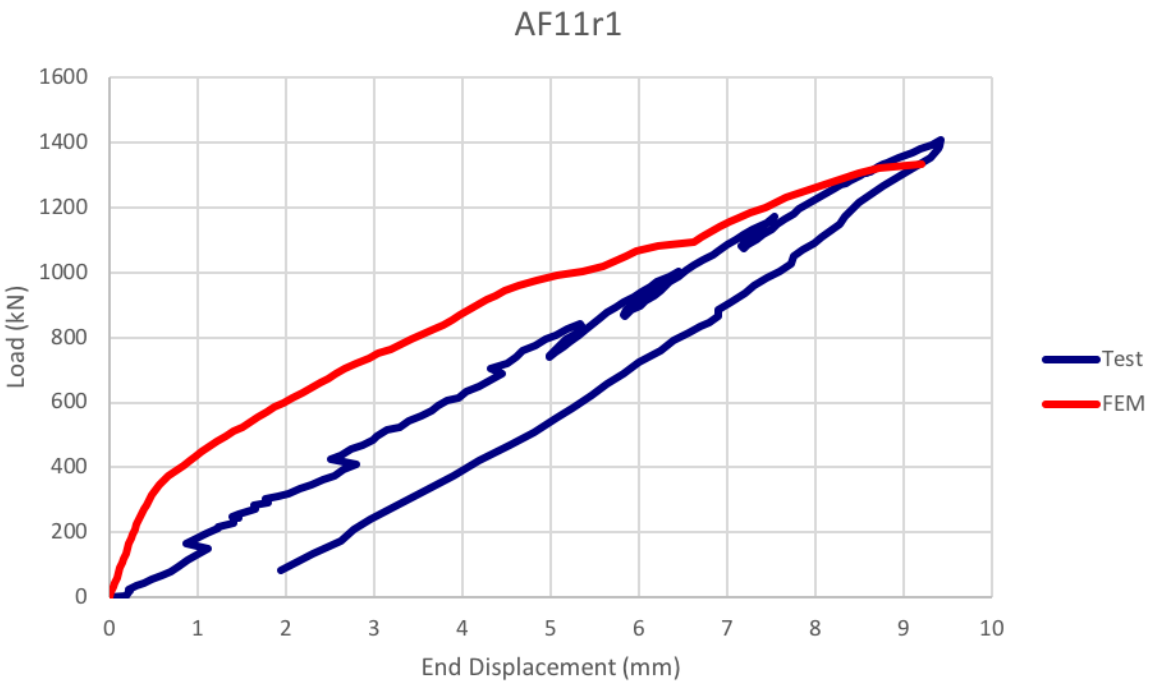

A.42: Load-Displacement plot for specimen AF11r1

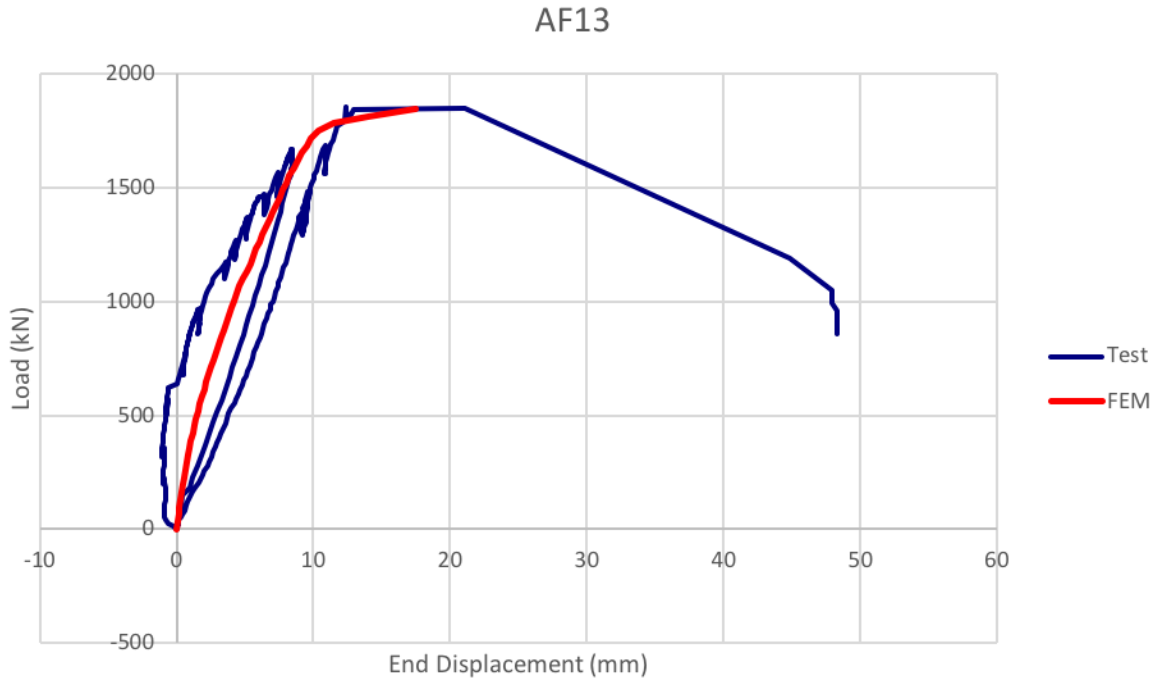

A.43: Load-Displacement plot for specimen AF13